Alma Mater Studiorum – Università di Bologna

DOTTORATO DI RICERCA IN

INGEGNERIA CIVILE, AMBIENTALE E DEI MATERIALI

Ciclo XXVII

Settore Concorsuale di afferenza: 08/A2

Settore Scientifico disciplinare: ING-IND/28

SOIL-STRUCTURE INTERACTION DURING TUNNELLING IN URBAN AREA: OBSERVATIONS AND 3D NUMERICAL MODELLING

Presentata da: Ing. VALENTINA FARGNOLI

Coordinatore Dottorato

Prof. Ing. Alberto LAMBERTI

Relatore

Prof. Ing. Daniela BOLDINI

Correlatore

Prof. Ing. Angelo AMOROSI

Esame finale anno 2015

Abstract

This work illustrates a soil-tunnel-structure interaction study performed by an integrated, geotechnical and structural, approach based on 3D finite-element analyses and validated against experimental observations. The study aims at analysing the response of reinforced concrete framed buildings on discrete foundations in interaction with metro-lines. It refers to the case of the twin tunnels of the Milan (Italy) metro-line 5, recently built in coarse-grained materials using EPB machines, for which subsidence measurements collected along ground and building sections during tunnelling were available. Settlements measured under free-field conditions are firstly back-interpreted using Gaussian empirical predictions. Then, the *in situ* measurements' analysis is extended to include the evolving response of a 9-storey reinforced concrete building while being undercrossed by the metro-line. In the finite-element study, the soil mechanical behaviour is described using an advanced constitutive model. This latter, when combined with a proper simulation of the excavation process, proves to realistically reproduce the subsidence profiles under free-field conditions and to capture the interaction phenomena occurring between the twin tunnels during the excavation. Furthermore, when the numerical model is extended to include the building, schematised in a detailed manner, the results are in good agreement with the monitoring data for different stages of the twin-tunnelling. Thus, they indirectly confirm the satisfactory performance of the adopted numerical approach which also allows a direct evaluation of the structural response as an outcome of the analysis. Further analyses are also carried out modelling the building with different levels of detail. The results highlight that, in this case, the simplified approach based on the equivalent plate schematisation is inadequate to capture the real tunnelling-induced displacement field.

The overall behaviour of the system proves to be mainly influenced by the buried portion of the building which plays an essential role in the interaction mechanism, due to its high stiffness.

Sommario

Questo lavoro illustra uno studio di interazione terreno-galleria-struttura messo a punto attraverso un approccio accoppiato, geotecnico e strutturale, basato su analisi tridimensionali agli elementi finiti e validato mediante il confronto con osservazioni sperimentali. Il principale obiettivo dello studio è l'analisi della risposta di edifici in cemento armato su fondazioni discrete in interazione con linee metropolitane. Questo studio si riferisce al caso delle due gallerie della linea 5 della metropolitana di Milano (Italia), costruita di recente in terreni a grana grossa mediante macchine di tipo EPB, per cui sono disponibili misure della subsidenza rilevate durante lo scavo, sia lungo sezioni sul terreno sia in corrispondenza di edifici situati lungo la tratta. I cedimenti misurati in condizioni di campo libero vengono prima interpretati mediante le classiche previsioni empiriche di tipo gaussiano. L'analisi delle misure in sito viene successivamente estesa ad analizzare la risposta di un edificio a nove piani in cemento armato sotto attraversato dalla linea metropolitana, che evolve durante lo scavo. Nello studio agli elementi finiti, la risposta meccanica del terreno è descritta mediante un modello costitutivo avanzato che, se associato ad una appropriata simulazione del processo di scavo, è in grado di riprodurre in modo realistico i profili di subsidenza di campo libero, nonché di cogliere la mutua interazione tra le due gallerie durante la costruzione della linea metropolitana. I risultati della simulazione condotta includendo nel modello numerico l'edificio schematizzato in dettaglio sono in buon accordo con i dati di monitoraggio per differenti fasi dello scavo. Ciò, dunque, conferma in modo indiretto la soddisfacente prestazione dell'approccio numerico adottato, consentendo, inoltre, una valutazione diretta della risposta strutturale come risultato dell'analisi. Ulteriori analisi numeriche eseguite con modelli semplificati dell'edificio mettono in luce che, in questo caso, l'approccio basato sul metodo della piastra equivalente è inadeguato a cogliere il reale campo di

spostamenti generato dallo scavo. La risposta globale del sistema, inoltre, risulta principalmente influenzata dalla porzione interrata dell'edificio che, data la sua elevata rigidezza, ha un ruolo essenziale nel meccanismo di interazione.

1. Introduction

1.1 Purpose of the study

The construction of new metro-lines in urban areas often requires tunnel excavation to be carried out in close proximity to residential buildings, cultural heritage monuments and underground services. The ability to correctly predict the tunnelling-induced settlements represents a key aspect to properly estimate potential damages on pre-existing structures and to design protective measures, when needed. It is widely recognised that the simplified approach for damage evaluation based on free-field subsidence profiles, thus disregarding the influence of the structure stiffness and weight, often leads to rather conservative solutions in terms of estimated differential settlements and, consequently, of damage intensity.

In the last few years two-dimensional (2D) approaches which incorporate the structure in the finite element analyses have been developed to overcome such limitations. However, in several cases, a detailed investigation of the soil-tunnel-structure interaction can only be performed by 3D numerical computations, which allow to account for any construction scheme, including the case of twin tunnels, and for any kind of surface structure and its relative position with respect to the tunnel axis.

Finite element simulations were mainly performed in the past with reference to masonry surface structures affected by tunnelling. Conversely, this class of interaction studies were more rarely carried out focusing on framed buildings, although being a structural typology widely diffuse in urban areas.

The reliability of the numerical approaches is strongly affected by different factors, such as the constitutive hypotheses for the soil, the correct simulation of the tunnel excavation sequence and the detail of the structural modelling.

This work proposes a coupled, geotechnical and structural, 3D finite element approach, performed by the code Plaxis 3D, aimed at investigating the soil-structure interaction during tunnelling, with specific reference to reinforced concrete framed buildings. It demonstrates the importance of a proper description of the soil mechanical behaviour, associated to a correct schematisation of the tunnel construction and to an appropriate structural modelling, to realistically simulate the response of the overall system to tunnelling.

The ability of the proposed procedure to effectively capture the soil-tunnel-structure interaction mechanism is validated against the available geotechnical and structural monitoring measurements from a real case-history, i.e. the recent construction of the two tunnels of the new Milan (Italy) metro-line 5 which, along its route, diagonally underpasses a multi-storey reinforced concrete framed structure dating back to the end of the 1950s.

1.2 Layout of the thesis

Chapter 2 presents a literature review on ground movements due to tunnel excavation with reference to free-field conditions and in presence of surface structures. The attention is given to closed-form empirical solutions for the prediction of tunnelling-induced subsidence as well as to 2D and 3D numerical approaches which allow a more accurate investigation of the soil-structure interaction. The methodology generally employed to assess the damage potentially caused by tunnel construction to surface buildings is also introduced and discussed.

Chapter 3 is focused on the case-history of the new metro-line 5 of Milan, excavated in coarse-grained soils partially below the water table by two earth pressure balance (EPB) machines that guaranteed low values of the surface volume loss. Settlement monitoring data collected under free-field conditions during and after the excavation of the twin

tunnels of the line are examined and back-interpreted using the classical Gaussian empirical curves. In addition, the influence of a few excavation parameters, in particular of the face and grouting pressures, on the final maximum settlement values is also evaluated and commented. The *in situ* measurement analysis is subsequently extended to explore the evolution of the structural response of the nine-storey framed building undercrossed by the metro-line as observed during different phases of tunnelling.

In Chapter 4 a preliminary study, carried out to validate the numerical tool with reference to the adopted soil constitutive formulation, the tunnel excavation procedure and the framed structure modelling, is presented and commented. The advanced soil constitutive model used in the finite element analyses, that is the *Hardening Soil model with small strain stiffness*, is described and calibrated based on the results of static and dynamic tests performed along and nearby the Milan metro-line route. In order to investigate the performance of the adopted constitutive hypothesis in this class of problems, a comparison of the computed subsidence troughs with the monitoring data is also proposed. The attention is then focused on the 3D numerical procedure defined for the simulation of the twin tunnel construction, validated against *in situ* measured settlements under free-field conditions. Finally, simple frame models subjected to different loading conditions are analysed by the codes Plaxis 3D and Sap 2000. This analysis is intended to assess the response of the structural elements schematised in the numerical code used in this study by comparing them with the results obtained by Sap 2000, a program widely used in the structural engineering practice.

Chapter 5 is devoted to the analysis of the interaction phenomena between the soil and multi-storey reinforced concrete framed structures during tunnelling. The study is firstly focused on 2, 4 and 8-storey ideal buildings with realistic geometry, stiffness and weight features, all of them being located in a symmetric position with respect to the

tunnel axis. The analysis aims at highlighting the modification of the free-field subsidence troughs, in the transversal and longitudinal directions to the tunnel, due to the presence of these buildings with different heights.

In the second part, the effects induced by the construction of the two metro-tunnels of the Milan line 5 on the real 9-storey framed building are analysed. The structure is first modelled in detail, taking into account its main structural components and also its secondary elements. Thus, the capabilities of the numerical model to correctly predict the response of the building to twin-tunnelling is evaluated by the comparison with measured settlements. The evolution of the building deformation modes during different phases of the excavation is also highlighted and commented. Then, additional numerical analyses with simplified building models are also carried out to clarify the role of different structural components on the behaviour of the whole system. They include the equivalent plate schematisation and a model only constituted by the buried portion of the building, whose upper portion was reduced to an equivalent load distribution. Finally, the results obtained adopting different levels of details in the modelling of the building are analysed and compared.

Concluding remarks are summarised in Chapter 6.

2. Tunnelling-induced movements on the ground under free-field conditions and on existing structures: state of the art

2.1 Purpose of Chapter 2

This chapter presents a literature review of methods used to predict tunnelling-induced settlements under free-field conditions (i.e. no structures on the ground surface) and in presence of existing buildings in interaction with the excavation.

In the first case, closed-form empirical solutions represent a well-established and effective tool to realistically predict the subsidence caused by the tunnel construction. Conversely, as the interaction with surface structures occurs, such expressions describe the worst scenario as they are often associated to the most cautious estimation of the structural damage.

In this case, a numerical approach can represent a valuable tool to accurately investigate the interaction phenomena and to likely estimate the potential damage due to tunnelling.

The success of such methods in practical applications strongly depends on many different variables, including the adopted soil constitutive model, the schematisation of the tunnel construction process and the accuracy to represent the essential features of the existing structures located nearby the metro-line works.

In several cases the main aspects of the soil-structure interaction problem can be investigated in detail only adopting a numerical approach based on a 3D discretisation.

2.2 Ground movements due to tunnelling under free-field conditions

2.2.1 Surface settlements: transversal and longitudinal empirical profiles

Tunnel construction is inevitably associated to ground movements which result in a surface settlement trough developing above and ahead of the tunnel (Fig. 2.1). They are

the result of different displacements occurring near the tunnel as shown in Figure 2.2 and presented in the following:

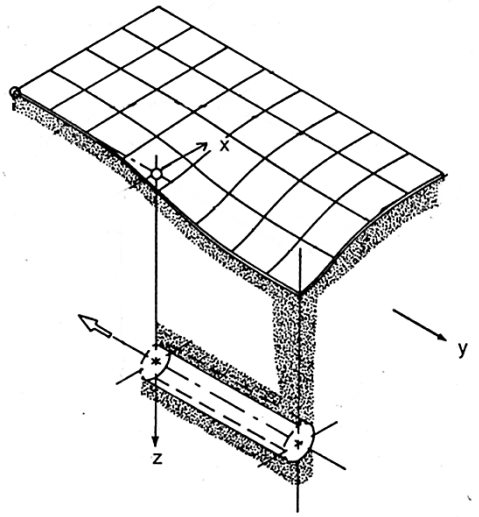

Figure 2.1. 3D settlement profile under free-field conditions (modified from Attewell et al., 1986).

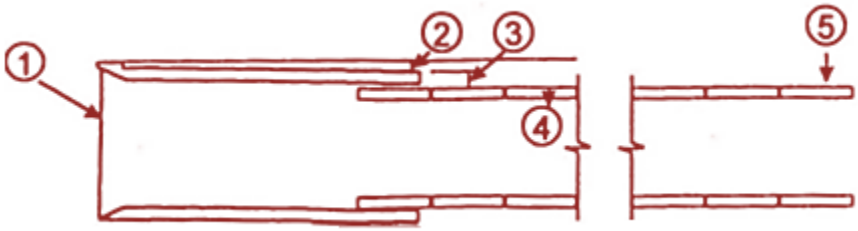

Figure 2.2. Main components of ground movements due to shield tunnelling (modified from Cording, 1991).

- *component 1*: face extrusion, i.e. ground displacement at the tunnel face resulting from the stress relief associated to the excavation. This latter can be minimised by applying a support pressure using slurry-shield or earth pressure balance (EPB) machines;

- *component 2*: displacement due to the shield passage. It depends on the amount of over-excavation and it is related to the shield geometry (e.g. cutting bead thickness, conicity) combined with the tendency of the machine, more marked in steering phases, to plough or yaw;

- *component 3*: loss due to the tail void, i.e. the existence of a gap between the tail of the shield and the lining which allows further radial ground movements that can be reduced by the immediate application of grouting injections;

- *component 4*: lining deflection as the ground loading develops, generally smaller than the other components if the lining is stiff enough;

- *component 5*: displacements due to the consolidation process in fine-grained soils.

The topic of ground movements associated with bored tunnel construction was extensively investigated in the past by several authors and many contributions were proposed in the literature on this theme for clays (e.g. Peck, 1969; Cording and Hansmire, 1975; Mair, 1979; Clough and Schmidt, 1981; Ward and Pender, 1981; O'Reilly and New, 1982; Attewell et al., 1986; Rankin, 1988; Grant and Taylor, 2000; Loganathan et al., 1998) and for coarse-grained soils (e.g. Potts, 1976; Atkinson and Potts, 1977; Kutter et al., 1994; Moh et al., 1996; Nomoto et al., 1995; Ata, 1996; Celestino et al., 2000; Jacobsz, 2002; Vorster, 2005; Marshall et al., 2012).

Field observations (Peck, 1969; Schmidt, 1969), collected from many case histories over the years, provided a description of the free-field settlement profile. At a sufficient distance from the tunnel face, the settlement profile in a section perpendicular to the tunnel axis (Fig. 2.3 *a*) can be expressed by a Gaussian distribution curve (Peck, 1969) having the following equation:

$$S_v(x) = S_{v,max}\, exp\left(-\frac{x^2}{2i_x^2}\right) \tag{2.1}$$

where:

$S_{v,max}$ is the maximum settlement on the tunnel centre line;

x is the horizontal distance from the centre line;

i_x is the horizontal distance of the inflection point of the settlement trough from the tunnel centre line.

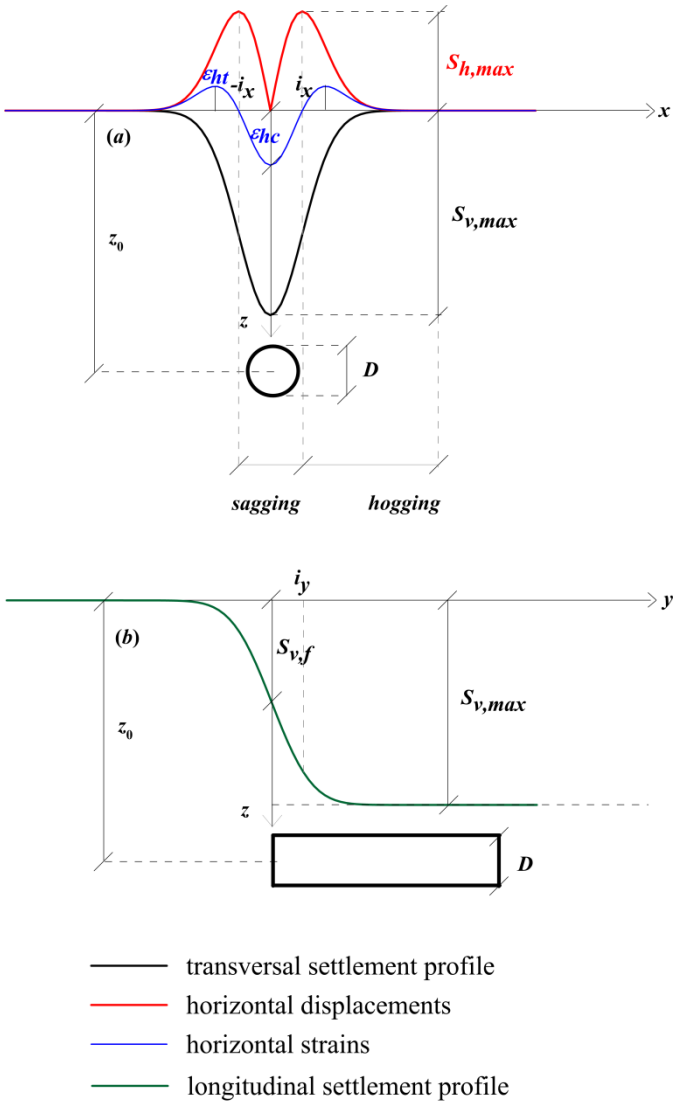

Figure 2.3. Transversal profiles of settlements, horizontal displacements and strains at the ground surface (*a*); longitudinal surface settlement profile (*b*).

The volume of the surface settlement trough per meter length of tunnel, V_S, can be evaluated by integrating Equation (2.1) along the distance x to give:

$$V_S = \int_{-\infty}^{+\infty} S_v(x)\,dx = \sqrt{2\pi}\, i_x\, S_{v,max} \tag{2.2}$$

The amount of volume lost in the region close to the tunnel, due to one or more of the displacement components 1-4 of Figure 2.2, is generally indicated as V_T. When tunnelling in coarse-grained soils $V_T \neq V_S$; in dense sands, for example, V_S is less than V_T due to dilation (Cording and Hansmire, 1975). When tunnelling in clays $V_T = V_S$, as ground movements occur at constant volume (i.e. in undrained conditions).

Of particular importance is the volume loss parameter, V_L, defined as:

$$V_L = \frac{V_S}{A_t} 100\% \tag{2.3}$$

where A_t is the nominal area of the tunnel section equal to $\pi D^2/4$ (D is the tunnel diameter).

In many real cases the volume loss is a design parameter and its value is estimated on the basis of excavation method, technological details of the tunnel boring machine (TBM) and previous tunnelling experiences in similar geotechnical conditions. As reported in Mair (1996), for open face tunnelling in stiff clays (e.g. London clay) the volume loss values are generally included between 1% and 2%; for closed face tunnelling, using earth pressure balance or slurry shields, a high degree of settlement control can be achieved, particularly in sands where the volume loss is often as low as 0.5% and even in soft clays where, excluding the consolidation settlements, it is of only 1%-2%.

The settlement distribution can be expressed as a function of V_L:

$$S_v(x) = \sqrt{\frac{\pi}{2}} \frac{V_L D^2}{4 i_x} e^{-\frac{x^2}{2 i_x^2}} \tag{2.4}$$

O'Reilly and New (1982), in a survey of the UK tunnelling monitoring data, shown that the point of inflection i_x results approximately to be a linear function of the depth of the

tunnel centre line, z_0, and they proposed the following simple relationship, also confirmed by other authors (Rankine, 1988; Lake et al., 1992):

$$i_x = K\, z_0 \tag{2.5}$$

where K is a constant depending solely on soil nature.

Field data collected all over the world during metro-line constructions, including shield tunnelling, indicated that K varies between 0.2 and 0.45 for sands and gravels, between 0.4 and 0.6 for stiff clayey soils and between 0.6 and 0.75 for soft clays (Mair and Taylor, 1997), regardless of the tunnel size and tunnelling method.

The settlement value in correspondence of $x = \pm\, i_x$ is about 0.6 $S_{v,max}$ and it is generally accepted that the extension of the surface subsidence basin is equal to about 6 i_x (Rankine, 1988).

The inflection point divides the central part of the Gaussian curve having upwards concavity (*sagging zone*) from the outer parts having downwards concavity (*hogging zone*) (Fig. 2.3 *a*): this aspect plays a key role in the tunnelling-induced potential damage on existing buildings, as discussed in the following.

As proposed by Clough and Schmidt (1981), the point of inflection i_x can be also influenced by the tunnel diameter. On the basis of past field data (Mair and Taylor, 1997), centrifuge data (Mair, 1979 for clays; Imamura et al., 1998 for sands and gravels) and monitoring results, Sugiyama et al. (1999) derived the following relationships between i_x /(D/2) and the cover to diameter ratio C/D for clays (Eq. 2.6) and for sands and gravels (Eq. 2.7):

$$\left(\frac{i_x}{D/2}\right) = 1.5\left(\frac{C}{D}\right)^{0.8} \tag{2.6}$$

$$\left(\frac{i_x}{D/2}\right)=\left(\frac{C}{D}\right)^{0.7} \tag{2.7}$$

The same Authors pointed out that the data can be reasonably approximated by the above equations, although a larger scatter is observed for sands and gravels as compared to the clayey soils.

Other studies on coarse-grained soils shown that i_x decreases with the increase in the volume loss (Hergarden et al., 1996; Jacobsz, 2002; Vorster, 2005; Marshall et al., 2012) due to the formation of a "chimney" mechanism (Cording, 1991), this latter also causing the i_x reduction with depth (Marshall et al., 2012). It was also observed that the parameter i_x reduces as the ratio C/D decreases (Marshall et al., 2012). In addition, it was also noted that the Gaussian curve does not always provide a good fit to settlement trough data in large-permeability soils (Celestino et al., 2000; Jacobsz et al., 2004; Vorster et al., 2005), in particular in proximity to the tunnel depth (Marshall et al., 2012).

New and O'Reilly (1991) suggested the following extension of Equation (2.5) for tunnels constructed in layered strata of both clay and coarse-grained soils:

$$i_x = \sum_{i=1}^{n} K_i z_i \tag{2.8}$$

where n indicates the number of the strata, K_i and z_i the trough with factor and the thickness of each layer, respectively.

The longitudinal settlement profile (Fig. 2.3 *b*) results to be well described by a cumulative Gaussian probability curve (Attewell and Woodman, 1982) with the following expression:

$$S_v(y)_{x=0} = S_{v,max}\Phi\left(\frac{y}{i_y}\right) \tag{2.9}$$

where $\Phi(y/i_y)$ is the cumulative probability function, defined as:

$$\Phi\left(\frac{y}{i_y}\right) = \frac{1}{i_y\sqrt{2\pi}}\int_{-\infty}^{y} exp\left(-\frac{y^2}{2i_y^2}\right)dy \tag{2.10}$$

The inflection distance of the longitudinal settlement trough, i_y, (Fig. 2.3 *b*) is often assumed to be equal to i_x (Attewell and Woodman, 1982).

Equation (2.9) is plotted in Figure 2.3 (*b*): it shows, in particular, that at $y = 0$ the tunnel face $S_{v,f}$ is equal to 0.5 $S_{v,max}$.

By examining a number of real case-histories (e.g. Mair and Taylor, 1997) it was observed that $S_{v,f} = 0.5\ S_{v,max}$ is valid only for tunnels constructed in stiff clays without face support, while in soft clays with face support or in coarse-grained soils (e.g. Moh et al., 1996; Nomoto et al., 1995; Ata, 1996) $S_{v,f}$ is generally less than 0.5 $S_{v,max}$, e.g. 0.25-0.40 $S_{v,max}$.

2.2.2 Subsurface settlements

It is often assumed that also the shape of the subsurface settlements can be reasonably approximated by a Gaussian distribution as at the ground surface. At a generic depth *z* below the ground surface, i_x parameter can be at first expressed by adapting Equation (2.5) (O'Reilly and New, 1982):

$$i_x = K(z_0 - z) \tag{2.11}$$

where *K* is the above defined settlement trough width factor.

However, filed measurements and centrifuge test results available in the literature for tunnels in clay (e.g. Mair et al., 1993) indicated that K parameter increases with depth, giving proportionally wider settlement profiles closer to the tunnel.

Mair et al. (1993) proposed the following expression, valid for tunnels in clay with $K = 0.5$ at the surface, which gives a linear trend of i_x parameter with depth:

$$i_x(z) = \left[0.175 + 0.325\left(1 - z / z_0\right)\right] z_0 \tag{2.12}$$

From similar observations of subsurface settlements for tunnels in silty sands below the water table, Moh et al. (1996) suggested this new relationship resulting in a non-linear trend of i_x parameter:

$$i_x(z) = bD\left(\frac{z_0 - z}{D}\right)^m \tag{2.13}$$

where b is a constant that can be deduced by equating Equations (2.13) and (2.5) at $z = 0$, while m parameter depends on the reference soils. A value of $m = 0.4$ was found to fit the data for sandy soils, while $m = 0.8$ appeared to be more appropriate for clayey soils.

2.2.3 Horizontal displacements and strains

Horizontal displacements are generally evaluated starting from the settlement profile and on the basis of assumptions concerning the direction of the displacement vectors. This allows the determination of the horizontal displacements at any point from the settlement value at the same point using simple geometrical considerations. For tunnels in clay in plane strain conditions and at constant volume, Attewell (1978) and O'Reilly and New (1982) proposed that, at a generic depth z, the surface ground displacement vectors are directed towards the tunnel axis, leading to the following simple relation:

$$S_h(x,z) = \frac{x}{z_0 - z} S_v(x,z) \tag{2.14}$$

Equation (2.14) at the ground surface can be expressed as:

$$S_h(x) \cong 1.65 \frac{x}{i_x} S_{h,\max} \exp\left(-\frac{x^2}{2i_x^2} \right) \tag{2.15}$$

The theoretical maximum horizontal displacement, $S_{h,max}$, occurs at the point of inflexion of the settlement trough (Fig. 2.3 *a*) and it is equal to 0.61 K $S_{v,max}$. This is only true in undrained conditions and if K parameter is constant with depth.

The horizontal displacements are considered positive as directed towards the tunnel axis.

Taylor (1995) shown that, for constant volume conditions, displacement vectors must be directed towards a point located at a depth equal to $0.175z_0/0.325$ below the tunnel axis and this results in a 35% reduction in surface horizontal displacements respect to those obtained using Equation (2.14).

Attewell and Yeates (1984) introduced a parameter, n, to be applied to the numerator of Equation (2.14) in order to take into account the variation in the focal point of the displacement vectors to a point above or below the tunnel axis along the tunnel centre line. They proposed values of n equal to 1 for clayey soils (undrained behaviour, i.e. displacement vectors directed towards the tunnel centre line) and less than 1 for coarse-grained soils (displacement vectors directed towards a point below the tunnel centre line). This latter condition implies that in coarse-grained soils the displacement vectors are increasingly vertical with depth and, as a consequence, the horizontal displacements are less than those observed in clays.

The horizontal strain distribution in the transversal direction to tunnel (Fig. 2.3 *a*) can be obtained by derivation of Equation (2.14):

$$\varepsilon_h(x,z) = \frac{S_v(x)}{z_0 - z}\left(\frac{x^2}{i_x^2} - 1\right) \tag{2.16}$$

where tensile strains are positive. In Figure 2.3 (*a*) the maximum values of the horizontal strains (compressive, ε_{hc}, or tensile, ε_{ht}) are also highlighted.

Assuming that the displacement vectors point towards the centre of the excavation face, the horizontal component at the surface along the tunnel centre line in the longitudinal direction can be expressed as:

$$S_h(y) = \frac{V_L D^2}{8 z_0}\exp\left(-\frac{y^2}{2 i_y^2}\right) \tag{2.17}$$

and the horizontal strains, being tensile ahead of the tunnel face and compressive behind it, can be obtained by derivation of Equation (2.17):

$$\varepsilon_h(y) = -y\frac{V_L D^2}{8 i_y^2 z_0}\exp\left(-\frac{y^2}{2 i_y^2}\right) \tag{2.18}$$

2.2.4 Settlements due to twin tunnels

Many tunnelling projects in urban environments require the construction of twin tunnels running side-by-side (e.g.: Bartlett and Bubbers, 1970; Cording and Hansmire 1975; Harris et al., 1996) or one above the other (e.g.: Higgins et al., 1996; Shirlaw et al., 1988).

New and O'Reilly (1991) extended the use of semi-empirical equations for predicting the movements above a single tunnel to the case of twin tunnels, providing the following expression:

$$S_v(x) = \left[S_{v,max}\, exp\left(-\frac{x^2}{2 i_x^2}\right)\right]^{(I)} + \left[S_{v,max}\, exp\left(\frac{(x-d)^2}{2 i_x^2}\right)\right]^{(II)} \tag{2.19}$$

where d is the axis-to-axis tunnel horizontal distance.

Equation (2.19) is obtained by the sum of two identical Gaussian curves due to the construction of two independent single tunnels, indicated by the apex (I) and (II). In the original formulation proposed by New and O'Reilly (1991) this expression, referring to two identical tunnels, characterised by the same diameters, depths and volume loss, does not take into account the asymmetry of the settlement profile (Fig. 2.4) shown by the available field data and physical modelling (e.g.: Cording and Hansmire, 1975; Barratt and Tyler, 1976; Perez Saiz et al., 1981; Lo et al., 1987; Shirlaw et al., 1988; Standing et al., 1996; Cooper et al., 2002; Chapman et al., 2007). The observed asymmetry in the settlement profile is generally related to the fact that tunnels are rarely driven simultaneously (e.g. Standing et al., 1996). As suggested by Cording and Hansmire (1975), on one side the ground in the region where the second tunnel has to be constructed has already experienced appreciable strains associated to the excavation of the first tunnel and this reduces its stiffness (Mair and Taylor, 1997), on the other side the excavation of the second tunnel may produce an increase in settlement in correspondence with the first one due to interaction effects. These latter mainly occur when tunnels are very closed spaced and, as expected, they increase as the axis-to-axis tunnel distance decreases (Cording and Hansmire, 1975; Addenbrooke and Potts, 2001; Cooper et al., 2002). In order to account for the typical asymmetry in the subsidence profile observed in the literature, Addenbrooke (1996) suggested to adopt in Equation (2.19) different values of $S_{v,max}$ and i_x for the two tunnels.

Hunt et al. (2005), on the basis of an extensive program of two-dimensional finite element analyses, demonstrated the potential inaccuracy of the Gaussian curve method in the case of settlements induced in clay by multiple tunnels and they proposed a new approach aimed at improving the subsidence empirical prediction.

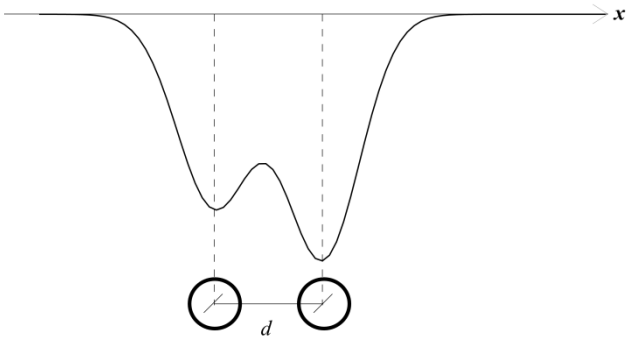

Figure 2.4. Asymmetric transversal profile induced by twin tunnel excavation.

The method is based on modifying the ground vertical displacements above the second tunnel in a zone, named overlapping zone, where the soil is assumed to be previously disturbed (Fig. 2.5).

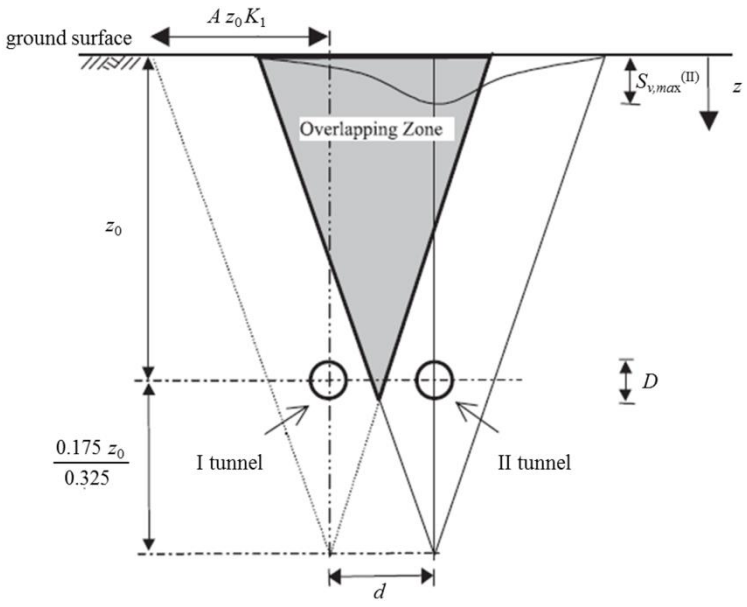

Figure 2.5. Modification factor method for calculating settlements above the second tunnel in clay (modified from Hunt, 2005).

The modified settlement profile, $S_{v,mod}^{(II)}(x)$, for the second tunnel can be determined by applying Equation (2.20) in the overlapping zone to the settlement distribution above the second tunnel, $S_v^{(II)}(x)$, expressed by Equation (2.1):

$$S_{v,mod}^{(II)}(x) = FS_v^{(II)}(x) \tag{2.20}$$

where the modification function, *F*, applicable for surface and subsurface settlements, is defined by Equation (2.21):

$$F = \left\{1 + \left[M\left(1 - \frac{|d+x|}{AK_1(z_0 - z)}\right)\right]\right\} \tag{2.21}$$

In Equation (2.21) *A* is a multiple of the trough width parameters (i.e. *K*) usually taken as 2.5. or 3.0 in half a settlement profile on the side of the first excavation, K_1 is the value of *K* parameter for the first tunnel and *M* is the value of the maximum modification assumed always acting in correspondence with the first tunnel axis. *M* parameter represents the maximum percentage of increase in settlement above the first tunnel and it is generally included between 0.6 and 1.5.

Chapman et al. (2007) applied the method to the results obtained from a series of small-scale (1/50) laboratory model tests (conducted at 1*g*) carried out in Speswhite kaolin clay to investigate the short term ground movements above twin tunnels. The Authors demonstrated that the modified approach produces an improvement of the subsidence prediction as compared to the traditional method based on the simple sum of individual Gaussian curves.

2.3 Soil-structure interaction related to tunnelling: experimental observations and numerical modelling

The displacement field generated by the tunnel excavation propagates up to the ground surface, activating interaction phenomena with existing buildings located in the area of the subsidence basin. The buildings in the proximity of the tunnel axis tend to assume a

deformed configuration with a upwards concavity (*sagging*), while those farther away from it, outside of the inflection point i_x, tend to assume a deformed configuration with a downwards concavity (*hogging*), as shown in Figure 2.6.

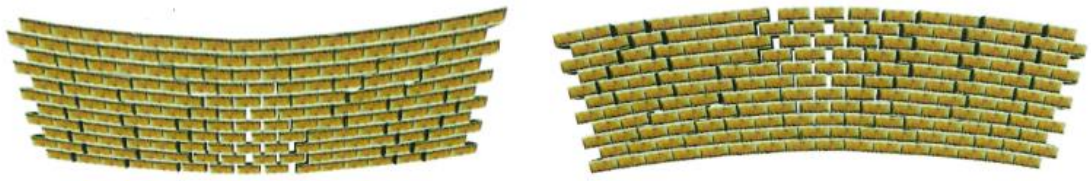

sagging *hogging*

Figure 2.6. Sagging and hogging deformation modes (Burghignoli, 2011).

Buildings undergoing hogging phenomena generally reveal more appreciable resentments than those experiencing a sagging deformation. In this latter case, in fact, the soil and the foundation system provide a constraint on the structure tending to limit the settlement effects in its lower portion. Conversely, when a hogging phenomenon occurs, settlements may induce larger effects in the upper portion of the structures, i.e. where the constructions are more prone to deform.

The building deformation parameters (Burland and Wroth, 1974), widely accepted in the literature and commonly used in soil-structure interaction studies, are shown in Figure 2.7 considering the maximum settlement at the foundation level of four points (i.e. A, B, C and D) and they are listed in Table 2.1.

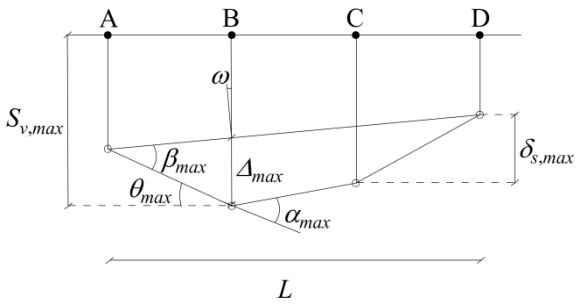

Figure 2.7. Definition of building deformation parameters.

Parameter	Name and Description
$S_{v,max}$	maximum absolute settlement
$\delta_{s,max}$	maximum differential (or relative) settlement
θ_{max}	maximum slope (or rotation): maximum change in gradient of a line joining two reference points, i.e. the ratio of their differential settlement and their distance
α_{max}	angular strain: algebraic difference of slopes of two consecutive segments
Δ_{max}	maximum relative deflection: maximum displacement of a point relative to the line connecting two reference points on either side
$(\Delta/L)_{max}$	maximum deflection ratio, where L is the distance between the two reference points defining Δ_{max}
ω	rigid body rotation of the whole structure
β_{max}	maximum value of the angular distortion: difference between θ_{max} and ω

Table 2.1. Structural deformation parameters.

2.3.1 Experimental observations

The conventional approach to evaluate possible tunnelling-induced damage, currently in use for a preliminary assessment of building performance, is based on the empirical prediction of the subsidence curve under free-field conditions (Peck, 1969; O'Reilly and New, 1982), neglecting any effect due to the presence of surface structures on the displacement field. The constructions resting on the ground, in fact, may modify the shape of the subsidence profile due to their stiffness and weight, generally reducing the differential settlement.

Breth and Chambosse (1974) shown field data for reinforced concrete framed buildings undercrossed by twin tunnel excavation in Frankfurt Clay, highlighting that they exhibit a different response: the structure deforming in sagging shows a more flexible behaviour with respect to that undergoing hogging.

Viggiani and Standing (2002) analysed settlements induced by the construction of the Jubilee Line Extension tunnels in London Clay, comparing the measurements recorded at the Treasury Building with those obtained in a nearby free-field section. The differential settlements under the structure result significantly smaller than the free-field ones, due to the building stiffness. Absolute settlements of the structure are smaller than

those measured at the ground in the sagging zone, while they are slightly larger in the hogging portion of the subsidence profile.

Mair (2003) presented measurements of settlements recorded in correspondence with an ordinary masonry building, named Neptune House, in interaction with the construction of twin tunnels, in order to highlight the stiffer response of the structure in the sagging zone. This experimental evidence confirms what observed by Burland et al. (1977) regarding the more flexible response of masonry buildings that experiment hogging deformation and what discussed by Son and Cording (2005), referring to the experimental results of scale model tests of masonry façades adjacent to deep excavations.

Dimmock and Mair (2008) analysed the settlement response of 2 and 3-storey masonry structures founded on shallow strip foundations. The observed settlement profiles of the Moodkee Street and Keetons Estate buildings, when compared to the equivalent free-field ones, reveal that these structures display close to fully flexible behaviour in hogging, but they are semi-flexible in sagging. The horizontal strains measured at the base of the building façades are negligible, indicating the high axial stiffness of these masonry buildings.

Many other Authors (e.g. Cording and Hansmire, 1975; Geddes and Kennedy, 1985; Boscardin and Cording, 1989; Viggiani and Standing, 2001; Withers, 2001; Mair, 2003) analysed the response of buildings resting on continuous foundations in interaction with tunnel excavations, concluding that such structures are interested by very small horizontal deformations with respect to what observed under free-field conditions.

Goh and Mair (2010) presented a case-history on the settlement response of two reinforced concrete framed buildings above the bored tunnelling works for a section of the Singapore Circle Line, showing that the framed building stiffness can influence their

response to excavation. The Authors proposed a method to quantify this influence based on the definition of a factor (named column stiffening factor) which puts in relation the bending stiffness of a framed building to that of a simple beam for which the deflection ratio can be estimated following the approach presented by Potts and Addenbrooke (1997) and discussed in the next Section 2.3.2.3.

Referring to the same case-study, Goh and Mair (2011) shown that the horizontal strains are significantly reduced for most buildings on continuous footings, while for structures on individual footings the horizontal strain values correspond to those under free-field conditions. The Authors illustrated the difference in horizontal strains between columns that are connected by ground beams and columns that are unconnected at ground level, but connected at first floor upwards. Using a combination of simplified structural analysis and finite element models, a design guidance was proposed to estimate excavation-induced horizontal strains in framed buildings on individual footings.

Farrell et al. (2011) analysed the response of 2 and 5-storey commercial masonry buildings with reinforced concrete floor slabs founded on strip footings and located in proximity to the excavation of a tunnel having a diameter equal to 12 m. The 5-storey building is characterised by larger vertical displacements when compared to the ground settlements recorded at a nearby control section, due to its stiffness and weight, while the 2-storey structure exhibits a more flexible response, deforming according to the free-field subsidence profile.

2.3.2 Numerical modelling

The use of two-dimensional (2D) and three-dimensional (3D) numerical approaches, developed in the last few years and nowadays common, allows a more realistic analysis of the soil-tunnel-structure interaction process. However, the success of such methods (finite-element or finite-difference methods) in practical application strongly depends

on different factors, including the constitutive hypotheses adopted for the soil, the 2D or 3D schematisation of the tunnel excavation sequence and the detail in modelling the structures in interaction with the tunnel.

2.3.2.1 Soil constitutive models

It is widely recognised that soil exhibits much higher stiffness at very small strains (e.g. strains $\leq 1 \times 10^{-6}$) than that measured in traditional laboratory tests on soil specimens. As the strain increases, the soil stiffness decays non-linearly and this feature, represented by the characteristic S-shaped stiffness reduction curve (e.g. Vucetic and Dobry, 1991), is incorporated into some constitutive models of soil behaviour proposed in the literature.

The first small-strain models for static applications were introduced by Mroz et al. (1981) and Burland et al. (1979) that used kinematic yield surfaces in the stress space and in the strain space, respectively.

Parallel to these models with kinematic surfaces, a different approach was proposed by Jardine et al. (1985, 1986) that, by fitting the strain-stiffness curves, directly calculate the soil stiffness as a mathematical function of the applied strain.

Al-Tabbaa (1987) presented the innovative idea of a very small inner yield surface, named bubble, and Al-Tabbaa and Wood (1989) published the two-surface bubble model as an extension of the Cam Clay model. Stallebrass (1990) introduced an additional history surface for the bubble extension within the Cam Clay framework. Then, a three-surface kinematic hardening model (3-SKH), able to simulate the non-linearity and the effect of recent stress history, was developed by Stallebrass and Taylor (1997).

Advanced mathematical descriptions of the strain-stiffness curve following the approach by Jardine et al. (1986) were proposed by Gunn (1993) and Tatsuoka (2000).

During the last few years, kinematic hardening models were further extended to take into account the effect of structure in natural soils (e.g. Rouainia and Muir Wood, 2000; Kavvadas and Amorosi, 2000; Baudet and Stallebrass, 2004). Grammatikopoulou et al. (2006) presented two new kinematic hardening models, which modify the pre-existing two-surface (Al-Tabba and Wood, 1989) and three-surface (Stallebrass and Taylor, 1997) models. The novelty consists in a hardening modulus resulting in a smooth elasto-plastic transition and in a realistic stiffness degradation curves.

A kinematic-hardening structured soil model incorporating structure and stiffness degradation was presented by Gonzalez et al. (2012) and used in numerical analyses performed to simulate the undrained excavation of a tunnel in London Clay. The work highlights as the choice of a representative small-strain stiffness value in the model calibration requires a considerable amount of engineering judgment.

Benz (2007) proposed an isotropic-hardening elasto-plastic constitutive model, named *Hardening Soil model with small-strain stiffness* (HSsmall), that represents an extension of the *Hardening Soil Model* (HS) previously developed by Shanz et al. (1999) and which is capable of taking into account the very high soil stiffness at very low strain levels, its variation with the strain level and the early accumulation of plastic deformations.

2.3.2.2 Tunnelling process: 2D and 3D numerical simulations

2D numerical simulation

Tunnelling process is characterised by a three-dimensional nature and this peculiarity has to be taken into account when the excavation is simulated by two-dimensional numerical analyses frequently adopted in engineering practice, assuming plane strain conditions.

Swoboda et al. (1979) proposed to simulate the excavation process by reducing the soil stiffness inside the tunnel. Panet and Guenot (1982) described the ground behaviour during the excavation and proposed a method based on the ground reaction curve (Fig. 2.8) which puts in relation the radial stress (σ_r) acting at the tunnel boundary with the corresponding radial displacement. In particular, as a degree of unloading inside the tunnel is allowed, it deforms inducing a volume loss.

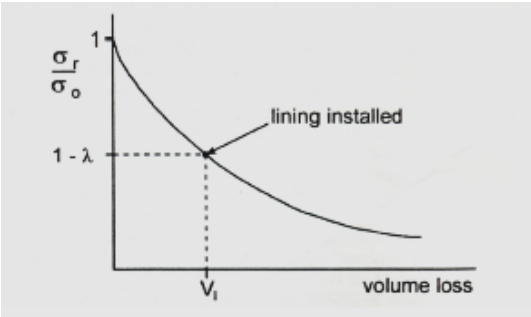

Figure 2.8. Ground reaction curve (modified from Panet and Guenot, 1982).

At a certain distance ahead the tunnel, the stress level around the cavity is not influenced by the excavation and it is equal to the original one (σ_0). Behind the tunnel, in the zone where the cavity is able to self-sustain, the stress level around the cavity is equal to zero. In between these two locations, the radial stress around the cavity (σ_r) varies between σ_0 and 0, i.e. $\sigma_r = (1-\lambda)\sigma_0$. The parameter λ is equal to 0 when $\sigma_r = \sigma_0$ and it is equal to 1 when $\sigma_r = 0$.

The ground reaction curve allows to calculate an amount of radial deformation for a given release of the original radial stress indicated as $\lambda\sigma_0$. In this way a certain volume loss can be achieved by installing a lining behind the tunnel face which supports the cavity by a pressure $p = (1-\lambda)\sigma_0$.

In the method of Panet and Guenot (1982), at the beginning of the excavation stage $\lambda = 0$; the soil elements inside the tunnel boundary are instantaneously removed, λ is

incrementally increased up to a given value and, at this point, the lining is activated. Then, λ is further increased until to 1 at the end of excavation.

In the gap method of Rowe et al. (1983) a predefined vertical distance, called "gap" parameter, is imposed in the finite element mesh between the tunnel profile and the lining to represent the expected volume loss.

In the method presented by Vermeer and Brinkgreve (1993) the volume loss is simulated by applying a contraction to the lining: in the first phase of the numerical procedure, the soil is removed and the lining installed at the same time, while in the second one a contraction is imposed to the lining in order to obtained a reference value of V_L.

In the volume loss control method proposed by Addenbrooke et al. (1997) the tunnel excavation is modelled in *n* increments. The volume loss value is evaluated at each step and the lining elements are activated when the desired V_L is obtained.

It was also shown by the same Authors that for soils characterised by a coefficient of earth pressure at rest $K_0 > 1$ the computed settlement profiles are wider than real observations and empirical predictions for the same values of the volume loss. Referring to the case of overconsolidated clays (i.e. London Clay), they proposed an improvement of the settlement numerical prediction by fictitiously altering the soil parameters and introducing an unrealistically low anisotropy ratio G_{vh}/E'_v, these latter being the shear stiffness and Young's moduli in the vertical direction, respectively. An alternative approach used by the same Authors consists in introducing a fictitious zone of reduced K_0 around the tunnel before simulating the excavation process.

An extension of the method proposed by Rowe et al. (1983) was presented by Tamagnini et al. (2005). It includes an ovalisation of the tunnel profile which provides a good agreement among numerical predictions, empirical relations and measurements.

A numerical schematisation of tunnelling inspired by the methods of Panet and Guenot (1982) and Addenbrooke (1997) was proposed by Altamura et al. (2007). In this procedure, the vertical and horizontal component of initial equilibrium nodal forces are independently released on the tunnel boundary until an adequate vertical to horizontal release ratio, calibrated for the single case, is found.

The computed settlement profiles result in good agreement with the empirical curves calculated for the same volume loss using realistic values of *K* parameter.

In the method proposed by Moller and Vermeer (2008), settlements are controlled by the simulation of the grouting action in the void between the lining and the soil.

3D numerical simulation

In several cases, the main aspects of the interaction between tunnels and existing buildings can be investigated only by adopting a numerical approach based on a 3D discretisation, which allows to capture the real geometry of the abovementioned soil-structure interaction problem. In this context, the correct 3D schematisation of all the excavation, support and lining sequences plays a key role for a realistic prediction of the subsidence phenomena.

In the past, the first 3D numerical simulations of tunnelling process were drastically simplified. Augarde et al. (1999) and Burd et al. (2000) proposed the simultaneous excavation method: tunnel excavation is simulated in a single step by removing the soil elements inside the tunnel boundary up to the desired face position and by simultaneously installing the lining over the whole excavated length. Subsequently, a uniform contraction is applied to the lining along the whole length. This method overcomes the geometry limitations of 2D analyses, but it simulates only in part the excavation sequence as a 3D process. It produces settlement trough widths larger than those predicted by the empirical equation for the same volume loss values.

Several Authors (e.g. Tang et al., 2000; Franzius, 2003; Franzius and Potts, 2005; Möller, 2006) used a step-by-step method to simulate the excavation process. In general, it consists in removing at each calculation step the soil elements inside the excavation profile over a length, indicated as L_{exc}, ahead of the tunnel face and in activating the lining at a certain distance behind the face, this latter being supported by a pressure acting on it. In some cases a support pressure, or a displacement field, may be also applied to the unsupported soil between the lining and the excavation face.

In a more recent version of this method available in the literature (Rampello et al., 2012), the tunnel cavity is lined by the shield or by the permanent lining, with the exception of the tunnel face, where a support pressure equal to the total horizontal stress at rest is applied, and of an intermediate 4 m long zone, where the displacements are forced. The shield extends for a total length of 8 m and the permanent lining is installed behind the shield. Tunnelling is modelled in discrete steps by removing a 2 m long slice of soil and advancing the support pressure, the shield and the lining by the same length.

Values of the maximum displacement, δ, imposed at the tunnel crown are determined by trial and error to meet the requirement that the design volume loss is achieved after the completion of the tunnel. The settlement troughs computed at the surface by the numerical analyses performed using the above described tunnelling sequence, in general, compare well with those given by the empirical procedure, both in terms of maximum settlement and width of the subsidence basin.

Examples of very realistic shield tunnelling simulation, capable of reproducing and explicitly modelling many details of the process (e.g. shield geometry, magnitude and distribution of the face support pressure, hydraulic jack thrust, volume and pressure of the grouting injections, etc.), were proposed in the literature (e.g. Komiya et al., 1999; Kasper and Meschke 2004, 2006 *a*, 2006 *b*). In some cases it emerges that such

complex simulations may give realistic results when combined with advanced constitutive hypotheses adopted for the soil.

Further research works (e.g. Melis et al., 2002; Migliazza et al., 2009; Lambrughi et al., 2012) compared numerical analyses with recorded data and explored the role of different shield-tunneling parameters on the surface settlements and stresses developed on the final lining. An extension of these methods to a full interaction of the TBM-EPB process was presented by Comodromos et al. (2014). In this case, the excavation process was simulated by a step-by-step procedure and the face support pressure, the tunnel lining, the tail gap grouting, the shield and the over-excavation were modelled in the numerical scheme. The influence of almost all relevant components of shield tunnelling was assessed by a parametric study and the sensitivity of the process to variations of the face support, of the pressure applied to the steering gap slurry and of the tail gap grouting was examined. It was found that the tunnel face pressure has the most influence on the surface settlements, while the steering and tail gap pressures affect the ground movements in a non-relevant way.

2.3.2.3 Numerical analysis of the interaction between structures and tunnels: 2D and 3D approaches

Numerical methods represent an attractive solution for the evaluation of the complex soil-tunnel-structure interaction phenomena which can be investigated by several approaches characterised by a different level of complexity.

In general, a fully-coupled approach is the most satisfactory tool, as it explicitly includes in the same numerical scheme all the ingredients of the problem: the soil, the tunnel and a full structural model of the building (e.g. Amorosi et al., 2014). Thus, it allows a direct estimation of the stress and strain fields acting in the structure and of the damage induced by the excavation process.

An alternative and strongly simplified uncoupled approach can also be employed, generally at the preliminary stage of the analysis. In this method, characterised by a limited computational effort, the displacements predicted under free-field conditions are simply applied at the base of the building. Separate numerical models are used for the soil and for the structure (e.g. Maleki et al., 2011), while their interaction is studied by an iterative process.

An intermediate solution is represented by a semi-coupled (or partly-uncoupled) approach (e.g. Losacco, 2011; Rampello et al., 2012, Losacco et al., 2014) that, although requiring a soil-structure interaction analysis, introduces a simplified equivalent model of the building. This method, limiting the required computational power and the calculation times, can be useful to investigate specific cases, for example the simultaneous effect of tunnelling on many existing buildings.

As will be discussed in the following, soil-structure interaction problems were explored by 2D or more advanced 3D numerical studies presented in the literature, frequently devoted to analyse the response to tunnelling of masonry buildings and, more rarely, of reinforced concrete framed structures.

2D approach

In the first studies aimed at investigating the structural response to ground settlements, the building was represented by a simple, weightless, 2D deep elastic beam undergoing sagging and hogging modes of deformation according to the soil displacement profile; the onset of cracking was related to the critical tensile strain within the beam associated with shear and bending modes of deformation (Burland and Wroth, 1974; Burland et al., 1977). This model was then improved to incorporate the influence of the horizontal strain (Boscardin and Cording, 1989; Burland, 1995).

An attempt to overcome this uncoupled approach, that disregards not only the mutual interaction between the soil and the structure, but also the influence of this latter on the tunnelling-induced soil movements, was proposed by Potts and Addenbrooke (1997), on the basis of a parametric finite-element study representative of the typical conditions encountered during tunnel excavations in London Clay. Their study involved more than 100 non-linear numerical analyses where the surface framed structure is modelled by an equivalent weightless beam located on the ground and characterised by different values of width, stiffness and eccentricity with respect to the tunnel axis. The results show that both the axial and bending stiffness of the beam influence the ground displacement field, this latter being very different to the free-field one. The presence of a structure has the effect of reducing settlements as compared to the free-field scenario; however, the vertical displacements can be larger than those evaluated without structure if this latter is characterised by a low bending stiffness and a realistic axial stiffness. The Authors defined two parameters, named relative bending stiffness (ρ^*) and relative axial stiffness (α^*); these parameters take into account the soil-structure relative stiffness and the so called modification factors for the deflection ratio (M^{DR}) and for the horizontal strain ($M^{\varepsilon h}$), which indicate as the structure modifies the free-field predictions of the relevant damage parameter. The design curves introduced by Potts and Addenbrooke (1997) in the assessment process of the building damage enable a more accurate prediction of the likely damage to existing structures.

Rampello and Callisto (1999) examined the case of a tunnel excavation in silty-sand passing under Castel Sant'Angelo in Rome (Italy), a massive masonry monumental building whose inner portion is of Roman age. In their work the structure is modelled as an isotropic linear elastic-perfectly plastic material with limited compressive strength and no tensile strength, while the soil behaviour is described by two different

constitutive models (i.e. an elastic-perfectly plastic model and an elastic-plastic model with isotropic deviatoric hardening). The results of the numerical analyses show that the high stiffness of the building plays a major role in the interaction process. The evaluated potential damage induced by tunnelling on the structure is shown to be significantly influenced by the choice of the soil constitutive model.

Liu et al. (2000) also used a continuum approach to study the response of masonry façades to tunnel excavation in London Clay, using a non-linear model for both soil (Houlsby, 1999) and surface building. In particular, the masonry material, elastic in compression, can crack when it reaches its tensile strength. Their study involves comparison of crack patterns obtained on plane stress façades by coupled and uncoupled analyses; in this latter case, the displacement filed obtained by a previous free-field analysis is applied at the base of the façade. Their analysis concentrates on the effects of the façade weight and stiffness and of the horizontal location of the façade with respect to the tunnel axis, finding that increasing weight tends to increase the damage, owing to larger horizontal strains. Increasing façade stiffness, however, appears to reduce the damage, since the differential settlements under the façade result inhibited.

Boonpichetvong and Rots (2002) presented the application of fracture mechanisms to predict the cracking damage in masonry buildings subjected to ground movements by tunnelling activity. They described the computational approach employed to capture the failure mechanism of a selected historical masonry façade, typical for the western part of The Netherlands. The soil-structure interaction process is studied by a finite element approach, testing various continuum crack models in large-scale fracture analyses. The results indicate some limitations of the utilised crack models in predicting the settlement damage, highlighting the need for reliable numerical techniques for highly brittle material.

Melis and Rodrìguez Ortiz (2003) illustrated a method of establishing the stiffness of several types of buildings (i.e. masonry buildings, framed buildings in steel or reinforced concrete) taking into account their main structural elements. The resulting values allow to model the reference structure as an equivalent beam with an associated modulus of deformation. This procedure was applied to a real case of study, i.e. the construction of the metro-line 7 of Madrid (Spain) by EPB-tunnelling, analysed by a finite element approach. The tunnel passes through hard and stiff soils, interacting with structures of different type. Actual observations confirm that stiff buildings rarely suffer damage, this latter being associated with very high angular distortions for the more flexible ones.

The response of buildings with different structural types resting on shallow foundations subjected to excavation-induced ground settlements was also compared by Son and Cording (2011), providing a better understanding of the complex soil-structure interaction in building response. The investigated structures include brick-bearing structures, open-frame structures and brick-infilled frame structures, that are often encountered near a construction area. In their research, numerical studies, performed by the distinct element method (DEM), were carried out to evaluate the response of such buildings subjected to an identical progressive ground settlement and to provide key features of their response in different soil conditions.

The structural behaviour was investigated using distortions and crack damages induced to the structures by ground settlements. Results indicate that such a response is highly dependent on structural type, cracking in a structure and soil condition, highlighting that their effects should be considered to better assess the potential damage due to tunnelling-induced ground subsidence.

In general, if the same magnitude of ground settlement occurs, a structure on stiffer soil is more susceptible to building damage caused by ground settlement than a structure on softer soil. This latter has a tendency to modify the ground settlement profile and undergoes less distortion. However, the effect of soil stiffness decreases when a structure has enough strength or it is restrained by some elements such as the frames in a brick-infilled framed structure. In particular, as cracking occurs in a brick-bearing structure, the subsequent cracks concentrate around the initial ones and propagate farther out with advancing ground settlements. However, for a brick-infilled framed structure the enclosed frame significantly confines the crack propagation, so that the structure undergoes relatively small distortion regardless of its conditions.

A finite element semi-coupled model including a cracking low for the masonry and a non-linear interface simulating the soil–structure interaction, was validated against experimental results (Giardina et al., 2012) by Giardina et al. (2013). The aim of this work is to produce a reliable validated numerical approach to improve the current procedures for the assessment of tunnelling-induced damage to masonry structures. The emphasis is on the crack modelling and on the robustness of the analysis for a critical case of a brittle façade on an elastic bedding. In particular, the feasibility of a continuum approach for the crack modelling of masonry was evaluated and, considering the convergence difficulties related to the non-linear modelling of quasi-brittle material, a new sequentially linear analysis scheme was also proposed. In comparison with previous works (e.g. Son and Cording, 2005), this study offers an evaluation of the structural damage evolution as a function of the applied deformation throughout the entire experimental and numerical tests, obtaining in this way new empirically validated results.

Alongside the same topic, Giardina et al. (2014) examined the masonry response to tunnelling by a sensitivity study on the effect of cracking and building weight. With the aim to improve the useful existing procedures for predicting damage due to tunnelling, their research considers the use of a finite element modelling, including non-linear constitutive laws for the soil and the structure, to analyse the response of a masonry structure, represented by a simple beam, subjected to tunnel excavation in sand. The numerical model was validated through a comparison with a series of centrifuge tests (Farrell, 2010). Results indicate a general increase in the beam deflection ratio with weight, suggesting a direct correlation between this latter, normalised to the relative stiffness between the structure and the soil (Potts and Addenbrooke, 1997), and the modification of the settlement profile. The weight can reduce the effect of an increment in relative stiffness and it is more evident for relatively high values of the volume loss and beam stiffness. A variation in the modified deflection ratio is also observed when a cracking model for masonry is included in the simulations, depending on the initial stiffness and material parameters.

The analysis of deformation and damage mechanisms induced by shallow tunnelling on masonry structures was carried out by Amorosi et al. (2014). The study, conducted by the finite-element code Abaqus, was performed in 2D conditions assuming plane strain and plane stress conditions for the soil and the structure, respectively.

As such, the analysed class of problems is that of a tunnel excavated under a masonry structure, this latter being characterised by its plane oriented perpendicularly to the tunnel axis.

The modelled structure represents an ancient masonry wall, schematised as a block structure with periodic texture and characterised by a non-linear anisotropic mechanical

response. The soil was modelled using a conventional linear elastic-perfectly plastic Mohr-Coulomb model.

The Authors performed a preliminary parametric study on the behaviour of a simple masonry structure affected by the excavation of a shallow tunnel, aimed at investigating the influence of the mechanical and geometrical properties of the structure. The numerical analyses carried out with different values of mortar joints' cohesion (0, 5 and 10 kPa) clearly demonstrate the role of the non-linear structural behaviour on the correct assessment of the masonry response. In particular, the influence of structure cohesion appears negligible in terms of overall settlement pattern, but more relevant for the damage development within the masonry wall. The analysis for a null cohesion displays a severe shear-induced damage pattern, while no significant differences are observed between the analyses carried out with cohesion values of 5 and 10 kPa.

A linear anisotropic-elastic analysis would have predicted the same level of damage in all the investigated cases.

Free-field preliminary analyses demonstrate that, despite the relatively simple constitutive hypothesis adopted for the soil, the displacement-controlled technique used in the study to reproduce the tunnel construction well captures the induced ground displacements, as highlighted by the comparison with the Gaussian curves for surface settlements at different volume losses. The numerical results are able to mimic the main features of the soil–structure interaction, including the modifications in the subsidence profile and the related deformative pattern in the structure.

In the same work the Authors presented a numerical back-prediction of the settlements induced in a complex historical masonry structure (the Felice Aqueduct in Rome, Italy) by the excavation of shallow twin tunnels. First, an uncoupled analysis was performed, by applying at the base of the structure the displacements obtained by the model under

free-field conditions. Then, a fully coupled simulation was carried out, thus highlighting the influence of soil–structure interaction on the computed deformative response of the structure, characterised by a reduced amount of tensile plastic strains, and in the ground, where horizontal displacements were dramatically decreased. In order to test the numerical approach, the computed ground and structural surface vertical displacements were compared with monitoring data. Numerical outcomes result to be in good agreement with experimental data, thus validating the numerical model for this class of soil–structure interaction problems.

3D approach

The effects of the weight and stiffness of surface structures on the ground settlements were studied by Burd et al. (2000) using a three-dimensional finite element analysis in which the tunnel, the soil and a masonry building were all included in a single numerical model. Although three-dimensional, the geometry of the problem is relatively simplified: the structure, in fact, consists of two identical façades, connected by two plane walls, with openings to model the windows and the door, while the roof, the floors, the internal walls and the foundation details were neglected. The excavation process of an unlined tunnel was simulated by incrementally removing the soil elements within a predefined zone. A multi-surface plasticity model (Houlsby, 1999) was adopted in the numerical study to describe the non-linear and irreversible behaviour of the soil, while a relatively straightforward model was assumed for masonry in which the material has a low tensile strength and infinite compressive strength. The presented results illustrate the mechanisms of interaction between the building and the ground considering two different tunnel positions (symmetric and non-symmetric with respect to the structure). In particular, it was pointed out that the performance of the building results highly dependent on the deformation mode: for façades subjected to sagging

deformation the soil-structure interaction process allows to reduce the predicted tendency of the building to suffer settlement-induced damage, while when the building deforms in a hogging mode, it results less effective in reducing the differential settlements.

Mroueh and Shahrour (2003) presented a numerical study of the interaction between a lined tunnel and an adjacent reinforced concrete structure conducted by a full three-dimensional calculation which takes into account the presence of the structure during tunnelling. The tunnel construction process was modelled by a simplified step-by-step procedure and the structure was schematised as a spatial frame composed by columns and beams. The soil behaviour was assumed to be governed by an elastic perfectly-plastic constitutive relation based on the Mohr–Coulomb criterion with a non-associative flow rule and the behaviour of the structure was assumed to be linear-elastic. The proposed study confirms that tunneling-induced movements are largely influenced by the presence of adjacent structures, showing as the simplified approach, which considers the free-field soil movements for the evaluation of structural damage, results very conservative. The performed numerical study also highlighted the importance of considering the building self-weight in the determination of the initial stress in the soil before tunnelling.

The soil-structure interaction phenomenon was also examined in the coupled numerical study proposed by Jenck and Dias (2004) who, however, considered all the component of the process in a simplified way. In particular, in their study the soil behaviour is elastic-perfectly plastic, the tunnel excavation is a simplification of the real phases of the TBM process based on the concept of volume loss and the reference building is an ideal reinforced concrete structure, with no eccentricity respect to the tunnel, founded on a raft foundation and composed by columns and floors. The main aim of the study is

the analysis of the role of the structural stiffness on the soil surface displacements. It was found, in accordance with previous studies, that the presence of the structure leads to negligible horizontal displacements under its foundations as compared to the free-field calculations and, consequently, the application of the free-field deformations to the building for damage estimation results to be conservative. This study also pointed out that the larger the building stiffness, the smaller the surface differential settlements.

Similar results were presented in the 3D numerical study proposed by Keshuan and Lieyun (2008). Their research is based on a finite element model which takes into account the presence of a strongly schematised spatial framed structure during the excavation of twin tunnels. A very simple structural scheme, consisting of beams, columns and live loads acting at each floor of the reinforced concrete building was also proposed by Liu et al. (2012) for the numerical analysis of ground movements due to metro-station driven with enlarging shield tunnels.

A finite element study aimed at demonstrating the importance of 3D modelling to evaluate the influence of the excavation advancement and tunnel-building relative position on damage mechanism was presented by Giardina et al. (2010). The Authors proposed a coupled scheme taking into account a damage model for the masonry building and the non-linear behaviour of the soil-structure interface. This latter was adopted to simulate the transmission of vertical and horizontal deformations from the ground to the structure through the shallow strip foundations. The structure, subjected to dead and live loads, only consists of external façades with openings and internal walls; the roof and the floor diaphragms were not represented due to their negligible stiffness with respect to that of the global building. The tunnelling process was simulated by subsequent stages of soil excavation and lining installation. The Authors investigated the effect of different factors (such as the expected volume loss and the location of the

building with respect to the tunnel) on the shape of the settlement profile. They also highlighted that crack pattern and failure mechanism evolve in the structure during tunnelling, pointing out, in particular, the importance of a three-dimensional description of the tunnel excavation process and building geometry for a complete analysis of the structural damage.

In the literature, several Authors defined simplified structural models with the aim to reproduce the behaviour of masonry or reinforced concrete buildings in the interaction analyses.

Franzius et al. (2006) proposed an extension of the study presented by Potts and Addenbrooke (1997), this time considering the building as an equivalent elastic shell with weight. The evaluation of the equivalent structural stiffness employs the parallel axis theorem, likely overestimating the stiffness of a real structure. In the proposed method the foundation system is not taken into account reducing, in contrast, the overall stiffness. Such methodology, however, is based on certain assumptions regarding the structural typology: it is mostly applicable to the buildings characterised by geometrical regularity, while it results not appropriate to those with more complicated features. This schematisation, for example, was applied in the theoretical study presented by Maleki et al. (2011) aimed at investigating the effect of structural characteristics (i.e. geometry, stiffness and weight) on tunnel-building interaction.

In the finite element procedure proposed by Pickhaver et al. (2010) to evaluate the structural damage due to tunnelling, the masonry building is represented in an approximate way by equivalent elastic Timoshenko beams. The Authors discussed the method to estimate the appropriate properties for the equivalent beams in terms of flexural and shear stiffness. The procedure is shown to compare favorably with the

results of a parametric numerical study of a range of building façades and internal wall subjected to applied displacements along their base.

The performed analyses shown that the response of the equivalent beams provides a good match with that of the masonry façades, modelled using a non-linear constitutive model, in the case of sagging deformation, while the proposed structural simplification requires the use of a reduced flexural stiffness to match the more flexible response of masonry panels which deform according to a hogging mode.

Rampello et al. (2012) illustrated the procedure adopted to evaluate the effect of tunnelling on existing monuments and historical buildings, with particular reference to the construction of the metro-line C of Rome (Viggiani and Soccodato, 2004; Losacco, 2011; Burghignoli, 2011). Specifically, the study of the interaction between construction activities and the built environment was carried out following two procedures at increasing levels of complexity: at the first level, free-field analyses were carried out neglecting the stiffness of the existing buildings for a simplified evaluation of the potential damage induced by tunnel excavation; at the second level, an interaction numerical study was performed accounting for the stiffness of existing buildings modelled in a simplified way.

The main aspects of such procedure were illustrated using, as an example, the case-study of Palazzo Grazioli. The mechanical behaviour of the soil was described by an elasto-plastic constitutive model with isotropic hardening and Mohr-Coulomb failure criterion (i.e. the *Hardening Soil model*), while the reference structure was modelled as an equivalent solid with simpler geometry and appropriate mechanical properties. This equivalent solid is fully embedded into the soil and it is assumed to behave as a linear-elastic material. This latter assumption may be valid only for relatively small volume loss, that is when the structure undergoes small distortions. In the simple

hypothesis of isotropy, the mechanical behaviour is completely described by the Poisson's ratio and Young's modulus. It is postulated that the actual and the simplified structures are equivalent if they show a similar response to a given perturbation, which consists in imposing the vertical displacements computed in the free-field analyses at the foundation level; the corresponding response is the distribution of the nodal forces at the same level. The Young's modulus of the equivalent solid is found iteratively, to produce a distribution of nodal forces at foundation level that matches the distribution computed using a complete structural model of the building.

In a subsequent step, the equivalent solid is introduced in the finite element model with its equivalent stiffness and weight reproducing those of the complete building. The numerical analyses produce a new displacement field, accounting for the stiffness and weight of the building, that is eventually applied to the complete structural model for a final evaluation of the effects induced by tunnel construction.

The study highlights the importance of a three-dimensional interaction analysis in cases of geometrical complexities. As a general result, explicit consideration of stiffness and weight of the building leads to larger settlements but smaller distortions, and therefore to a predicted less damage than the free-field analysis.

2.4 Evaluation of building damage

2.4.1 Damage classification

The control of tunnelling-induced ground movements and the protection of the built environment from potential damage represent the principal design and construction requirements (Viggiani and Soccodato, 2004). The ability to predict with confidence the displacements due to tunnelling is a crucial aspect as ground movements transmit to adjacent structures as settlements, rotations and distortions of foundations which can induce damage affecting visual appearance and aesthetics, serviceability or function

and, in most severe cases, stability of the structures (Burland and Wroth, 1974; Burland et al., 1977; Boscardin and Cording, 1989).

Skempton and MacDonald (1956) provided some design indications about maximum admissible settlements likely to cause either architectonic or structural damage on the basis of the examination of a large number of real cases, mainly framed construction buildings deforming under their self-weight. They recognised that the curvature of the settlement profile of the foundations is related to damage. They chose the maximum relative rotation β_{max} (see Fig. 2.7) as an indicator of damage and they assigned a limit value to this parameter equal to 1/300 and 1/150 for architectonic and structural damage, respectively. The Authors also proposed a relation between maximum absolute or differential displacements and maximum relative rotation for rafts and isolated foundations on either sandy or clayey soil, as reported in Table 2.2.

Isolated foundations		**Rafts**	
Clay	**Sand**	**Clay**	**Sand**
$S_{v,max} = 1000\ \beta_{max}$	$S_{v,max} = 600\ \beta_{max}$	$S_{v,max} = 1250\ \beta_{max}$	$S_{v,max} = 750\ \beta_{max}$
$\delta_{s,max} = 550\ \beta_{max}$	$\delta_{s,max} = 350\ \beta_{max}$	$\delta_{s,max} = 550\ \beta_{max}$	$\delta_{s,max} = 350\ \beta_{max}$

Table 2.2. Relations between maximum absolute or differential displacement and maximum relative rotation (Skempton and MacDonald, 1956).

Most of the existing classifications refers to crack widths in masonry resulting from tensile strain. Analysing the deformation and cracking state of existing masonry building, Polshin and Tokar (1957) established a relation between the geometry ratio L/H (where L is the length of the structure and H is its height) and the deflection ratio Δ/L causing cracking in the walls. They identified a common critical tensile strain, ε_{crit}, corresponding to the onset of visible cracks.

Burland and Wroth (1974) proposed a method to relate the building foundation settlements to the onset of visible cracking, developing the concept of critical tensile

strain (Polshin and Tokar, 1957). In particular, they investigated the relation between the maximum deflection ratio $(\Delta/L)_{max}$ and the maximum tensile strain occurring in a building idealised as an isotropic, linear-elastic deep beam (Timoshenko, 1955) subjected to either pure bending or pure shear deformation. In pure bending the maximum tensile strain $\varepsilon_{b,max}$ is horizontal, while in shear it is indicated as $\varepsilon_{d,max}$ and it is oriented at 45° (the subscript *d* stands for diagonal). For such specified deformation modes, the relation between the maximum deflection ratio $(\Delta/L)_{max}$ and the maximum tensile strain is described by the following equations:

$$\frac{\Delta}{L} = \varepsilon_{b,max} \frac{L}{12y}\left[1+\frac{18EJ}{L^2HG}\right] \tag{2.22}$$

$$\frac{\Delta}{L} = \varepsilon_{d,max}\left[1+\frac{L^2HG}{18EJ}\right] \tag{2.23}$$

where *y* is the distance of the neutral axis, whose position is assumed either at the base or at mid-height of the beam, from the bottom; *L* and *H* are the length and the height of the beam, respectively; *J* is the second moment of area of the beam; *E* and *G* are the Young's and shear stiffness moduli, respectively.

The Authors also highlighted, however, that the ratio *E*/*G* for a real structure can be very different from that calculated by assuming an isotropic behaviour as for the beam.

Burland et al. (1977) introduced a classification with six categories of increasing damage, which is based on the ease of repair and also provides several indications on the likely width and number of cracks associated to each category. Such classification is reported in Table 2.3: categories from 0 to 2 are essentially associated to aesthetic

damage, category 3 to the attainment of some serviceability limit state for the structure, while in categories 4 and 5 the structure reaches an ultimate limit state.

This classification was developed to provide a guide for standard domestic and office buildings in brickwork or blockwork and stone masonry. Although widely adopted in the geotechnical engineering practice, its applicability to monumental and historical structures may be questionable (Viggiani and Soccodato, 2004).

In an important development, Boscardin and Cording (1989) replaced the concept of critical tensile strain with that of limiting tensile strain, ε_{lim}. They analysed case histories of a number of brick-bearing-wall and framed buildings affected by excavation with regard to the limiting tensile strain.

The Authors, in particular, overcame the model presented by Burland and Wroth (1974) adding the effect of horizontal strains ε_h on the onset of visible cracking. Assuming homogeneous horizontal straining across the whole beam, it is possible to superimpose ε_h to $\varepsilon_{b,max}$ or $\varepsilon_{d,max}$, separating bending and shear deformation modes. The resultant strains are expressed as in the following equations:

$$\varepsilon_{b,r} = \varepsilon_{b,max} + \varepsilon_h \tag{2.24}$$

$$\varepsilon_{d,r} = \varepsilon_h \frac{1-\nu}{2} + \sqrt{\varepsilon_h^2 \left(\frac{1-\nu}{2}\right)^2 + \varepsilon_{d,max}^2} \tag{2.25}$$

Based on the data collected by Boscardin and Cording (1989), Burland (1995) proposed that the attainment of each category of damage might be broadly related to characteristic values of the limiting tensile strain, as reported in Table 2.4. The Author integrated the previous classification of Burland et al. (1977) and defined damage charts of deflection ratio Δ/L versus horizontal strain ε_h, as shown in the example of Figure 2.9.

Category of damage	Normal degree of severity	Description of typical damage (easy of repair in italic type)
0	Negligible	Hairline cracks less than about 0.1mm
1	Very slight	*Fine cracks which are easily treated during normal decoration*. Damage generally restricted to internal wall finishes. Close inspection may reveal some cracks in external brickworks or masonry. Typical crack widths up to 1mm.
2	Slight	*Cracks easily filled. Re-decoration probably required. Recurrent cracks can be masked by suitable linings*. Cracks may be visible externally and some repointing may be required to ensure weather-tightness. Doors and windows may stick slightly. Typical crack width up to 5mm.
3	Moderate	*The cracks require some opening up and can be patched by mason. Repointing of external brickwork and possibly a small amount of brickwork to be replaced*. Doors and windows sticking. Service pipes may fracture. Weather-tightness often impaired. Typical crack widths are 5÷15mm or several up to 3mm.
4	Severe	*Extensive repair work involving breaking-out and replacing sections of walls, especially over doors and windows*. Windows and door frames distorted, floor sloping noticeably. Walls leaning or bulging noticeably, some loss of bearing in beams. Service pipes disrupted. Typical crack widths are 15÷25mm but also depends on the number of cracks.
5	Very severe	*This requires a major repair job involving partial or complete rebuilding*. Beams lose bearing, walls lean badly and require shoring. Windows broken with distortion. Danger of instability. Typical crack widths are greater than 25mm but depends on the number of cracks.

Table 2.3. Damage classification (Burland et al., 1977).

Category of damage	Normal degree of severity	Limiting tensile strain (%)
0	Negligible	0÷0.05
1	Very slight	0.05÷0.075
2	Slight	0.075÷0.15
3	Moderate	0.15÷0.3
4 and 5	Severe to Very severe	>0.3

Table 2.4. Damage category and limiting tensile strain (Boscardin and Cording, 1989; Burland, 1995).

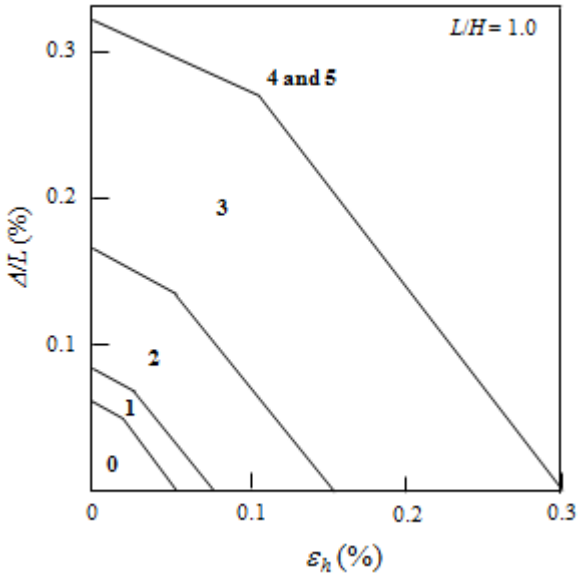

Figure 2.9. Burland's damage classification.

2.4.2 Methodological approach to damage evaluation

Mair et al. (1996) described the assessment procedure of building damage induced by settlements that was firstly applied on the Jubilee Line Extension (JLE) of London.

The methodology consists of three phases (Mair et al., 1996) which are referred to "preliminary assessment" (Phase 1), "second phase assessment" (Phase 2) and "detailed evaluation" (Phase 3).

In Phase 1 the presence of buildings is not considered and the free-field settlement profiles are calculated by empirical expressions. Maximum absolute settlement and rotation are calculated in correspondence with the area of the building and, if these values are lower than 10 mm and 1/500 respectively, no further action is required, otherwise a Phase 2 assessment has to be carried out. This indication is obviously conservative, because the stiffness of the neglected surface structure, in general, tends to reduce the differential displacements, as previously discussed.

In Phase 2 free-field horizontal and vertical displacements are calculated for each building individually. Each structure is assumed to follow the ground movements and it

is represented as an elastic beam, described by its length L, its height H and the ratio of Young's modulus over the shear stiffness modulus E/G (Burland and Wroth, 1974).

The deflection ratio and the average horizontal strain along the building are evaluated and in this approach the zones of hogging (i.e. tension) and sagging (i.e. compression) are treated independently. In particular, the deflection ratio and the average horizontal strain are calculated for each hogging and/or sagging zone of the building; these can be related to categories of potential damage (Table 2.4). Alternatively, the category of damage can be obtained by calculating the tensile strain developing in the building as outlined by Mair et al. (1996). For damage categories of 2 (Slight) or smaller, only aesthetic damage is predicted and, thus, no further analysis is required, while for buildings with a potential damage category of 3 (Moderate) or higher a detailed evaluation is required.

Although the Phase 2 calculation is more detailed than the preliminary assessment, it is conservative since the building is assumed to follow the free-field settlement trough (i.e. its stiffness is completely neglected).

In Phase 3 more details of the building and of the tunnel construction are taken into account. This includes the orientation of the building with respect to the tunnel, building features such as the foundation design and structural continuity and their effect on the soil-structure interaction. Mair et al. (1996) pointed out that, due to the conservative assumptions of the second phase assessment, the detailed evaluation will usually predict lower categories of damage than obtained from the previous phase. However, if the risk remains high (i.e. damage category of 3 or higher), protective measures have to be considered, when necessary.

A new generic approach to the second stage of the assessment of the potential building damage was developed by Harris and Franzius (2005). Such methodology aims at

improving the effectiveness and efficiency of the process whilst maintaining consistency with Phase 3 of the method outlined by Mair et al. (1996). The ambition is to reduce the effort expended in producing a large number of Phase 2 calculations for individual buildings which show, in most cases, that the potential damage is within acceptable limits. The Authors discussed about the inefficiency of the Phase 3 approach to settlement assessment on the base of a specific experience (i.e. the Jubilee Line Extension Contract 102 in London): for many of the Phase 2 assessments undertaken, a low damage category is evident a priori and, consequently, a detailed evaluation for all buildings is not justified. The proposal for generic Phase 2 assessments is to apply the same assumptions and calculation methods as used previously for the assessment of individual buildings, but applying these only to representative sections taken through the surface settlement profiles determined in the Phase 1 assessment. Along each section, a high number of different building geometries are analysed and the worst case, i.e. the maximum tensile strain, for any building geometry located along the section is then determined. This approach avoids the production of hundreds or thousands of Phase 2 calculations for individual buildings, it gives improved insight into the variation of maximum tensile strain along the route alignment and it identifies potentially problematic areas to be more efficiently targeted for further assessment.

This generic method, however, cannot take into account of varying foundation depths due to the fact that it is based on surface settlement contours.

3. Tunnelling-induced settlements in coarse-grained soils: the case of the new Milan metro-line 5

3.1 Purpose of Chapter 3

This chapter proposes a detailed analysis of the displacement field induced by tunnelling activities in granular soils, taking as reference the case study of the new metro-line 5 of Milan (Italy). The two twin tunnels of the line were recently constructed in sand and gravel, partially below the water table, with earth pressure balance (EPB) machines to safely perform the excavation and to minimise the surface subsidence.

Measurements of tunnelling-induced settlements collected during the construction of the line 5 are discussed and interpreted. The attention is firstly given to the monitoring data recorded under free-field conditions (i.e. no structures on the ground surface) during and after the construction of the first and the second tunnel. Settlement data are back-analysed using the classical empirical predictions, both in the transversal and longitudinal directions, providing an exhaustive description of the EPB tunnelling effect under this specific geotechnical conditions.

Then, the influence of different excavation parameters (such as face pressure, grouting pressure, machine thrust, etc.) on the subsidence due to the construction of the first and the second tunnel of the metro-line is also investigated in detail.

Finally, measurements of the vertical displacements observed in correspondence with a 9-storey reinforced concrete building in interaction with the metro-line are analysed, providing specific information on the evolution of the surface structure response during tunnelling.

3.2 Tunnel construction

The twin tunnels of the metro-line 5 recently constructed in Milan (Italy) run from north to west of the city with a total length of 12.6 km and 19 access stations (Fig. 3.1) (Fargnoli et al., 2013).

The portions of the metro-line considered in this study extend for about 1.3 km between *San Siro* and *Segesta* stations and for a length of about 600 m between *Lotto* and *Portello* stations (Fig. 3.1).

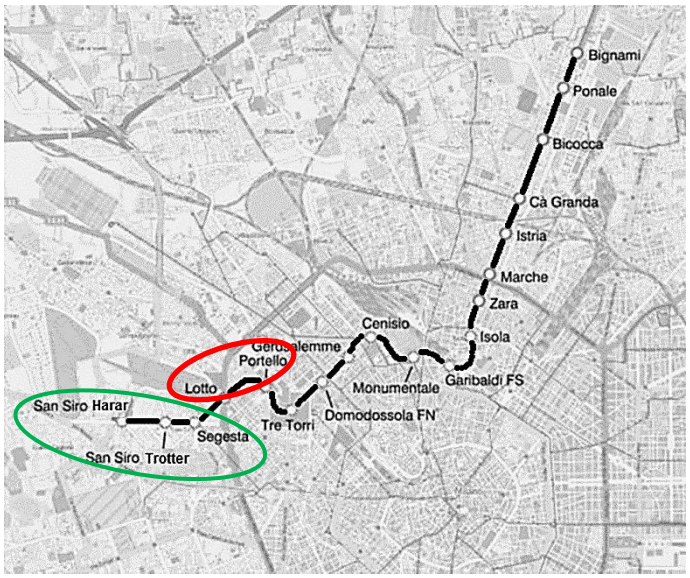

Figure 3.1. Metro-line 5 of Milan (the reference segments of the route between the stations of *San Siro-Segesta* and *Lotto-Portello* are underlined by the green and red circles, respectively).

The tunnels, partially excavated under the water table, have a separation between the two axes, d, of about 15 m and a mean depth z_0 = 15 m. This latter reaches its maximum value of about 23 m at *Lotto* station.

In order to effectively minimise ground movements in these highly-populated areas, EPB machines were selected.

The EPB machine makes use of a rotating cutter-head as a tool of excavation; the excavated material, kept under pressure in the bulk chamber, ensures face stability and

it limits surface settlements. Face pressure is generally set as a function of the total horizontal lithostatic pressure at rest acting at the depth of the tunnel.

In this case study the EPB shields have a total length of about 10 m and a thickness of 30 mm. They are characterised by an outer diameter of 6.69 m at the face and an inner one of 6.67 m at the tail. The maximum excavation diameter at the face can be increased up to 6.71 m. Six pressure cells are located on each EPB face as shown in Figure 3.2.

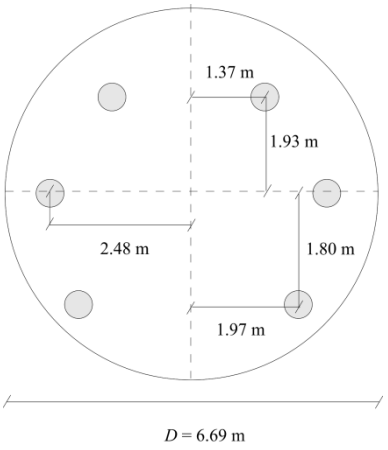

Figure 3.2. Location of the pressure cells on the EPB face.

A total thrust of about 50500 kN is required for the advancement of each machine. It is provided by 38 hydraulic jacks located on the perimeter of the shield body, acting on the already cast in place lining.

The tunnel lining, set in place inside the shield tail to support the tunnel as the machine advances, consists in concrete cast-in-place rings characterised by a length of 1.4 m and a thickness of 30 cm. The outer and inner diameters of the lining ring are equal to 6.40 m and 5.80 m, respectively. The external diameter of the final lining is always smaller than the excavated one, in order to allow the advancement of the machine and of the shield.

The gap created behind the lining segments after their erection is promptly filled in order to minimise the settlement. A two-component back-filling grouting, consisting in

cement paste and grip accelerator, is injected from the shield to fill the void between the lining and the soil.

The tunnel advancement along the examined portion of the route is shown in Figure 3.3.

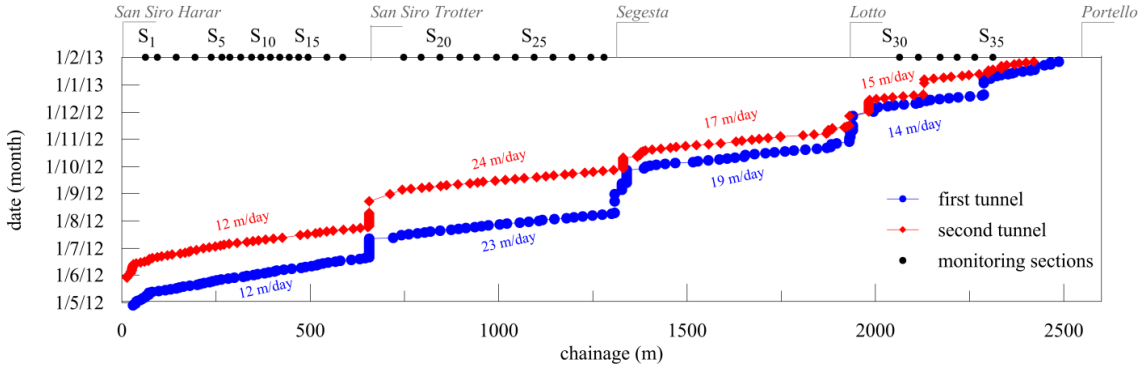

Figure 3.3. Advancement of the twin tunnel excavation along the examined portion of the route (the ground monitoring sections and the metro-line stations are also shown).

Tunnelling activities started at the beginning of May 2012 for the first tunnel and about one month later for the second tunnel. The excavation works proceeded regularly, with relatively short stop time only in correspondence with the metro-line stations and, occasionally, between *Lotto* and *Portello* stations. Figure 3.3 also reports the average values of the excavation rate, evaluated between consecutive stations, which results to be similar for both tunnels. It is possible to note, in particular, that lower excavation rates characterise the initial portion of the route, due to the start-up phase of the EPB machines, and the *Lotto-Portello* segment where the twin tunnels interacted with pre-existing surface structures.

During the various phases of the shield tunnel construction, an extensive geotechnical and structural monitoring was carried out along the line using a precise levelling survey, with recording intervals varying between 12 and 24 hours.

3.3 Ground conditions and geotechnical characterisation

The city of Milan is located in northern Italy, in the central part of the Padana plain, and it rests on a deep glacial and alluvial Pleistocene formation. The upper part of this deposit mainly consists of sand and gravel, with a percentage of silt increasing with depth. A formation of conglomerate and sandstone underlies this upper deposit, while sand and clay are present at greater depth. The new metro-line is located within the granular unit of the upper formation, mainly consisting of gravel and sand of fluvioglacial and alluvial origin.

Along the metro-line an extensive geotechnical investigation was carried out at the design stage of the work, as summarised in Table 3.1.

Granulometric analyses were conducted on the disturbed samples taken from the core drillings.

investigation	**reference portion of the route**	
	San Siro-Segesta	*Lotto-Portello*
core drillings instrumented with open pipe piezometers	3 boreholes (CD_1, CD_2 and CD_3) to a depth of 21-27 m from the ground surface	2 boreholes (CD_4 and CD_5) to a depth of 24-30 m from the ground surface
SPT tests	13 tests conducted in CD_1, 11 in CD_2 and 11 in CD_3	14 tests conducted in CD_4 and 12 ones in CD_5
constant-head Lenfranc-type permeability tests	2 tests in CD_1, 1 test in CD_2 and 1 test in CD_3	2 tests in CD_4 and 1 test in CD_5
disturbed samples taken from the core drillings	19 samples	14 samples

Table 3.1. Details of the geotechnical investigation carried out along the reference portions of the route.

The soil stratigraphy at the reference sites is shown in Figure 3.4 together with the hydrostatic water level, measured with open pipe piezometers and detected on average at 15 m below the ground surface. The gravelly-sand soil results as the main component

of the deposit; it can be considered fairly homogeneous at the two investigated segments of the route, with the exception of a 5 m thick layer of sandy-silt identified at the depth from 20 m to 25 m only at the location between *Lotto* and *Portello* stations.

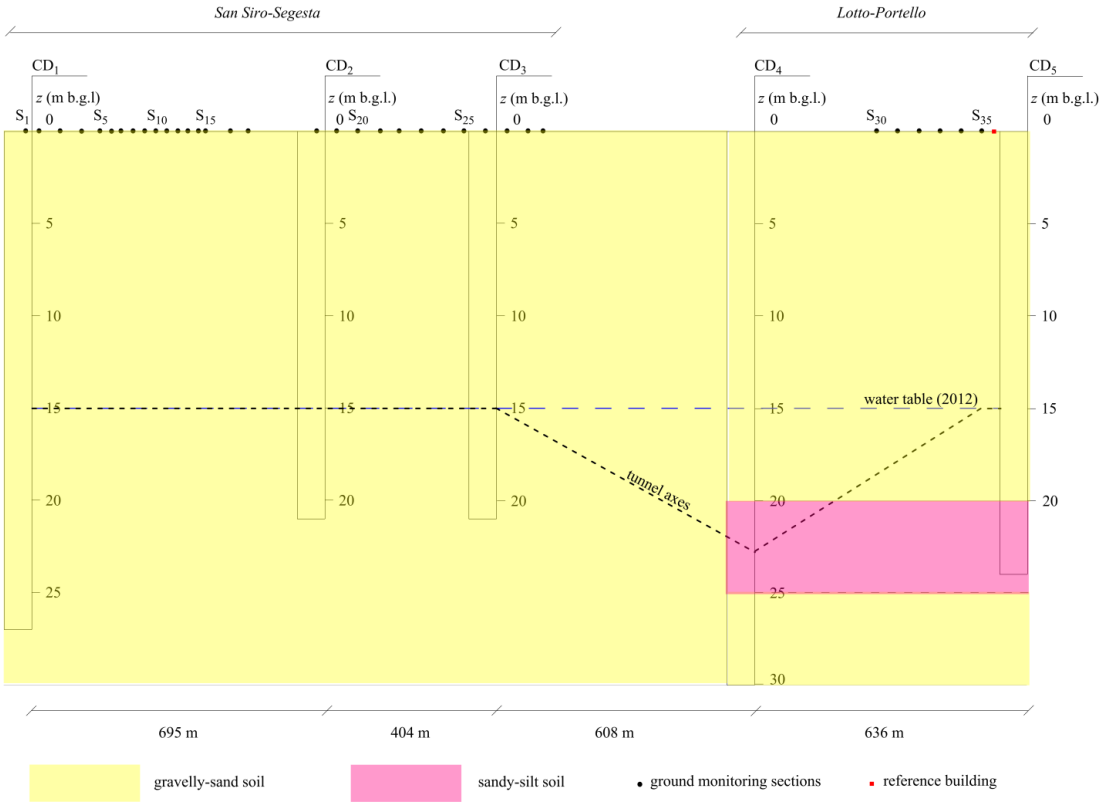

Figure 3.4. Soil stratigraphy along the reference portion of the route (the position of the tunnels and the monitoring sections are also shown).

The total unit volume weights under saturated conditions for the gravelly-sand and for the sandy-silt soils are equal to 20 kN/m^3 and 17.5 kN/m^3, respectively.

Results of SPT tests conducted in the gravelly-sand stratum were elaborated following Skempton (1986), leading to a relative density equal to 70 % on average and to an effective friction angle, ϕ', equal to 33°. SPT tests were not considered appropriate to characterise the sandy-silt layer; as such, its strength parameters were assumed equal to $c' = 5$ kPa and $\phi' = 26°$, based on pre-existing geotechnical characterisations carried out in the Milan area (Fargnoli et al., 2015 *b*).

The permeability coefficients, *k*, were observed to vary at different depths between 5.5 x 10^{-3} m/s and 1.1 x 10^{-2} m/s.

No geophysical investigations were specifically carried out at the construction site. The one closest to the investigated portion of the metro-line route is a down-hole test performed at a distance of about 400 m from the *Lotto-Portello* segment, for very similar geotechnical conditions. The resulting small strain shear modulus (G_0) profile with depth is shown in Figure 3.5.

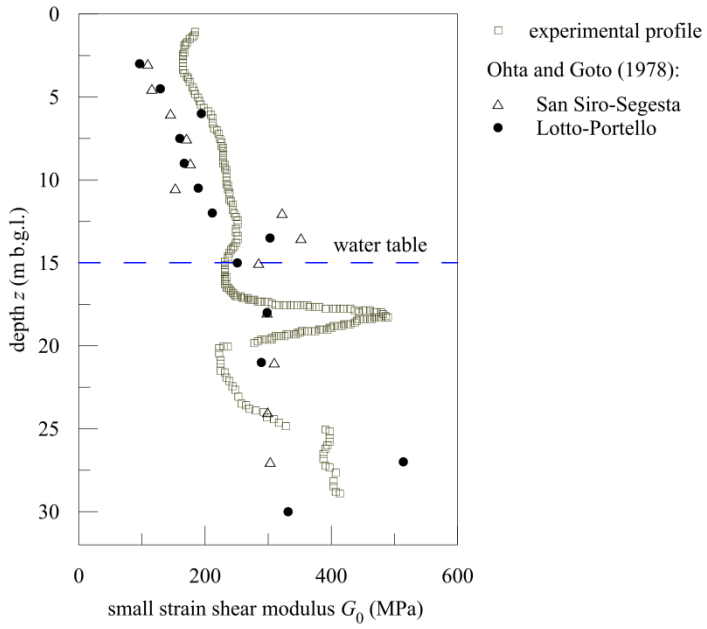

Figure 3.5. Experimental profile of the small strain shear modulus representative of the investigated segments of the route.

The same figure also shows the G_0-*z* profiles obtained from SPT tests (see Tab. 3.1) following Ohta and Goto (1978): although based on an empirical approach, the data do not differ significantly from those directly obtained by the down-hole test.

3.4 Monitoring measurements: analysis and discussion

3.4.1 Ground settlements recorded between San Siro and *Segesta stations*

The data analysed and discussed in this section are vertical ground movements recorded during the excavation of the right tunnel (i.e. the first excavated tunnel) at 29 free-field surface sections located along the initial portion of the metro-line. Several monitoring points (from 5 to 9), characterised by different distances *x* from the tunnel axis, were surveyed on each instrumented location (Fig. 3.6), as reported in Table 3.2.

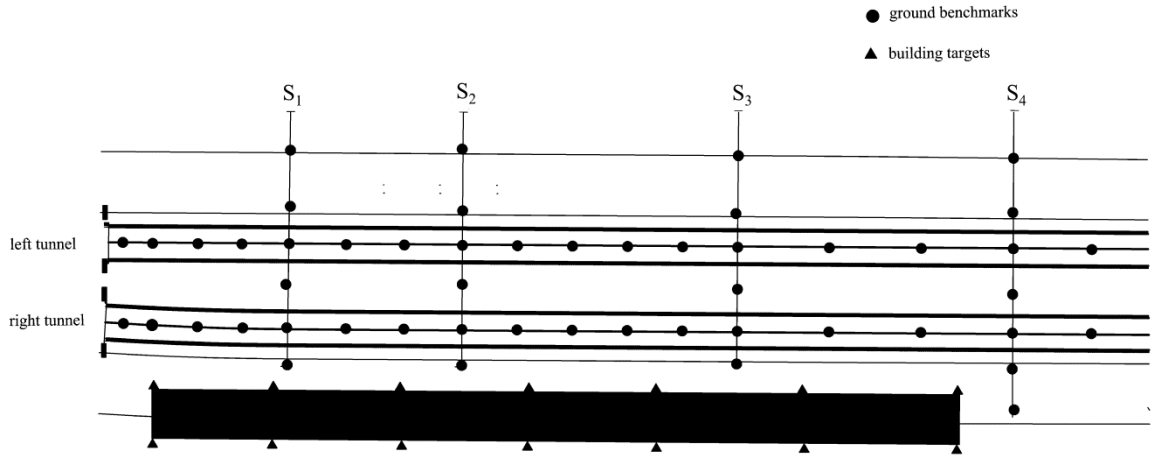

Figure 3.6. Plan view of the initial portion of the examined route (four investigated monitoring sections are also shown).

Along the *San Siro-Segesta* segment of the route several structures are located on the ground surface with a minimum tunnel axis-building distance of about 15 m. This allows to neglect any influence of the surface structures on the tunnelling-induced ground movements and to consider the discussed measurements as occurred under free-field conditions.

Transversal and longitudinal settlements troughs were obtained on the basis of the recorded measurements.

Monitoring sections										
S_1	number	10006	10005	10004	10003	10002	10001			
	x (m)	-32.3	-22.1	-15.4	-8.0	-0.1	6.6			
S_2	number	10012	10011	10010	10009	10008	10007			
	x (m)	-32.7	-21.5	-15.3	-8.2	-0.3	6.5			
S_3	number	10018	10017	10016	10015	10014	10013			
	x (m)	-31.8	-21.3	-15.3	-7.6	0.0	5.9			
S_4	number	10025	10024	10023	10022	10021	10020	10019		
	x (m)	-31.7	-21.9	-15.3	-7.0	0.0	6.5	13.9		
S_5	number	10032	10031	10030	10029	10028	10027	10026		
	x (m)	-30.4	-21.4	-14.7	-7.3	0.0	6.9	14.6		
S_6	number	10039	10038	10037	10036	10035	10034	10033		
	x (m)	-31.5	-21.5	-15.3	-7.6	0.0	6.5	16.2		
S_7	number	10046	10045	10044	10043	10042	10041	10040		
	x (m)	-31.3	-21.6	-15.3	-7.5	0.0	7.0	15.9		
S_8	number	10051	10050	10049	10048	10047				
	x (m)	-21.6	-15.3	-7.7	0.2	6.6				
S_9	number	10056	10055	10054	10053	10052				
	x (m)	-21.5	-15.3	-7.8	0.0	6.6				
S_{10}	number	10061	10060	10059	10058	10057				
	x (m)	-21.8	-15.2	-7.9	0.0	6.5				
S_{11}	number	10066	10065	10064	10063	10062				
	x (m)	-21.9	-15.3	-7.9	0.0	6.6				
S_{12}	number	10071	10070	10069	10068	10067				
	x (m)	-21.9	-15.2	-7.7	0.0	6.6				
S_{13}	number	10076	10075	10074	10073	10072				
	x (m)	-22.0	-15.3	-7.7	0.0	6.5				
S_{14}	number	10081	10080	10079	10078	10077				
	x (m)	-21.4	-15.2	-7.7	0.0	6.6				
S_{15}	number	10086	10085	10084	10083	10082				
	x (m)	-19.4	-15.2	-7.6	0.0	6.4				
S_{16}	number	10092	10091	10090	10089	10088	10087			
	x (m)	-21.2	-15.2	-7.6	0.0	6.5	16.1			
S_{17}	number	10098	10097	10096	10095	10094	10093			
	x (m)	-21.5	-15.3	-8.1	-0.4	5.3	15.9			
S_{18}	number	20006	20005	20004	20003	20002	20001			
	x (m)	-31.3	-21.7	-13.6	-7.5	0.0	5.9			
S_{19}	number	20011	20010	20009	20008	20007				
	x (m)	-21.6	-14.0	-7.7	0.0	6.8				
S_{20}	number	20016	20015	20014	20013	20012				
	x (m)	-21.6	-14.3	-7.7	0.0	6.5				
S_{21}	number	20023	20022	20021	20020	20019	20018	20017		
	x (m)	-33.5	-22.1	-16.1	-8.3	0.0	5.7	16.7		
S_{22}	number	20030	20029	20028	20027	20026	20025	20024		
	x (m)	-29.1	-21.7	-14.9	-7.7	0.0	5.1	15.5		
S_{23}	number	20035	20034	20033	20032	20031				
	x (m)	-21.5	-14.2	-6.4	0.0	6.4				
S_{24}	number	20040	20039	20038	20037	20036				
	x (m)	-21.1	-14.2	-7.6	0.0	6.3				
S_{25}	number	20045	20044	20043	20042	20041				
	x (m)	-21.8	-13.9	-7.6	0.0	6.7				
S_{26}	number	20050	20049	20048	20047	20046				
	x (m)	-21.0	-14.2	-7.7	0.0	6.1				
S_{27}	number	20055	20054	20053	20052	20051				
	x (m)	-21.1	-15.2	-6.4	0.0	6.8				
S_{28}	number	20060	20059	20058	20057	20056				
	x (m)	-14.3	-5.6	0.0	6.1	14.6				
S_{29}	number	20069	20068	20067	20066	20065	20064	20063	20062	20061
	x (m)	-40.4	-31.4	-20.0	-14.7	-7.2	0.0	5.6	17.4	27.1

Table 3.2. Monitoring benchmarks on the instrumented sections between *San Siro-Segesta* stations.

Surface settlement profiles evolve with the excavation advancement. Figure 3.7 shows their final configuration as recorded at each of the 29 monitoring sections at steady-state conditions, i.e. for a sufficiently large distance between the section and the tunnel face. In each monitoring section the maximum settlement, $S_{v,max}^{(I)}$, varying in the range 6.0-21.4 mm, is observed at the tunnel centre line ($x = 0$) and gradually decreases moving away from it, as expected in the case of a single tunnel excavation.

These measurements were fitted by a Gaussian distribution curve (Eq. 2.1 of Chap. 2; Peck, 1969), using K values appropriate to coarse-grained soils (0.25-0.45; Mair and Taylor, 1997; Puzrin et al, 2012). In this way, it was possible to evaluate for each location the corresponding volume loss, $V_L^{(I)}$ (%), as shown in the example of Figure 3.8, referring to the section S_7. The tunnelling influence zone extends symmetrically for about 15-20 m from the tunnel axis.

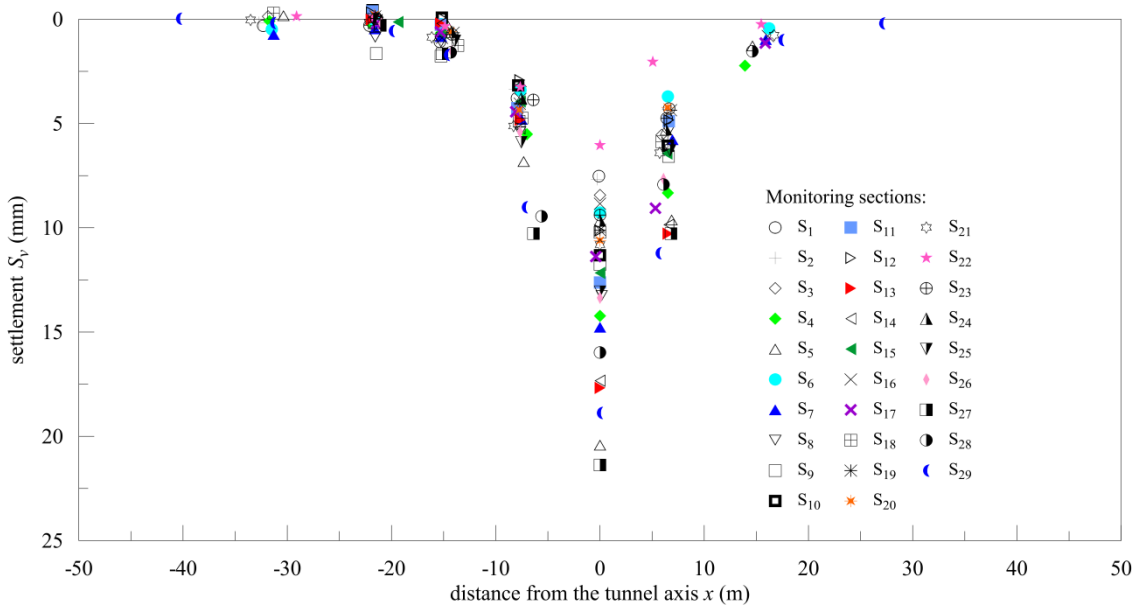

Figure 3.7. Settlements measured at ground surface after the first tunnel construction.

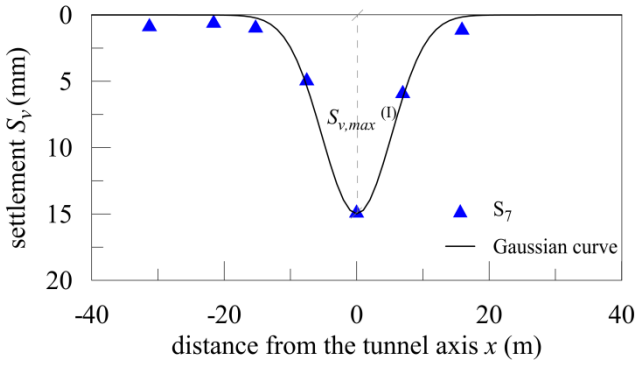

Figure 3.8. Example of measurement interpretation by a Gaussian empirical curve.

The resulting maximum settlement, $S_{v,max}^{(I)}$, volume loss, $V_L^{(I)}$ (%), and inflection point, i_x, are summarised in Table 3.3 and shown in Figure 3.9 as a function of the tunnel chainage.

It can be seen that $S_{v,max}^{(I)}$ is lower than 22.0 mm with an average value of about 12.0 mm, while $V_L^{(I)}$ is always lower than 0.90% with an average value of 0.50%, demonstrating a good achievement in the control of tunnelling. The range of $V_L^{(I)}$ varies from 0.27% to 0.82%, consistently with typical performances reported in the literature for tunnelling in granular soils with EPB or slurry shield (Leblais and Bochon, 1991; Ata, 1996). In fact, the magnitude of volume loss mainly depends on the type of ground and on the tunnelling method, as pointed out by Mair and Taylor (1997) based on several case histories discussed in the literature (e.g.: Peck, 1969; Cording and Hansmire, 1975; Clough and Schmidt, 1981; O'Reilly and New, 1982; Attewell et al. 1986; Uriel and Sagaseta, 1989; Mair, 1996). In particular, for closed face tunnelling adopting EPB machines in coarse-grained soils, a possible reference value for the average volume loss is $V_L^{(I)} = 0.50\%$ (Mair, 1996), which corresponds with that observed in the present study (see Tab. 3.3).

The observed inflection distance i_x, summarised in Table 3.3 and shown in Figure 3.9, varies only between 5.25 m and 6.45 m, indicating fairly uniform ground conditions.

Monitoring sections	$S_{v,max}^{(I)}$ (mm)	$V_L^{(I)}$ (%)	i_x (m)
S_1	7.5	0.33	6.00
S_2	7.7	0.33	6.00
S_3	8.4	0.37	6.00
S_4	14.2	0.58	5.55
S_5	20.4	0.80	5.25
S_6	9.3	0.38	5.70
S_7	14.8	0.56	5.25
S_8	13.3	0.54	5.70
S_9	11.8	0.45	5.25
S_{10}	11.3	0.42	5.25
S_{11}	12.6	0.47	5.25
S_{12}	10.1	0.41	5.55
S_{13}	17.7	0.70	5.55
S_{14}	17.3	0.67	5.40
S_{15}	12.2	0.46	5.25
S_{16}	8.8	0.40	6.45
S_{17}	11.4	0.50	6.00
S_{18}	10.2	0.44	6.00
S_{19}	10.1	0.39	5.25
S_{20}	10.6	0.41	5.25
S_{21}	10.8	0.48	6.00
S_{22}	6.0	0.27	6.00
S_{23}	9.4	0.36	5.25
S_{24}	9.6	0.39	5.55
S_{25}	13.1	0.50	5.25
S_{26}	13.4	0.54	5.55
S_{27}	21.4	0.82	5.25
S_{28}	16.0	0.70	6.00
S_{29}	18.9	0.82	6.00
average value	12.4	0.50	5.60

Table 3.3. Values of $S_{v,max}^{(I)}$, $V_L^{(I)}$ (%) and i_x at the monitoring sections between *San Siro* and *Segesta* stations.

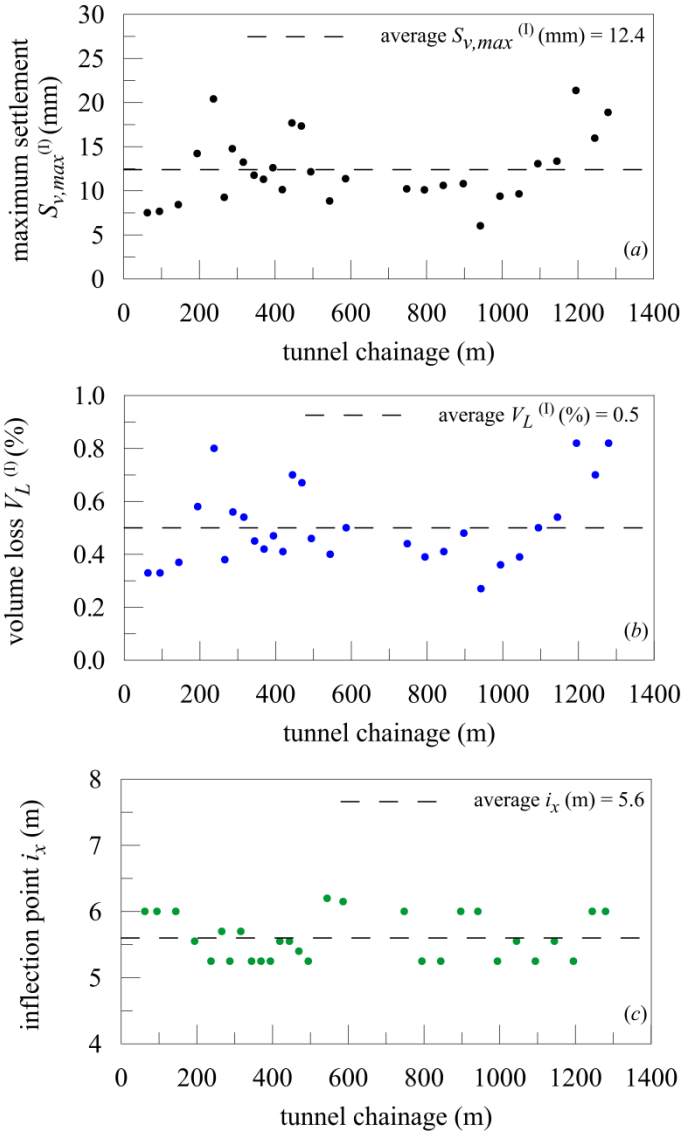

Figure 3.9. Values of $S_{v,max}^{(I)}$ (*a*), $V_L^{(I)}$ (*b*) and i_x (*c*) at the examined monitoring sections along the initial portion of the metro-line route.

A vast majority of the settlements measured at the ground surface falls in the range delimited by the Gaussian empirical predictions for K values equal to 0.25 (upper bound) and 0.45 (lower bound), as shown in Figure 3.10 in terms of normalised settlement curves. In particular, the figure shows that the Gaussian curve for $K = 0.35$ (i.e. $i_x = 5.25$ m) nicely fits the measurements within a horizontal distance of $x = \pm 2i_x$, while data recorded at larger distances are best-fitted by a Gaussian curve characterised by $K = 0.45$. A similar pattern was also observed by Grant and Taylor (2000) in

centrifuge model tests. It indicates that the Gaussian distribution as obtained for K = 0.35 may underestimate the magnitude of the settlements in the outer region of the subsidence trough.

This experimental evidence can be more effectively highlighted by plotting the same set of measurements in an alternative way, as illustrated in Figure 3.11. In this plot the curves are linearised in such a way that the inverse of their gradient is the inflection point, i_x.

Figure 3.12 illustrates the comparison between measured settlements at selected instrumented sections and the associated best empirical predictions as obtained for different K values in the range 0.35-0.40. Despite the limited variability of i_x (see Fig. 3.9 *c*), it is possible to observe from Figure 3.12 that the maximum settlement magnitude increases as i_x decreases, in accordance with Cording (1991).

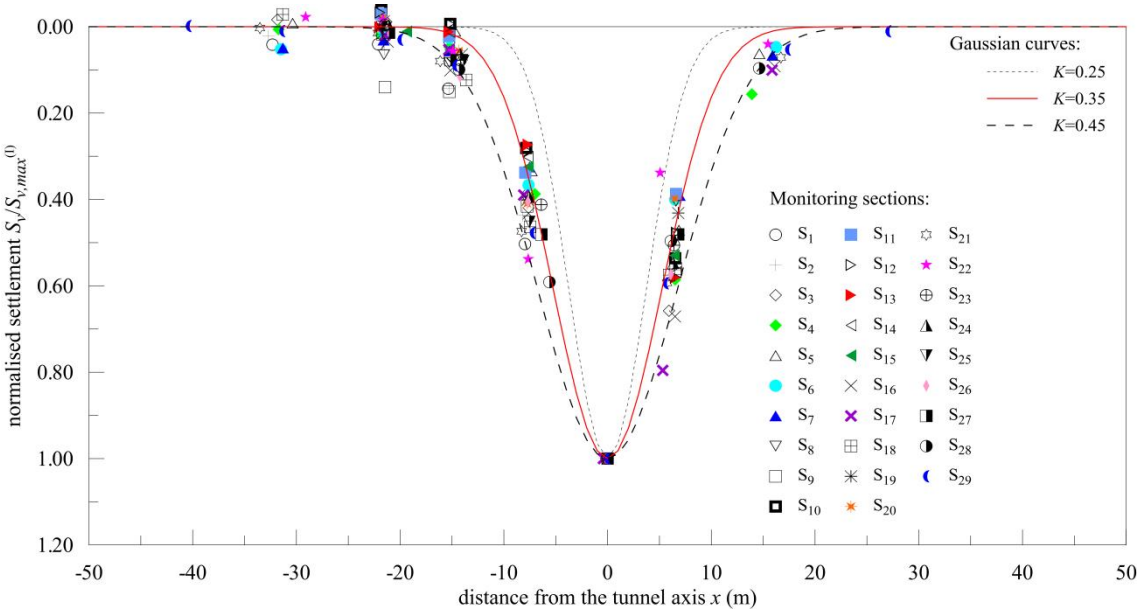

Figure 3.10. Normalised settlements measured at ground surface and comparison with Gaussian empirical curves.

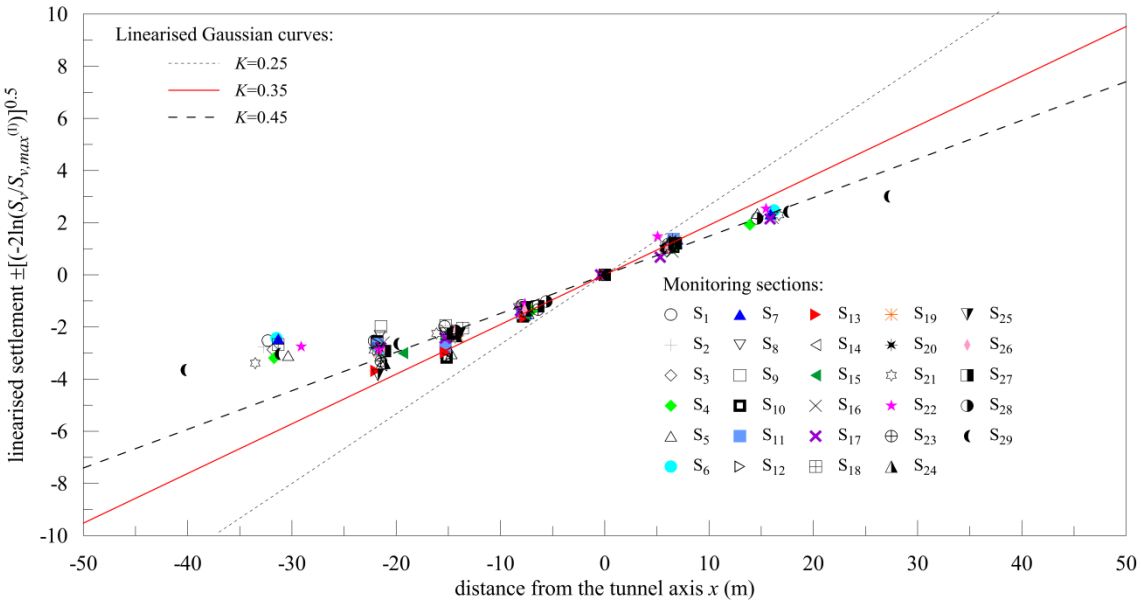

Figure 3.11. Linearised settlements at ground surface.

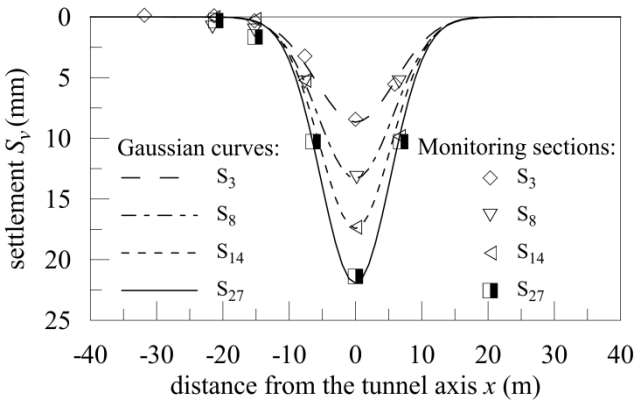

Figure 3.12. Transversal settlement profiles: trough widths and settlement magnitudes (i_x values for each section are reported in Table 3.3).

A possible explanation of such a feature can be provided with reference to limit conditions. In fact, several case-histories of tunnel failures in sand (Chambon and Corté, 1994) and in clay (Mair, 1979) shown that the corresponding mechanisms are markedly different: in clays it propagates upwards and outwards from the tunnel invert, becoming significantly wider than the tunnel diameter; in sands, failure involves a narrow "chimney" mechanism propagating almost vertically from the tunnel up to the ground surface. This latter mechanism was also observed in laboratory studies on tunnels in

sands (Cording et al., 1975; Potts, 1976). Although being far from failure conditions, the data reported in Figure 3.12 confirm such a trend, showing that larger settlements in granular soils tend to produce narrower troughs, consistently with the "chimney" mechanism discussed above.

The evolution of the measured settlements at the tunnel centre line ($x = 0$) is presented in Figure 3.13 as a function of the face distance. Figure 3.14 shows in detail the example of section S_{11}, where the settlement evolution is interpreted by the cumulative Gaussian probability curve (Eq. 2.9 of Chap. 2) to define the longitudinal settlement trough, assuming the values of volume loss and i_x reported in Table 3.3 and considering $i_y = i_x$. A similar approach was adopted for all the sections under study.

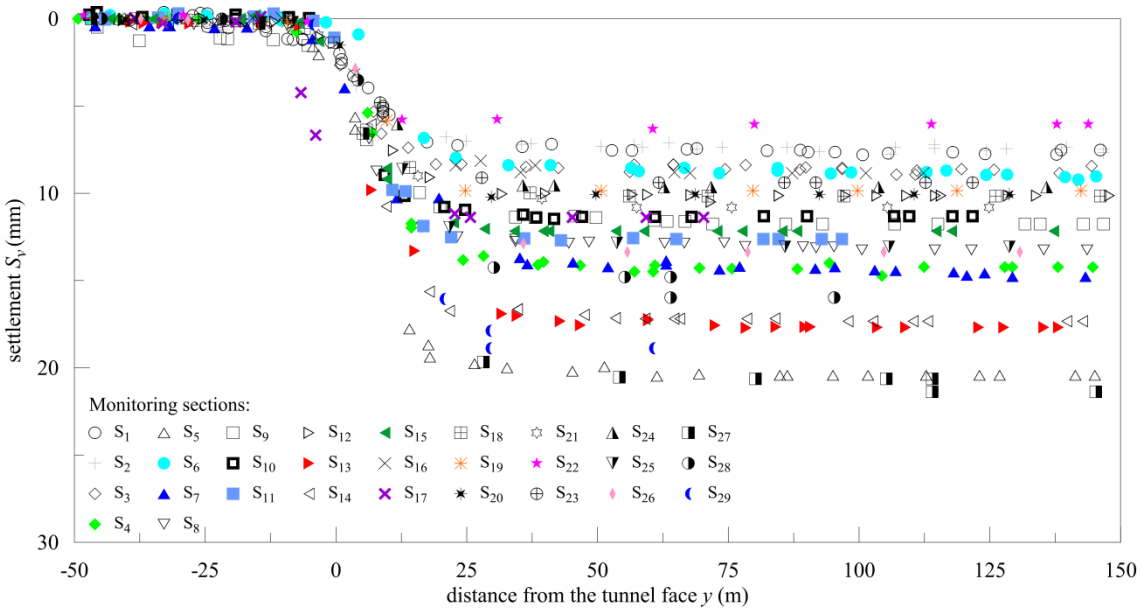

Figure 3.13. Settlement measured at the ground surface above the first tunnel axis as a function of the tunnel face distance.

The settlement magnitude at the tunnel face depends on the tunnel construction technology. Attewell and Woodman (1982) examined several case-histories of tunnelling in clays, concluding that the surface settlement directly above the tunnel face generally corresponds to about 0.5 $S_{v,max}$ for tunnels excavated in stiff clays without

face support, while showing values lower than 0.5 $S_{v,max}$ for tunnels in soft clays with face support provided by compressed air, as also reported in Mair and Taylor (1997).

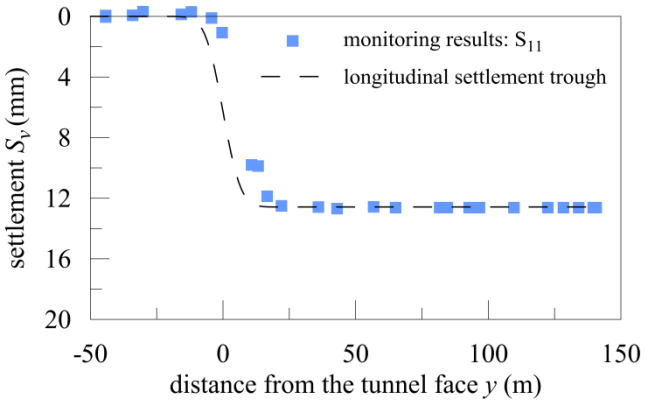

Figure 3.14. Example of measurement interpretation by a cumulative Gaussian curve.

This is due to the fact that pressurised face tunnelling tends to limit ground movements ahead of the tunnel face.

Field observations for shield tunnelling in loose silty-sand and soft clay (Moh et al., 1996), in sands or silts (Nomoto et al., 1995) and in medium to dense sands overlain by a clay layer (Ata, 1996), indicate that the major construction settlement is related to the tail void, leading to surface settlement directly above the tunnel face generally much lower than 0.5 $S_{v,max}$. This typically induces a horizontal translation of the Gaussian cumulative curve (Mair and Taylor, 1997). This evidence is also supported by centrifuge data (Imamura et al., 1998), irrespective of the ground condition (Sugiyama et al., 1999).

Measurements of vertical displacements close (i.e. ± 1m) to the tunnel face, $S_{v,f}$ $^{(I)}$, in this segment of the route, were only available for 6 sections (i.e.: S_1; S_3; S_7; S_{11}; S_{18}; S_{20}) out of the 29 ones examined. For those monitoring sections the surface settlements at the tunnel face are in the range of 0.09-0.32 $S_{v,max}^{(I)}$, as summarised in Table 3.4, indicating a satisfactory control of the face support during the excavation process.

Monitoring sections	$S_{v,max}^{(I)}$ (mm)	$S_{v,f}^{(I)}$ (mm)	$S_{v,f}^{(I)}/S_{v,max}^{(I)}$
S_1	7.5	2.0	0.26
S_3	8.4	2.7	0.32
S_7	14.8	4.0	0.27
S_{11}	12.6	1.1	0.09
S_{18}	10.2	1.4	0.13
S_{20}	10.6	1.5	0.14

Table 3.4. Maximum settlement $S_{v,max}^{(I)}$, tunnel face settlement $S_{v,f}^{(I)}$ and $S_{v,f}^{(I)}/S_{v,max}^{(I)}$ ratio at the monitoring sections between *San Siro* and *Segesta* stations.

Figure 3.15 shows the original and translated cumulative curves for the 6 monitored sections, the latter being obtained equating the empirical ratio $S_{v,f}^{(I)}/S_{v,max}^{(I)}$ to the measured one: the consistency between the longitudinal surface settlement trough and the translated cumulative curve indicates that the main source of settlements is far from the face, as suggested in the literature (Mair and Taylor, 1997; Ata, 1996; Imamura et al., 1998; Sugiyama et al., 1999).

For all the other sections, where face settlement measurements were not available, the corresponding translation ratio $S_{v,f}^{(I)}/S_{v,max}^{(I)}$ was obtained by the settlement best-fitting curve: its lowest value is equal to 0.02, an even lower value as compared to that observed in the fully monitored 6 sections mentioned above.

Figure 3.16 illustrates all the available longitudinal data as plotted in terms of normalised settlements, together with the best-fitting translated longitudinal troughs obtained for sections S_6 ($S_{v,f}^{(I)}/S_{v,max}^{(I)}$= 0.02) and S_3 ($S_{v,f}^{(I)}/S_{v,max}^{(I)}$= 0.32). The figure shows that a vast majority of data falls in the range delimited by these curves within a distance from the face of $y_1 = -i_y$ and $y_2 = 3.5i_y$ (for $i_y = i_x = 5.6$ m, the average i_x value indicated in Fig. 3.11). However, the empirical profile is not able to accurately predict the settlements occurring for $y < y_1$, nor to capture the correct distance from the face at which, for $y > y_2$, steady-state conditions are achieved, this latter condition being predicted at a shorter distance from the face than observed.

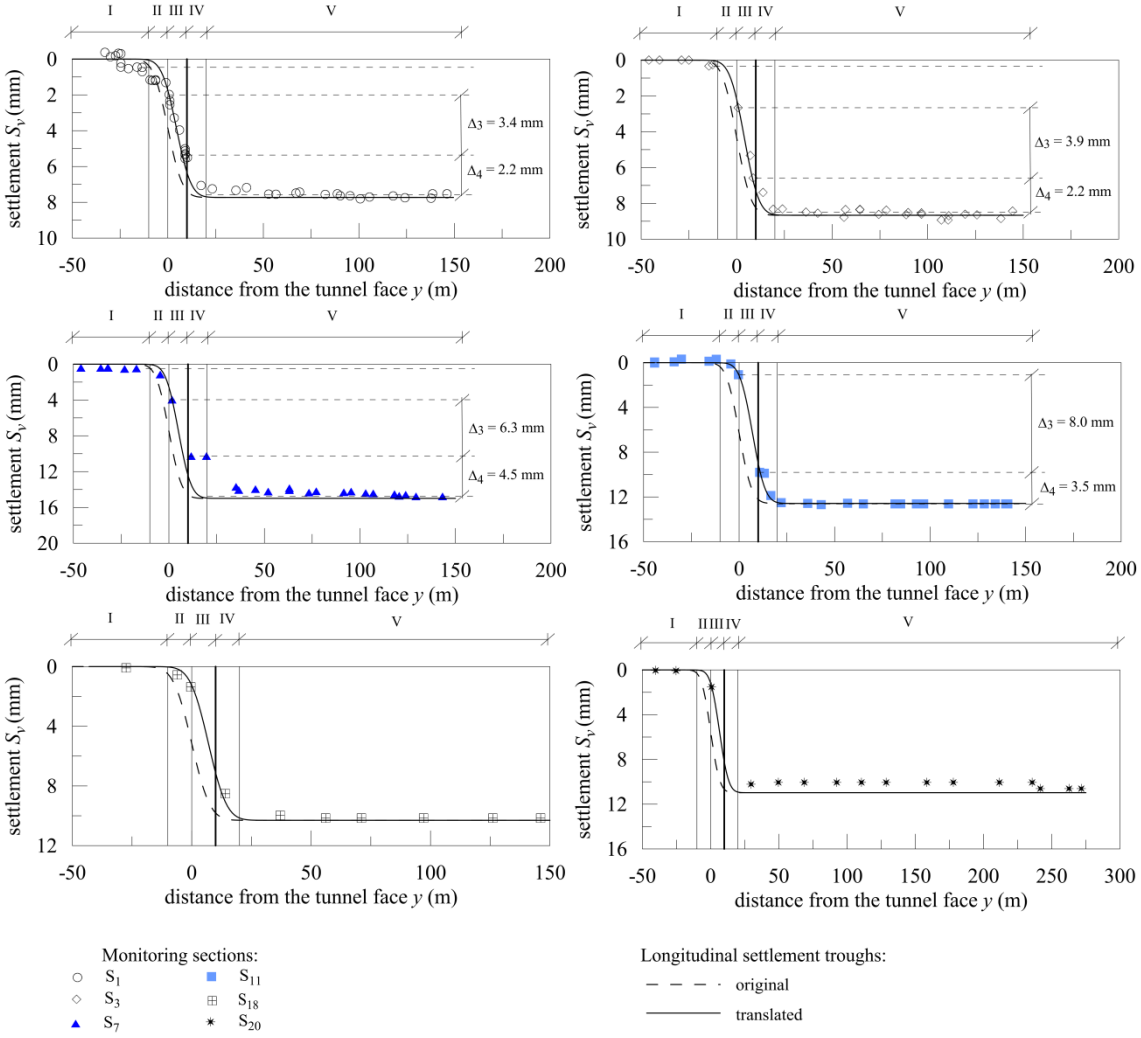

Figure 3.15. Settlements measured at the ground surface above the first tunnel axis and longitudinal settlement troughs.

In an ideal problem, longitudinal settlements over tunnel axis can be divided into 3 different main components (Mho et al., 1996; Hulme et al., 1990): the first one associated with the shield advancing, the second one related to the tail void and the third one eventually due to consolidation in fine-grained soils. When analysing ground movements, it is proposed to consider only the first two components, as the long-term consolidation settlement is governed by a different mechanism which should be examined separately (Moh and Hwang, 1993). This latter settlement component is not relevant in the case under study, since the excavation is carried out in coarse-grained

soils. More in detail, with reference to Figure 3.15 the following stages can be considered in the case under study, following Sugiyama et al. (1999): settlements cumulated ahead of the tunnel face, generally negligible (I); settlements occurring at the arrival of the tunnel face in the monitoring section (II); settlements added during the passage of the TBM from the face to the shield tail (III) and the final contribution accounting for the residual settlement, due to the interaction with the lining, up to the steady-state condition (IV).

Settlement measurements recorded immediately after the shield passage (i.e. at a distance from the face of about 10 m) are available only for the sections S_1; S_3; S_7; S_{11}.

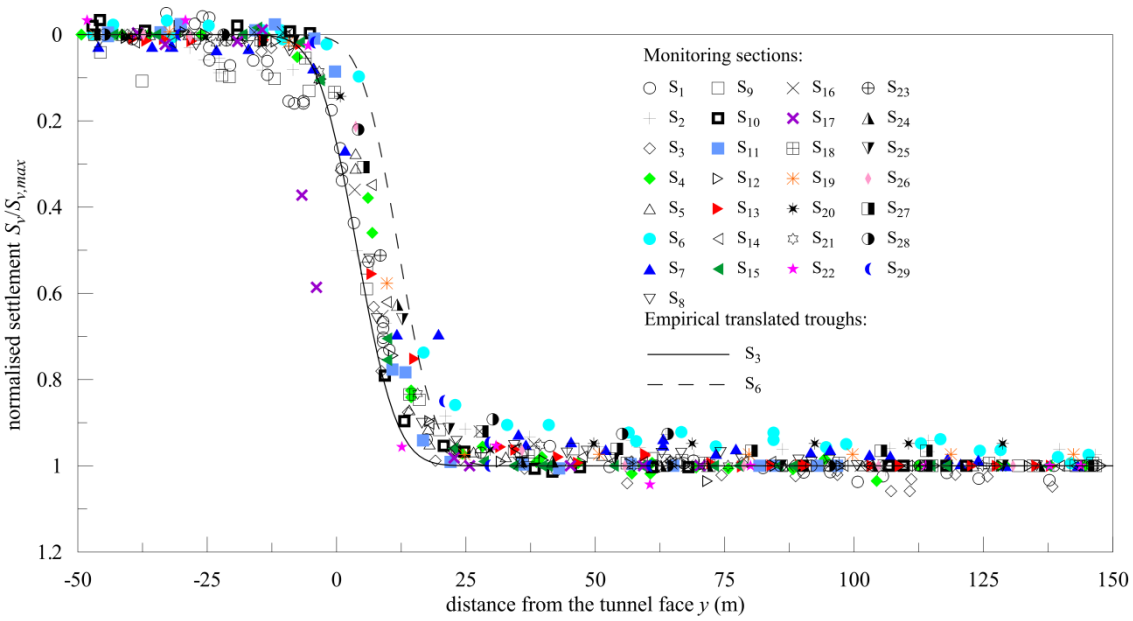

Figure 3.16. Normalised settlements measured at the ground surface above the tunnel axis and longitudinal settlement troughs.

At these 4 locations the settlement components (Δ_3, Δ_4) associated to the III and IV stages of tunnel excavation were evaluated and reported in Figure 3.15. The mean ratio Δ_4/Δ_3 is of about 60%. It can be observed that the majority of the settlements occurs at the shield passage (III), with a smaller portion taking place at the tail void (IV): this should be related to the efficiency of the grouting injection activity carried out soon

after the passage of the TBM to fill the tail void at the scope of minimising the ground movements. This aspect is further discussed in the following.

3.4.2 Ground settlements recorded between Lotto and Portello stations

Transversal and longitudinal ground settlement profiles induced by the excavation of the first tunnel along the *Lotto-Portello* segment of the metro-line (Fig. 3.17) are represented in Figure 3.18 (*a*) and (*b*), respectively.

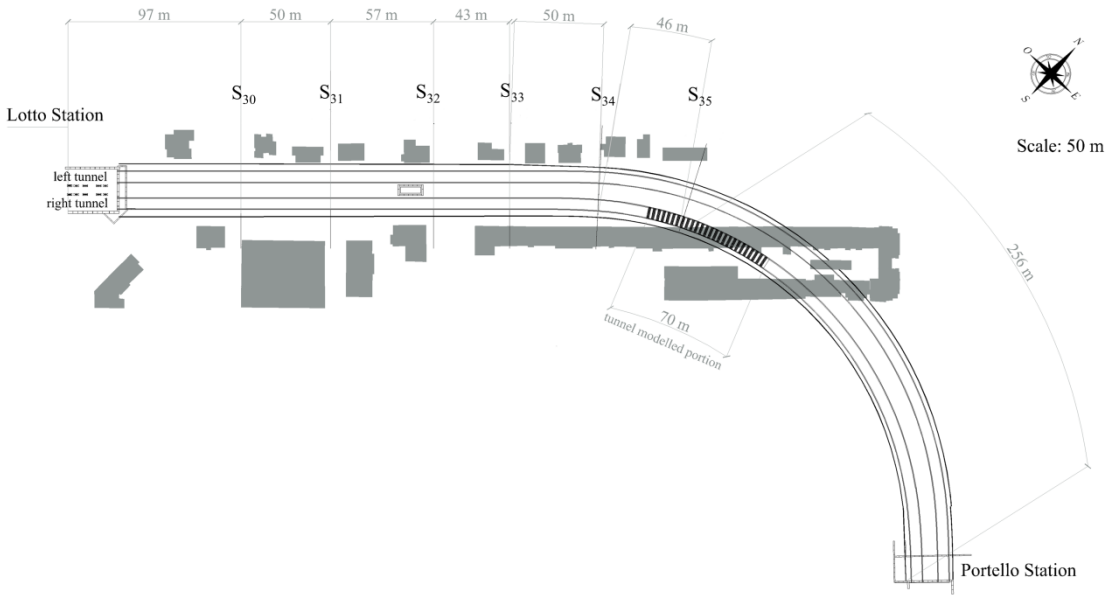

Figure 3.17. Plan view of the *Lotto-Portello* segment of the Milan metro-line 5.

Transversal profiles, in particular, refer to fully developed settlements achieved when the first tunnel face was at a sufficient distance from the monitoring sections. The maximum settlement $S_{v,max}$ (I) is generally very low and never exceeds 7 mm.

Along this portion of the route too, the transversal settlement troughs result to be sufficiently well fitted by a Gaussian distribution curve with K values in the range 0.40-0.45, with the exception of the leftmost points of each section, whose values are under-predicted by the empirical relation (Fig. 3.19); this is probably due to the influence of nearby surface structures located along this segment (see Fig. 3.17).

The above interpolation allowed to back-evaluate the corresponding volume loss, $V_L^{(I)}$ (%), which varies from 0.30% to 0.38% with an average value equal to 0.33%, indicating, along this portion of the metro-line too, a well-performing EPB excavation (e.g. Ata, 1996; Leblais and Bochon, 1991; Mair, 1996; Mair and Taylor, 1997).

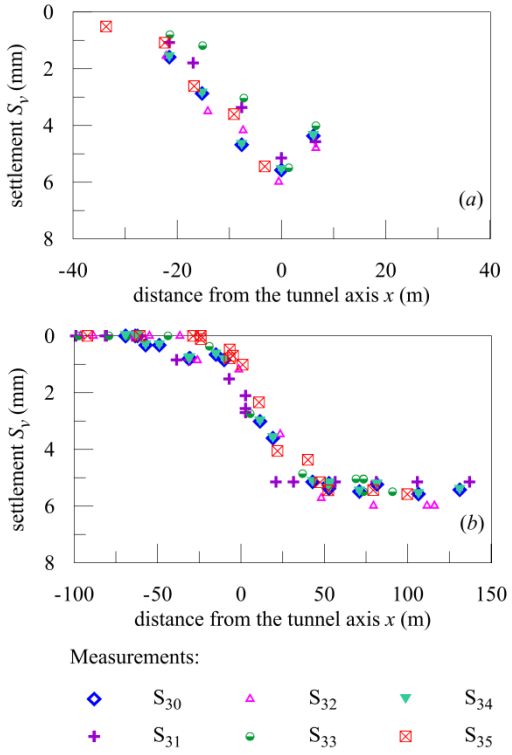

Figure 3.18. Settlement measurements at ground sections in transversal (*a*) and longitudinal (*b*) directions.

The values of maximum settlement $S_{v,max}^{(I)}$, K parameter and volume loss $V_L^{(I)}$ for all the considered sections (i.e. from S_{30} to S_{35}) are summarised in Table 3.5. The table also reports the different depth of the tunnel axis, z_0, at each location and the recording date of the analysed settlement measurements.

Settlements surveyed at section S_{35} located near a multi-storey reinforced concrete building undercrossed by the first tunnel of the metro-line was investigated with special accuracy.

Monitoring sections	$S_{v,max}^{(I)}$ (mm)	K (-)	$V_L^{(I)}$ (%)	z_0 (m)	date
S_{30}	5.6	0.45	0.38	20.0	16/12/2012
S_{31}	5.2	0.42	0.30	19.0	18/12/2012
S_{32}	6.0	0.45	0.37	18.0	20/12/2012
S_{33}	5.5	0.42	0.30	17.0	08/01/2013
S_{34}	6.5	0.40	0.31	16.0	10/01/2013
S_{35}	5.5	0.45	0.34	15.0	15/01/2013

Table 3.5. Values of maximum settlement, *K* parameter, volume loss, axis depth and surveying date at the reference monitoring sections.

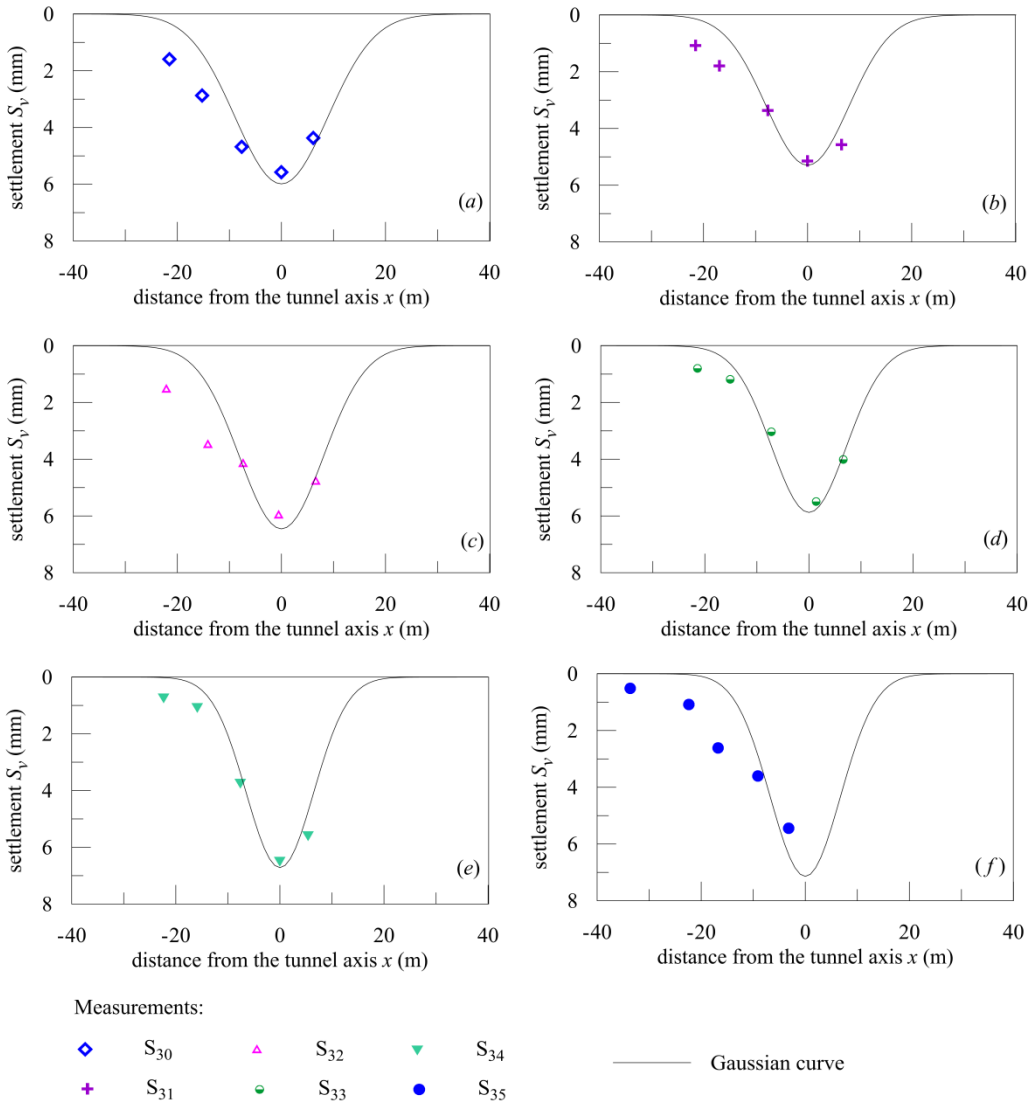

Figure 3.19. Transversal settlement troughs: measurements and best-fitting Gaussian curves.

Measurements recorded at such section at the passage of the tunnel face and of the shield tail are shown in Figure 3.20 together with the best-fitting empirical curves ($K = 0.45$). The estimated volume loss values are equal to 0.06% and 0.14%, respectively.

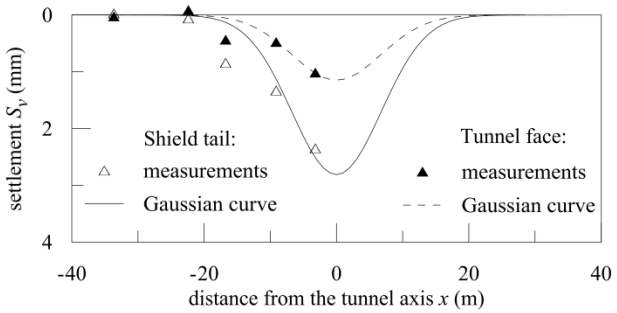

Figure 3.20. Measurements collected at section S_{35} after the passage of the tunnel face and of the shield with the corresponding best-fitting Gaussian curves.

The evolution of settlement above the tunnel centre line is presented in Figure 3.21 as a function of the face distance for sections S_{32} and S_{35}, for which measurements of vertical displacements close to the tunnel face (i.e. ± 1m) were available.

The tunnel face settlement, $S_{v,f}^{(I)}$, at these locations is equal to about 1 mm, indicating a very satisfactory face support during the excavation process.

Measurements were interpreted at each location by the cumulative Gaussian probability curve (Attewell and Woodman, 1982) in order to define the longitudinal settlement trough, assuming the volume loss and K values reported in Table 3.5 and considering $i_y = i_x$. As shown in Figure 3.21, at these sections too face settlements are best-fitted by the translated Gaussian cumulative curve (Mair and Taylor, 1997), obtained equating the ratio $S_{v,f}^{(I)}/S_{v,max}^{(I)}$ to the measured one. This translated profile, however, is not able to capture the further evolution of settlements, predicting the achievement of steady-state conditions well before what observed *in situ*.

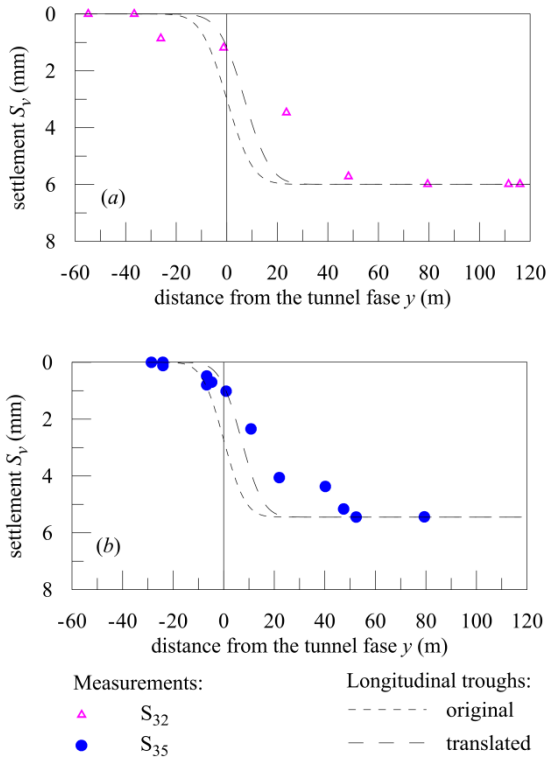

Figure 3.21. Settlements measured above the tunnel centre line at the monitoring sections S_{32} (*a*) and S_{35} (*b*) with original and translated longitudinal profiles.

3.4.3 Effects induced on ground settlements by the excavation of the second metro-line tunnel

Maximum settlements measured after the second excavation above the second tunnel axis, $S_{v,max}^{(II)}$, are summarised in Table 3.6 for the 29 monitoring ground sections (from S_1 to S_{29}) between *San Siro* and *Segesta* stations and for the 6 sections (from S_{30} to S_{35}) between *Lotto* and *Portello* stations. It varies from 8.0 mm to 27.8 mm with an average value of about 12.0 mm.

The construction of the second tunnel produces an increase in settlement above the axis of the first tunnel on average equal to 30%. The final vertical displacement recorded above the first tunnel axis after the second excavation, identified as $S'_{v,max}^{(I)}$ and reported in Table 3.6, ranges from 6.0 mm to 24.8 mm with an average value of about 15.0 mm.

Monitoring sections	$S'_{v,max}^{(I)}$ (mm)	$S_{v,max}^{(II)}$ (mm)	$V_L^{(TOT)}$ (%)
S_1	10.0	11.0	0.88
S_2	10.2	10.8	0.88
S_3	11.1	12.3	0.99
S_4	17.5	17.9	1.41
S_5	23.1	8.0	1.19
S_6	10.0	8.7	0.75
S_7	16.2	9.5	0.98
S_8	14.4	10.7	1.02
S_9	13.5	13.7	1.03
S_{10}	13.2	11.7	0.95
S_{11}	14.6	10.7	0.96
S_{12}	12.2	13.8	1.03
S_{13}	20.5	27.8	1.89
S_{14}	19.4	15.1	1.33
S_{15}	14.2	11.6	0.97
S_{16}	11.3	10.6	0.95
S_{17}	15.1	11.0	1.06
S_{18}	12.7	11.3	0.99
S_{19}	12.6	9.6	0.84
S_{20}	13.2	9.5	0.85
S_{21}	13.3	9.3	0.94
S_{22}	6.0	8.8	0.62
S_{23}	12.4	10.1	0.85
S_{24}	12.9	11.0	0.94
S_{25}	16.6	12.7	1.10
S_{26}	17.7	12.5	1.18
S_{27}	24.8	15.7	1.51
S_{28}	20.1	16.1	1.50
S_{29}	23.8	19.7	1.81
S_{30}	11.4	12.1	1.05
S_{31}	10.3	11.9	1.00
S_{32}	8.3	9.6	0.81
S_{33}	8.2	8.4	0.74
S_{34}	10.1	10.0	0.85
S_{35}	8.7	9.2	0.84

Table 3.6. Values of final settlements and volume loss at the end of the second tunnel excavation.

In addition, different values of the final settlement above the two tunnel axes along the same monitoring section typically occur, suggesting an asymmetry of the subsidence troughs (Fig. 3.22), with a maximum vertical displacement localised in correspondence with the first tunnel for 22 sections out of the 35 ones examined.

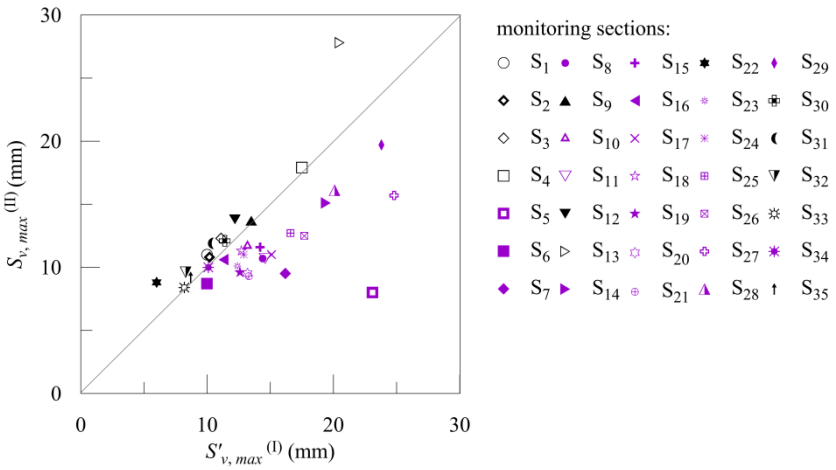

Figure 3.22. Final settlements recorded above the first and the second tunnel axis.

Tunnelling-induced settlements were fitted by the empirical relation proposed by New and O'Reilly (1991) (Eq. 2.19 of Chap. 2) for the case of twin tunnels using, for each monitoring section, the same *K* values adopted for the single tunnel configuration (see Tabs. 3.3 and 3.5). This interpolation allows to evaluate the corresponding final volume loss $V_L^{(TOT)}$ in Table 3.6, which ranges from 0.62% to 1.89% with a mean value equal to about 1.0 % (that is twice $V_L^{(I)}$).

The comparison between measurements and empirical back-predictions for the final configuration of twin tunnels, shown as an example in Figure 3.23 for sections S_{16}, S_{19} and S_{35}, is fairly consistent in all the analised sections; however, the magnitude of the settlement at the measuring point between the tunnel axes is most of the times underestimated by the empirical curve proposed by New and O'Reilly (1991), as shown Figure 3.23 (*b*) and (*c*).

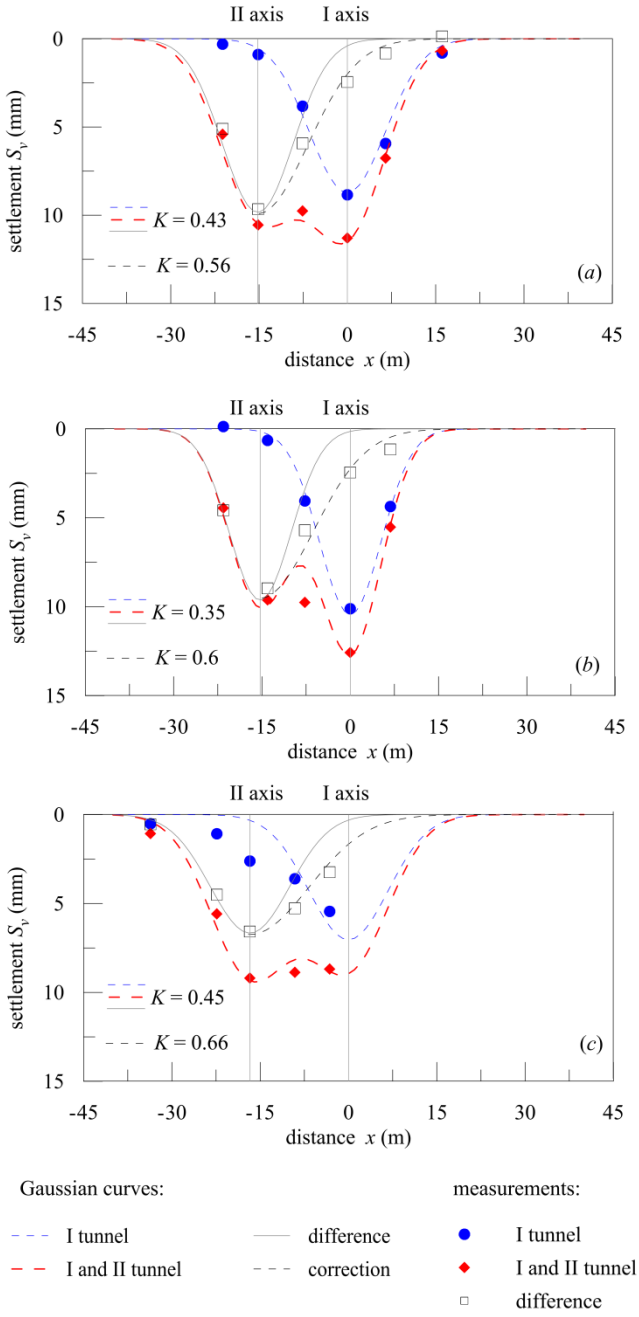

Figure 3.23. Interpretation of measurements by Gaussian empirical curves at monitoring sections S_{16} (*a*), S_{19} (*b*) and S_{35} (*c*) (the reference *K* values are also reported in each plot).

The analysis carried out in the present study indicates that, in general, the sum of the individual Gaussian curves for a single tunnel to predict the vertical movements above twin tunnels, neglecting any interaction effect, may not give realistic settlement profiles (Addenbrooke and Potts, 2001; Cooper et al., 2002; Chapman et al., 2007). This

procedure, in fact, does not take in account that the soil around the first tunnel has already experienced a certain amount of stress relief and strain accumulation which is very likely to reduce its initial stiffness.

This aspect becomes more evident when looking at the vertical displacements obtained by subtracting the settlements measured after the first tunnel excavation from the final values (Fig. 3.23). These data, which represent the settlements induced only by the second excavation (Perez Saiz et al., 1981; Suwansawat and Einstein, 2007), are not symmetric: in fact, the values on the left side of the axis of the second tunnel are well interpreted by the empirical Gaussian curve proposed by Peck (1969) (Eq. 2.1 of Chap. 2,) which, conversely, underestimates the data on the right side.

As suggested in the literature (e.g. Chapman et al., 2007), the trough width parameter i_x could be increased for the second tunnel on the side nearest to the first tunnel in order to take into account the interaction effects. For the investigated case, such a parameter was increased in the region where x > -15 m (Fig. 3.23) using K values included in the range 0.42-0.70 to obtain a more adequate interpolation of the measurements. The above evidence confirms that, also for this case-history, the presence of an existing tunnel alters the expected pattern of vertical ground movements induced by a new excavation.

The evolution of the settlement profile with the excavation advancement along three different transversal sections during the critical construction stages of the second tunnel (i.e. the passage of the face and shield) is shown in Figure 3.24. At these locations the components of settlement Δ_2, Δ_3 and Δ_4, already defined in the previous Section 3.4.1, were evaluated above the second tunnel.

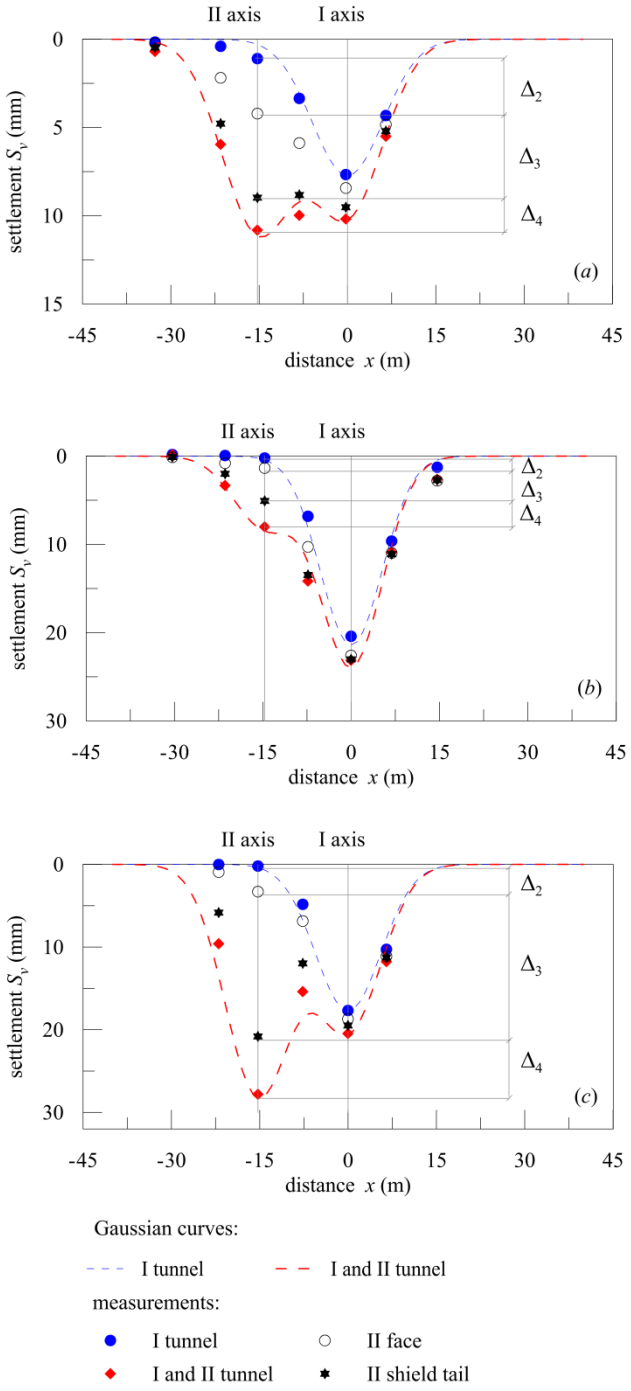

Figure 3.24. Settlement evolution during reference stages of the second tunnel construction at selected sections S_2 (*a*), S_5 (*b*) and S_{13} (*c*).

These data confirm that the largest contribution is that related to the shield passage (Δ_2), with a smaller but non-negligible fraction occurring later (Δ_4), probably during the back-filling operation (e.g.: Sugyama et al., 1999; Fargnoli et al., 2013).

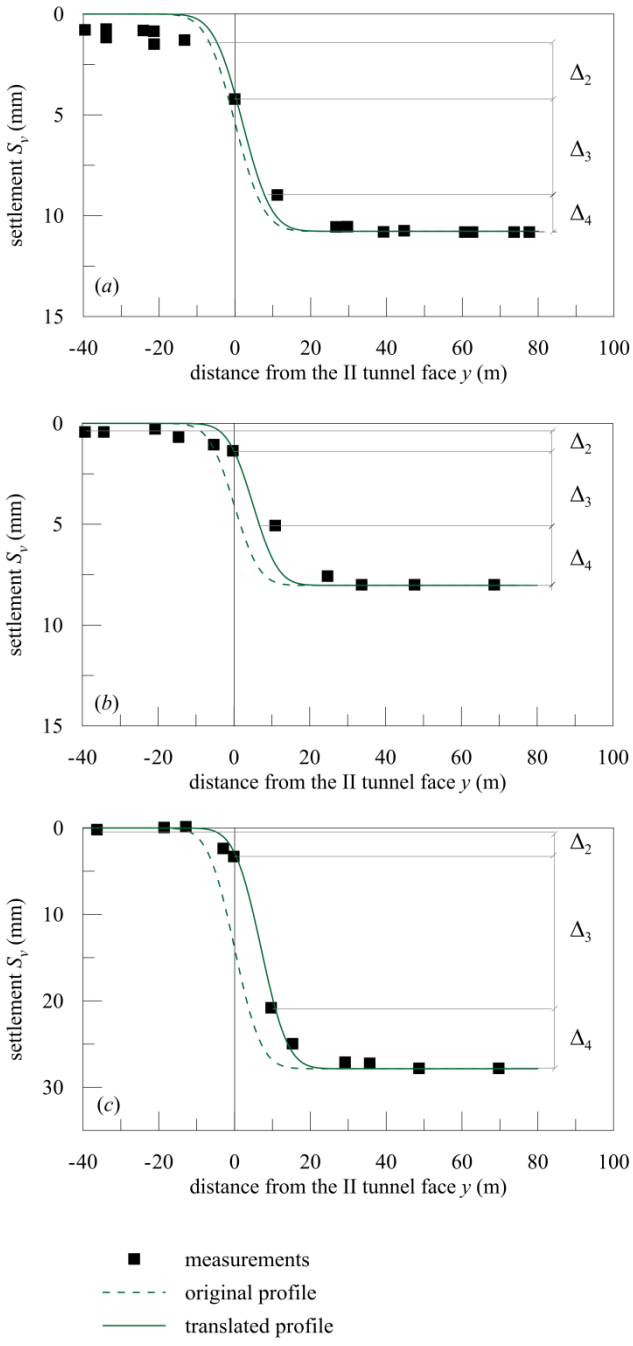

Figure 3.25. Interpretation of measurements above the second tunnel by original and translated cumulative Gaussian curves at sections S_2 (*a*), S_5 (*b*) and S_{13} (*c*).

Figure 3.25 illustrates, with reference to the same sections (S_2, S_5 and S_{13}), a longitudinal representation of the settlements above the second tunnel axis together with the original (Eq. 2.9 of Chap. 2; Attewell and Woodman, 1982) and translated (Mair and Taylor, 1997) Gaussian cumulative curves.

The figure highlights that, also in these sections, the face settlements are best-fitted by the translated Gaussian cumulative curve and it confirms the above discussed limits of the empirical relation that predicts the attainment of final conditions too early with respect to what indicated by *in situ* measurements.

3.4.4 Excavation parameters influencing ground settlements

EPB machine parameters were continuously monitored during the excavation works in order to control tunnelling-induced subsidence.

In this section the effect of the following parameters on the ground settlements due to the first tunnel excavation is firstly analysed: support pressure at the tunnel face (Branque et al. 2002; Dimmock et al., 2002; Guedes de Melo and Santos Pereira, 2002; Shirlaw et al., 2002; Suwansawat, 2002; Phienwej et al., 2006; Sirivachiraporn and Phienwej, 2012); grouting pressure for the back-filling of the concrete lining (Peila et al., 2011; Bilotta and Russo, 2012; Russo et al., 2012; Sirivachiraporn and Phienwej, 2012); machine stop time at monitored sections (Sirivachiraporn and Phienwej, 2012); installation time for one-ring tunnel lining; machine thrust against the existing tunnel lining to advance during the boring process (Branque et al., 2002; Dimmock et al., 2002).

The excavation parameters are plotted in Figure 3.26, while their average values are summarised in Table 3.7. In particular, Figure 3.26 (*a*) highlights that the face pressure values applied along the initial portion of the route, on average equal to about 200 kPa, are higher than the total horizontal stress acting at rest in correspondence with the tunnel invert (i.e. 185 kPa) and this is probably due to the start-up phase of tunnelling. After this stage, in fact, the values of the face support pressure were lower and, on average, equal to 132 kPa. Figure 3.26 (*b-e*) shows a more regular trend of all the other excavation parameters along the examined metro-line route.

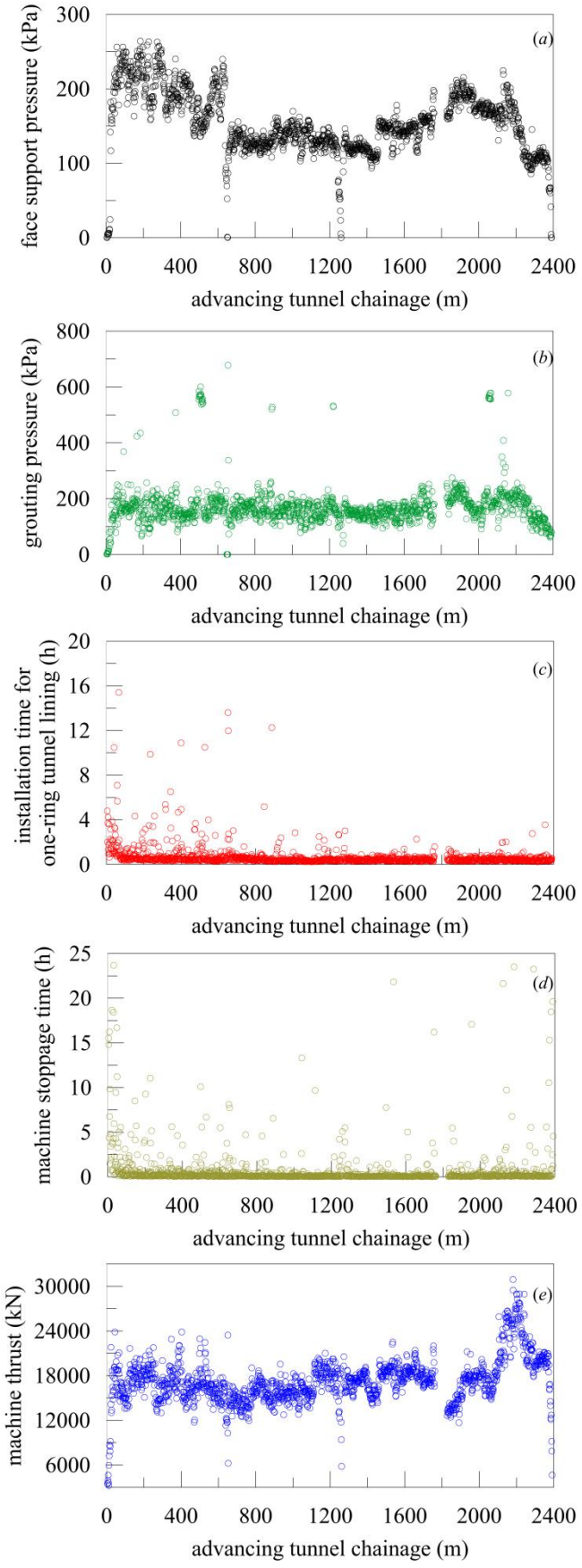

Figure 3.26. Excavation parameters recorded during the first tunnel advancement.

As observed in the previous Section 3.4.1, most of the construction settlement is associated to the shield passage. However, the ground movements induced by this tunnelling stage cannot be controlled during the machine advancement (Sugiyama et al., 1999).

In this study an attempt was first made to relate face settlements (available in a few monitored sections) to face pressure, but in this respect no direct correlation could be extracted from the few analysed monitoring data. However, all the data indicates that face pressure clearly contributes in limiting the settlements at the tunnel face, as previously discussed with reference to the values of the ratio $S_{v,f}^{(I)}/S_{v,max}^{(I)}$.

A second and more extended analysis, performed on all the 35 monitoring sections, was carried out to explore the existence of possible correlations between the volume loss $V_L^{(I)}$ associated to the settlement $S_{v,max}^{(I)}$ and the excavation parameters, as recorded along a tunnel length of 8.4 m (that is six times the size of the tunnel lining ring, i.e. 4.2 m ahead and 4.2 m behind the monitored section).

Correlations are observed in the case of face and grouting pressures, as shown in Figure 3.27 (*a*) and (*b*). In detail, the figure plots both the recorded data and their average values, grouped according to eight classes of pressure defined in the interval 90-250 kPa. The data, although relatively dispersed, indicate a trend which proves the role of face and grouting pressures in mitigating settlements and in reducing the related volume loss. Grouting pressure plays a direct role in the settlement contribution Δ_4, which is related to the injection activity carried out soon after the passage of the TBM to fill the tail void. As already discussed above, this contribution is small as compared to that due to the shield passage, in contrast to what shown in Figure 3.27 (*b*) where an evident reduction of the overall $V_L^{(I)}$ is observed for increasing values of grouting pressure.

This feature can be interpreted assuming that the tail grouting can also play a non-negligible role in inhibiting volume losses induced by the shield passage, in relation to possible longitudinal arching effects, which can extend its supporting role towards the shield.

Excavation parameters	Average values
face support pressure (kPa)	168
grouting pressure (kPa)	150
installation time for one-ring tunnel lining (h)	0.65
machine stop time (h)	0.62
machine thrust (kN)	17300

Table 3.7. Average values of the excavation parameters recorded during the first tunnel advancement.

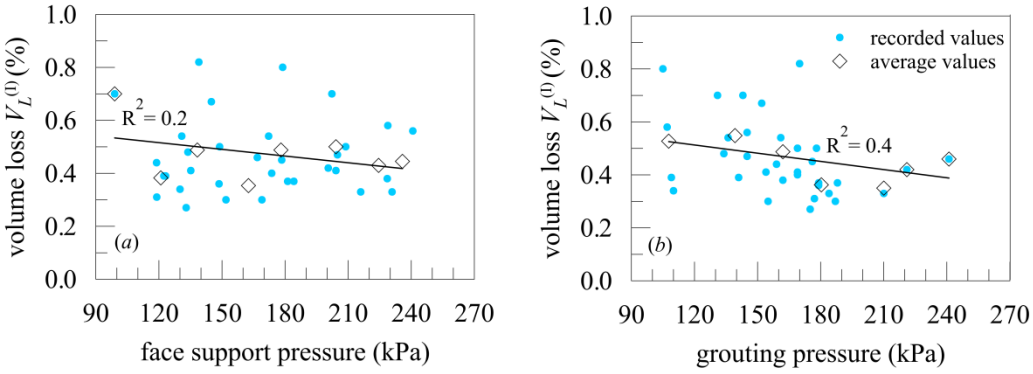

Figure 3.27. Observed trend of face pressure (*a*) and grouting pressure (*b*) with volume loss due to the first tunnel excavation.

As discussed in Section 3.4.3, monitoring data show that the maximum vertical displacement is generally recorded in correspondence with the first or the second tunnel axis. Maximum vertical displacements above the two tunnel axes are reported in Figure 3.28 (*a*) together with the corresponding face and grouting pressure values (Fig. 3.28 *b* and *c*, respectively) that were found to be the main excavation parameters influencing the settlements due to the first tunnel construction.

Figure 3.28 (*b* and *c*) shows, in particular, the average values of these excavation parameters as recorded along a tunnel length of 8.4 m, already defined as a function of the size of one tunnel lining ring.

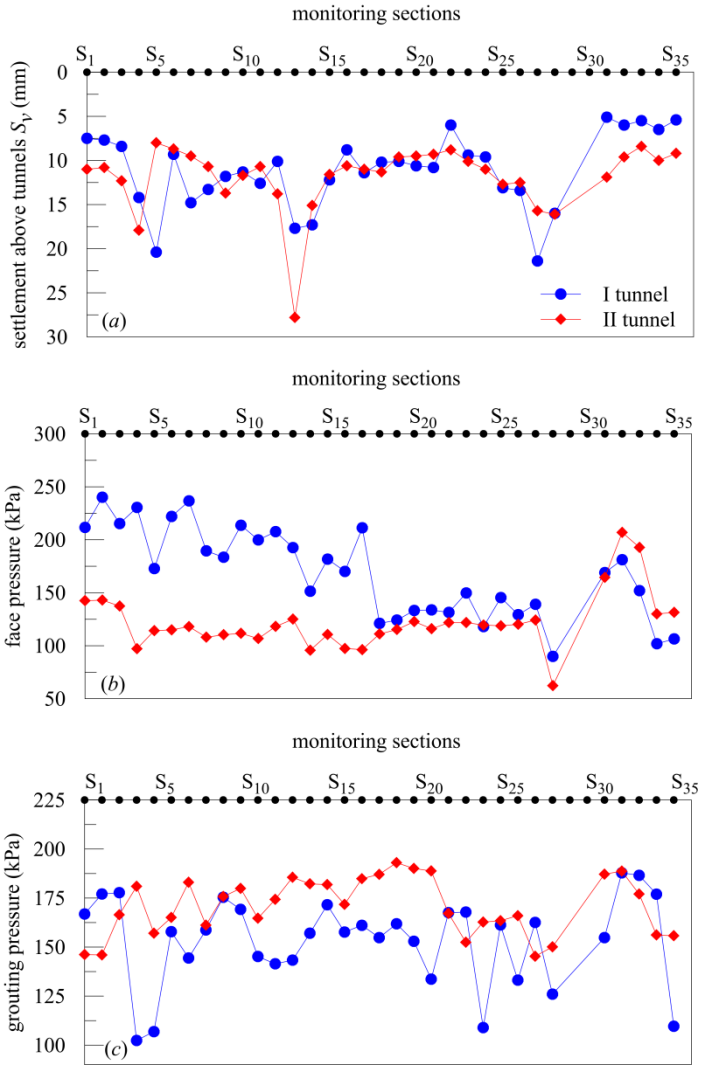

Figure 3.28. Recorded settlements above the tunnel axes (*a*) with grouting (*b*) and face (*c*) pressure values at the reference sections (the grouting and face pressure values at sections S_{29} and S_{30} are not available).

Figure 3.28 (*b*) shows that, after the start-up phase of tunnelling (i.e. from section S_{17} on), the values of the support pressure at the first tunnel face are almost coincident with those applied, more regularly, during the excavation of the second tunnel (mean value of about 122 kPa) along the entire examined route.

Concerning the grouting pressure, it is possible to observe (Fig. 3.28 *c*) a larger variability of the recorded data during the whole excavation of the first tunnel with respect to the second one, despite the rather similar average values (equal to 150 kPa and 170 kPa for the first and the second tunnel, respectively).

No statistic correlations between such excavation parameters and the recorded final settlements emerge from the analysis of the data. It is possible to highlight, however, some trends in specific areas of the route.

In particular, the sections interested by rather constant settlements above the two tunnel axes (e.g. from section S_{18} to section S_{26}) are also characterised by rather regular values of the face pressure (Fig. 3.28 *a*, *b*). In some occasional cases, a decrease in the face support pressure is associated to an increase in the settlement (e.g. section S_{28}) and vice versa (e.g. section S_{31}).

Moreover, it is possible to notice that, in general, the higher the settlement above the first tunnel axis, the lower the values of the grouting pressure (Fig. 3.28 *a*, *c*). In particular, the monitoring sections interested by higher vertical displacements above the first tunnel axis are also characterised by larger settlements above the second one, despite the generally larger values of the grouting pressure applied for the second excavation.

3.4.5 Structural monitoring

The data presented and discussed in this section are vertical displacements recorded during the excavation of the twin tunnels of the metro-line 5 in correspondence with a 9-storey reinforced concrete framed structure (Fig. 3.29) located nearby the ground section S_{35} between *Lotto* and *Portello* stations (see Fig. 3.17) and diagonally undercrossed by the first tunnel (Fig. 3.30).

(*a*) (*b*)

Figure 3.29. General view of the main left side façade (*a*) and detail of the garage zone on the right longitudinal side (*b*) of the building.

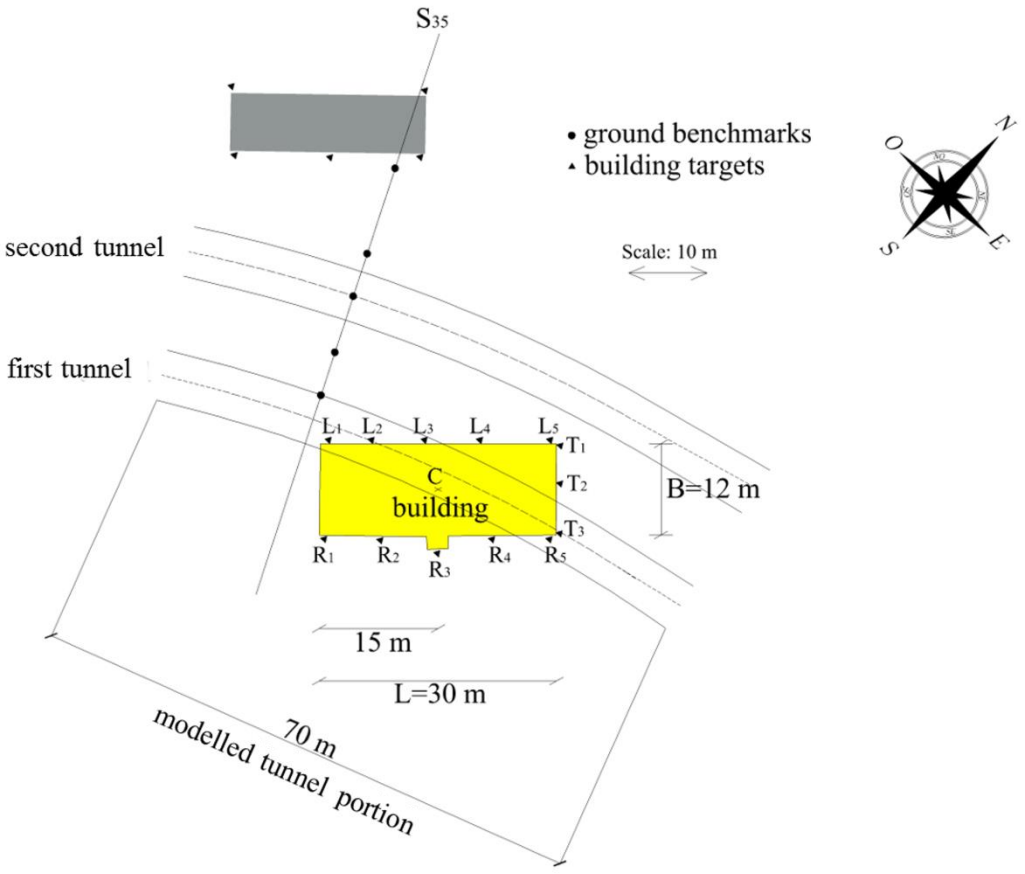

Figure 3.30. Detail of the examined portion of the route.

The 30 m high structure dates back to 1959 and it is characterised by a total weight of about 41000 kN. Its plan dimensions and the position of its middle-point C are reported in Figure 3.30.

The building inter-storey height is equal to 3.2 m, with the exception of the ground floor and of the basement floor, having a height of 4.2 m and 2.5 m, respectively.

The main structural components of the building have the following dimensions: the sections of the beams are equal to 40 cm x 45 cm at the lower floors, 70 cm x 20 cm and 45 cm x 20 cm within or along the perimeter of the upper floors, respectively; the column section is equal to 40 cm x 40 cm; the floor slab thickness is of 26 cm at the lower floors and 22 cm at the upper ones; the sections of the reinforced concrete interior panels are equal to 0.2 m x 3.26 m.

The structure is founded on five strip footings (0.65 m high, indicated as F_I, F_{II}, F_{III}, F_{IV} and F_V in Fig. 3.31) at 4 m below the ground surface; more specifically, the building rests on the foundation beams F_I, F_{II} and F_{III}, while the garage zone (Fig. 3.29 *b*), situated at the basement floor level along the right longitudinal side of the structure, stands on the other ones (F_{IV} and F_V). Three raft foundations (0.7 m high, indicated as F_{VI}, F_{VII} and F_{VIII} in Fig. 3.31) are located at the same level under the elevator shafts and the stairwell, both situated on the right longitudinal side of the building. Reinforced concrete retaining walls (40 cm thick and 3.5 m high) surround the buried portion of the structure along its three sides, with the exception of the right longitudinal side for the access to the garage zone.

Several ground benchmarks (from 5 to 9) were installed on each instrumented ground section, while building targets were placed along the base of the longitudinal façades and on its transversal right side (Fig. 3.30). Structural vertical displacements were gathered during tunnelling by the monitoring targets identified by capital letters L, R and T and a sequential number in Figure 3.30. The target relative distance and their distance from the tunnel axes are listed in Tables 3.8 and 3.9, respectively.

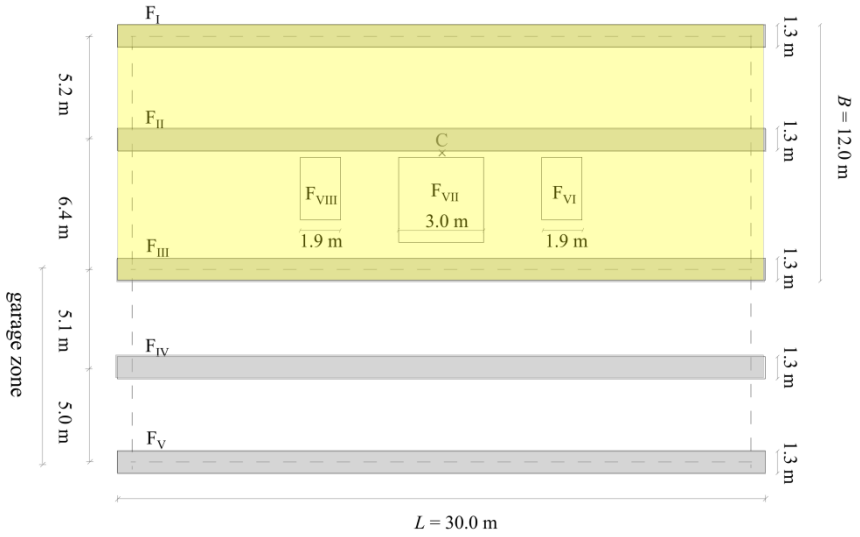

Figure 3.31. Plan view of the building foundations.

Monitoring points	Relative distance (m)
L_1- L_2	5.54
L_2- L_3	6.80
L_3- L_4	7.09
L_4- L_5	8.44
R_1- R_2	7.18
R_2- R_3	7.32
R_3- R_4	6.97
R_4- R_5	7.33
T_1- T_2	4.84
T_2- T_3	6.38

Table 3.8. Target relative distance.

Monitoring points	Distance from the right tunnel axis (m)	Distance from the left tunnel axis (m)
L_1	1.53	18.27
L_2	0.33	17.07
L_3	2.84	13.90
L_4	5.84	10.90
L_5	9.82	6.92
R_1	13.35	30.09
R_2	10.76	27.50
R_3	9.26	26.00
R_4	4.51	21.25
R_5	1.02	17.76
T_1	11.23	7.47
T_2	6.89	11.80
T_3	0.00	16.70

Table 3.9. Target distance from the right and left tunnel axes.

Figure 3.32 (*a, b* and *c*) shows the settlement evolution at each monitoring point during tunnelling. As expected, the structural response changes as the excavation advances.

Along the longitudinal sides of the building the subsidence profile is characterised by a hogging-type mode of deformation when the face of the first TBM is located in correspondence with the middle of the structure (measurements recorded on 11.1.2013), while the deformative pattern seems to be mainly of sagging-type after the first tunnel passage (i.e. from 15.01.2013 on). Measurements gathered on 15.1.2013, when the distance of the first tunnel face from section S_{35} was about 50 m (i.e. about 8*D*), range from 4.7 mm to 6.5 mm along the longitudinal left façade, from 3.5 mm to 6.6 mm along the longitudinal right one and from 4.6 mm to 5.7 mm along the transversal side. In particular, it is possible to note that the monitoring targets closer to the first tunnel axis (i.e. points L1, L2, L3 along the longitudinal left side; R4, R5 along the longitudinal right side; T2, T3 along the transversal one) are characterised by higher settlements.

On 18.1.2013 the face of the second EPB machine approached the ground section S_{35}. As shown in Figure 3.32, settlements increase with the advancement of the second excavation and the subsidence pattern changes: larger increments in the vertical displacements are progressively observed, in particular in correspondence with the targets closer to the second tunnel along the left longitudinal side (i.e. points L4 and L5) and along the transversal one (point T1). Conversely, the right longitudinal side of the structure shows a modest increment in the settlement profile with progressively larger vertical displacements from R1 to R5 and an increasing maximum differential settlement (Fig. 3.32 *b*).

When the second tunnel is about 30 m far from the building, i.e. about 5*D*, (measurements recorded on 24.1.2013), the settlements reach the final configuration: they are included in the intervals 8.4 mm - 10.6 mm, 4.1 mm - 8.1 mm and

8.6 mm - 9.9 mm along the left and right longitudinal sides and along the transversal one, respectively.

No evidence of damage was detected on this structure during tunnelling, due to the relatively low values of the absolute settlement induced by the excavation works. This is also consistent with the maximum values of the differential settlement characterising the subsidence profiles, equal to 2.7 mm on the left longitudinal side, as detected on 19.1.2013, and to 4.1 mm and 1.3 mm respectively on the longitudinal and transversal right sides, as recorded at the end of excavation process.

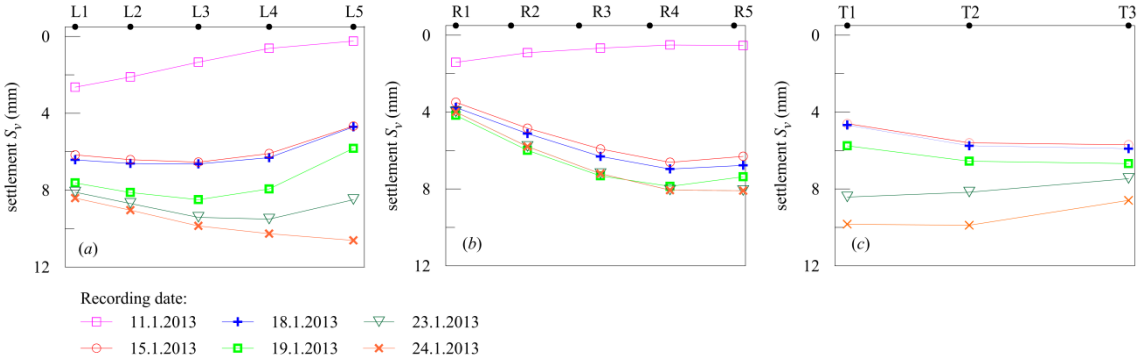

Figure 3.32. Structural vertical displacements recorded in correspondence with the monitoring targets L1-L5 (*a*), R1-R5 (*b*) and T1-T3 (*c*) during tunnelling. Settlements recorded at targets T1-T3 before 11.1.2013 are equal to zero.

4. Preliminary numerical study on the key ingredients of the interaction problem: the soil, the tunnel and the structure

4.1 Purpose of Chapter 4

This chapter is focused on the results of a preliminary study, performed by the finite element code Plaxis (Plaxis, 2012), aimed at investigating the response of the main ingredients influencing the analysis of a soil-tunnel-structure interaction problem.

The first part of the chapter is devoted to the soil constitutive model adopted in the numerical study (i.e. *Hardening Soil model with small strain stiffness*, HSsmall; Benz, 2007). This model is firstly presented and explored; then, it is used in a two-dimensional (2D) finite element study to describe the mechanical response of a soil layer interested by the excavation of a single tunnel. A comparison with the steady-state surface settlements recorded under free-field conditions at a monitoring section of the Milan metro-line 5 is proposed to validate the performance of the adopted constitutive formulation in this class of problems.

The excavation of the first and the second tunnel of the metro-line is then simulated under free-field conditions by a three-dimensional (3D) step-by-step procedure. Although simplified, the schematisation of the excavation sequence, which principally aims at simulating the subsidence at the ground surface in a realistic fashion, takes into account the main aspects of the EPB-tunnelling (e.g. the action of a support pressure applied at the tunnel face linearly variable with depth, the grouting injection at the shield tail, the installation of reinforced concrete lining rings, etc.).

In the final part of the chapter the response of a number of structural models subjected to different loading conditions is analysed by the codes Plaxis 3D and Sap 2000. The goal of such a comparison is the assessment of the performance of the structural

elements in the finite element code adopted in this study as compared to that obtained by the well-known Sap 2000, a widely used program for structural analyses.

4.2 The constitutive model *Hardening Soil with small strain stiffness*

4.2.1 Description of the soil constitutive model

The *Hardening Soil model with small-strain stiffness* (HSsmall; Benz, 2007) is a constitutive model capable of taking into account the very high soil stiffness observed at very low strain levels, its reduction with the strain level and the early accumulation of plastic deformations. It represents an extension of the *Hardening Soil model* (HS) developed by Schanz et al. (1999).

The reversible response of the soil is described by an isotropic non-linear elastic law. The small strain shear modulus, G_0, is a function of the stress state by the following expression:

$$G_0 = G_0^{ref} \left(\frac{c' \cdot \cos\phi' + \sigma'_3 \cdot \sin\phi'}{c' \cdot \cos\phi' + p^{ref} \cdot \sin\phi'} \right)^m \tag{4.1}$$

where G_0^{ref} is the small strain shear modulus at the reference pressure p^{ref} = 100 kPa, σ'_3 is the minimum principal effective stress, m is a constant, c' is the effective cohesion and ϕ' is the angle of shear resistance.

The evolution of the shear modulus with the increase in the shear strain is included in the constitutive formulation by the expression of the stiffness reduction curve proposed by Hardin and Drnevich (1972), successively modified by Santos and Correia (2001):

$$\frac{G_s}{G_0} = \frac{1}{1 + a\left|\frac{\gamma}{\gamma_{0.7}}\right|} \tag{4.2}$$

where G_s is the secant shear modulus, a is a constant equal to 0.385 and $\gamma_{0.7}$ is the shear strain at which the shear modulus is reduced to about 70% of its initial value.

The derivative of Equation (4.2) with respect to the shear strain provides the tangent shear modulus, G_t, expressed as:

$$\frac{G_t}{G_0} = \frac{1}{\left(1 + a\left|\frac{\gamma}{\gamma_{0.7}}\right|\right)^2} \tag{4.3}$$

The tangent shear modulus is bounded by a lower limit corresponding to the shear modulus G_{ur}:

$$G_t > G_{ur} = \frac{E'_{ur}}{2(1+\nu_{ur})} \tag{4.4}$$

This latter is selected by the user, referring to a medium value of the shear strain level, $\gamma_{cut\text{-}off}$, after which the reversible response is characterised by a constant value of the tangent stiffness with the strain. In Equation (4.4) ν_{ur} is the Poisson's ratio for unloading/reloading.

The expression of $\gamma_{cut\text{-}off}$ is provided in the following:

$$\gamma_{cut-off} = \frac{1}{0.385}\left(\sqrt{\frac{G_0^{ref}}{G_{ur}^{ref}} - 1}\right) \cdot \gamma_{0.7} \tag{4.5}$$

A graphic representation of Equations (4.2) and (4.3) is provided in Figure 4.1.

The Young's modulus corresponding to G_{ur} is also a function of the stress state according to a relation analogous to Equation (4.1):

$$E'_{ur} = E'^{ref}_{ur} \left(\frac{c' \cdot \cos\phi' + \sigma'_3 \cdot \sin\phi'}{c' \cdot \cos\phi' + p^{ref} \cdot \sin\phi'} \right)^m \tag{4.6}$$

Similar expressions are defined in the model for the secant stiffness at 50% of failure load in drained triaxial test, E'_{50}, and the tangent stiffness for primary oedometer loading, E'_{oed}:

$$E'_{50} = E'^{ref}_{50} \left(\frac{c' \cdot \cos\phi' + \sigma'_3 \cdot \sin\phi'}{c' \cdot \cos\phi' + p^{ref} \cdot \sin\phi'} \right)^m \tag{4.7}$$

$$E'_{oed} = E'^{ref}_{oed} \left(\frac{c' \cdot \cos\phi' + (\sigma'_3 / K_0^{nc}) \cdot \sin\phi'}{c' \cdot \cos\phi' + p^{ref} \cdot \sin\phi'} \right)^m \tag{4.8}$$

In Equation (4.8) K_0^{nc} is the coefficient of earth pressure at rest estimated with reference to a normal consolidated state.

The above equations are valid until the material remains in the elastic region (Brinkgreve et al., 2007).

The irreversible response of the HSsmall model is governed by two yield surfaces which evolve according to isotropic hardening laws: a shear hardening yield surface f_s, that is a function of the deviatoric plastic strain and a cap yield surface f_v, which is

introduced to bound the elastic region for compressive stress paths and it depends on the plastic volumetric strain. The elastic region of the model is further reduced for tensile stress states by means of a *tensile cut-off* surface. The shear hardening yield surface can expand up to the ultimate Mohr-Coulomb failure surface.

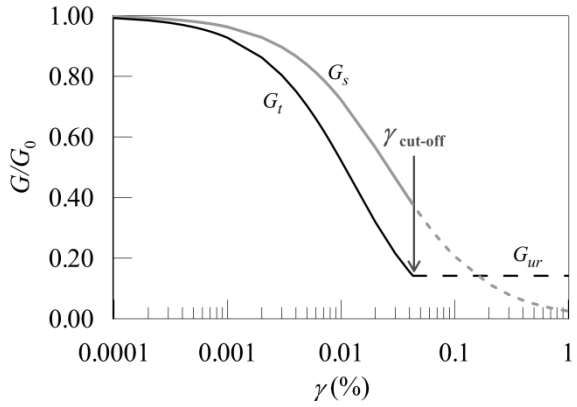

Figure 4.1. Decay curves of the tangent and secant shear stiffness moduli of the *Hardening Soil model with small strain stiffness*.

The flow rule adopted for the cap yield surface f_v is associate, while a non-associate rule is employed for the f_s, adopting a formulation inspired by the well-known stress-dilatancy theory.

4.2.2 Verification and validation of the soil constitutive model

A preliminary study was performed for a first validation of the model, considering an ideal material having the physical and mechanical properties (γ = 18 kN/m^3, c' = 0 kPa, ϕ' = 30°) of a loose sand (e_0 = 0.83). The G_0-z profile (Fig. 4.2) was determined according to the relation proposed by Hardin (1978):

$$\frac{G_0}{p_a} = S \cdot \left(\frac{p'}{p_a} \right)^n \cdot f(e) \cdot OCR^m \tag{4.9}$$

where $f(e)$ is a function of the void ratio (Hardin and Black, 1968) expressed as:

$$f(e) = \frac{(2.973 - e)^2}{1 + e} \tag{4.10}$$

p_a is the atmospheric pressure (100 kPa), p' is the average effective stress, *OCR* is the overconsolidation ratio and *S*, *n* and *m* are parameters depending on the plasticity index I_P of the material, as proposed by Vinale et al. (1996). They are equal to 300, 0.5 and 0 respectively, being $I_P = 0$.

For the calibration of the model, the parameters G_0^{ref} and *m* (equal to 85 MPa and 0.5, respectively) were determined so as to best-fit the G_0-*z* semi-empirical profile (Fig. 4.2). In order to investigate the role of $\gamma_{cut\text{-}off}$ parameter, different values of the ratio G_{ur}^{ref}/G_0^{ref} were selected and three different sets of model parameters (named M_I, M_II and M_III) were defined as reported in Table 4.1. The values of G_{ur}^{ref}/G_0^{ref} and $\gamma_{cut\text{-}off}$ for these materials are equal to: 0.15 and 0.042% for M_I, 0.25 and 0.026% for M_II, 0.34 and 0.018% for M_III, respectively. The same value was assumed for E_{50}^{ref} and E_{oed}^{ref} and it was set equal to half of E_{ur}^{ref}.

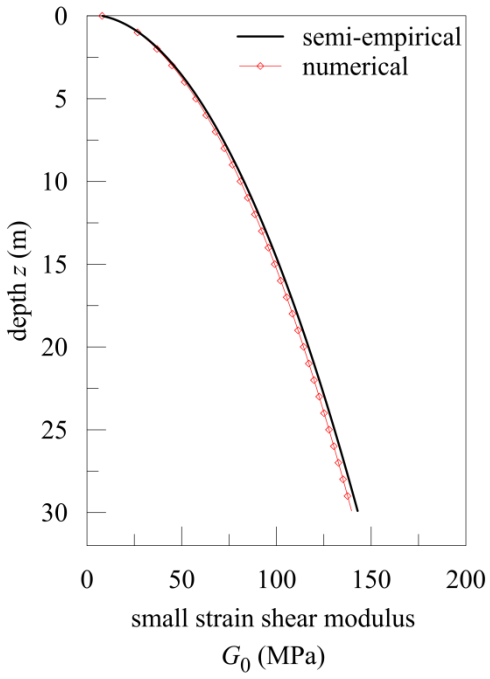

Figure 4.2. Semi-empirical and numerical small strain shear modulus profile with depth.

	c' (kPa)	ϕ' (°)	m (-)	G_0^{ref} (MPa)	E_{ur}^{ref} (MPa)	E_{50}^{ref} (MPa)	E_{oed}^{ref} (MPa)	$\gamma_{0.7}$ (%)	ν_{ur} (-)
M_I	0	30	0.5	85	30	15	15	0.01	0.2
M_II	0	30	0.5	85	50	25	25	0.01	0.2
M_III	0	30	0.5	85	70	35	35	0.01	0.2

Table 4.1. Parameters of the constitutive model assumed for the preliminary study.

Numerical simulations of displacement-control cyclic shearing tests (Fig. 4.3) were carried out on a weightless soil volume (0.1 m x 0.1 m x 0.1 m) subjected to the following loading phases:

- isotropic loading (p'=150 kPa; q = 0 kPa);

- isotropic unloading (p'=100 kPa; q = 0 kPa);

- deviatoric loading (p'=133.33 kPa; q = 100 kPa);

- deviatoric unloading (p'=100 kPa; q = 0 kPa);

- cyclic shearing.

In order to obtained the required deformation level (γ), in the last phase of the test a horizontal displacement distribution was applied on the soil volume; it is uniform on the head of the sample, while it linearly decreases with depth along its lateral faces. The soil volume is fixed at the base. The material is characterised by an initial strain of elastic type, due to the isotropic and deviatoric loading/unloading process, which produces the expansion of the yield surface and, consequently, of the elastic domain.

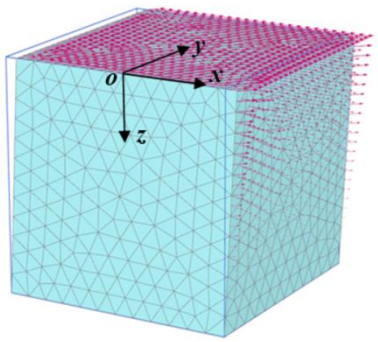

Figure 4.3. Numerical simulation of cyclic shearing tests on a soil sample (0.1 m x 0.1 m x 0.1 m).

Figure 4.4 illustrates, as an example, a result of the test presented in terms of τ-γ response; it also shows the initial stiffness G_0, the secant stiffness G_s and the unloading/reloading stiffness G_{ur} on the reference curve.

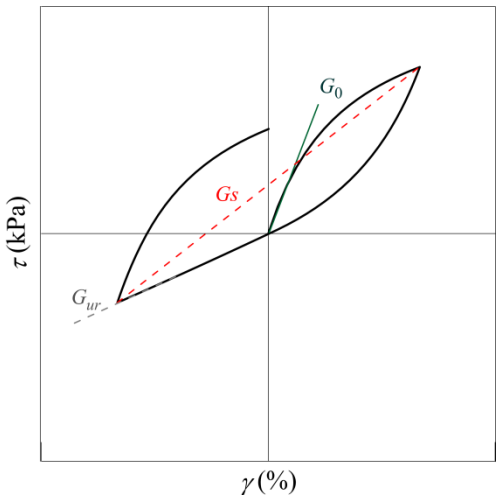

Figure 4.4. Example of τ–γ curve obtained from the numerical simulation of the cyclic shearing test (the initial, secant and unloading/reloading stiffness are also shown).

The stress-strain curves obtained from the numerical tests performed on the ideal materials for different selected deformation levels are reported in Figure 4.5 (*a-f*).

It is possible to notice that the curves overlap for low values of the strain (Fig. 4.5 *a-d*), while, as the strain increases (γ_{max} = 0.1%, Fig. 4.5 *e*), the materials exhibit a different elastic response due to their different stiffness (materials M_III and M_I are characterised by the highest and the lowest stiffness, respectively). A plastic behaviour is then observed in correspondence with higher deformation levels (Fig. 4.5 *f*).

The secant shear modulus G_s, normalised with respect to the initial value G_0, was finally evaluated at each deformation level γ_{max} for the reference materials and compared with the reference theoretical G_s/G_0-γ curve (Fig. 4.6) proposed by Hardin and Drnevich (1972) (Eq. 4.5).

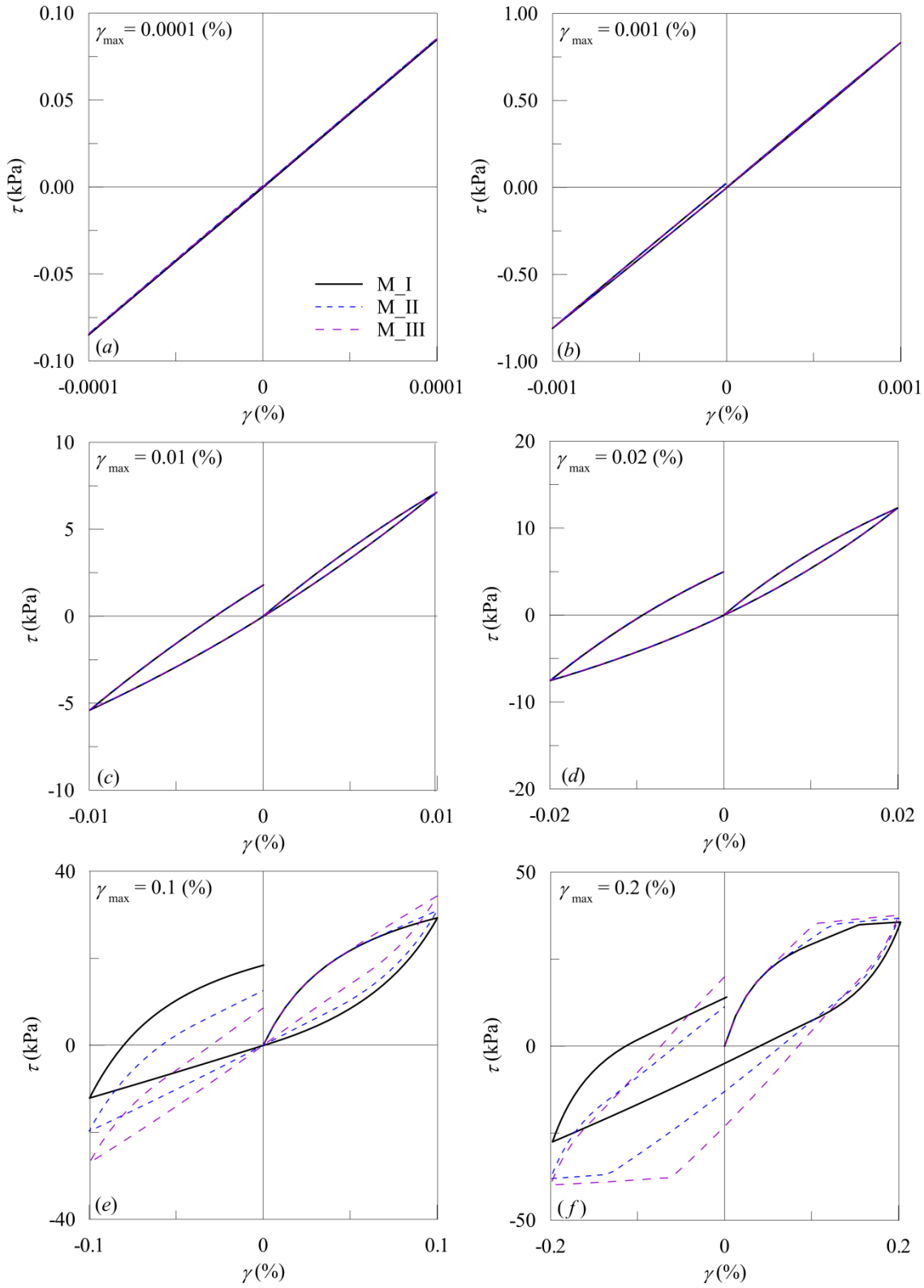

Figure 4.5. Stress-strain curves obtained from the numerical cyclic shearing tests at different deformation levels.

The comparison highlights a very good agreement between the computed and theoretical values for strain levels lower than the reference $\gamma_{cut\text{-}off}$, while, as expected, the two trends diverge for larger γ values.

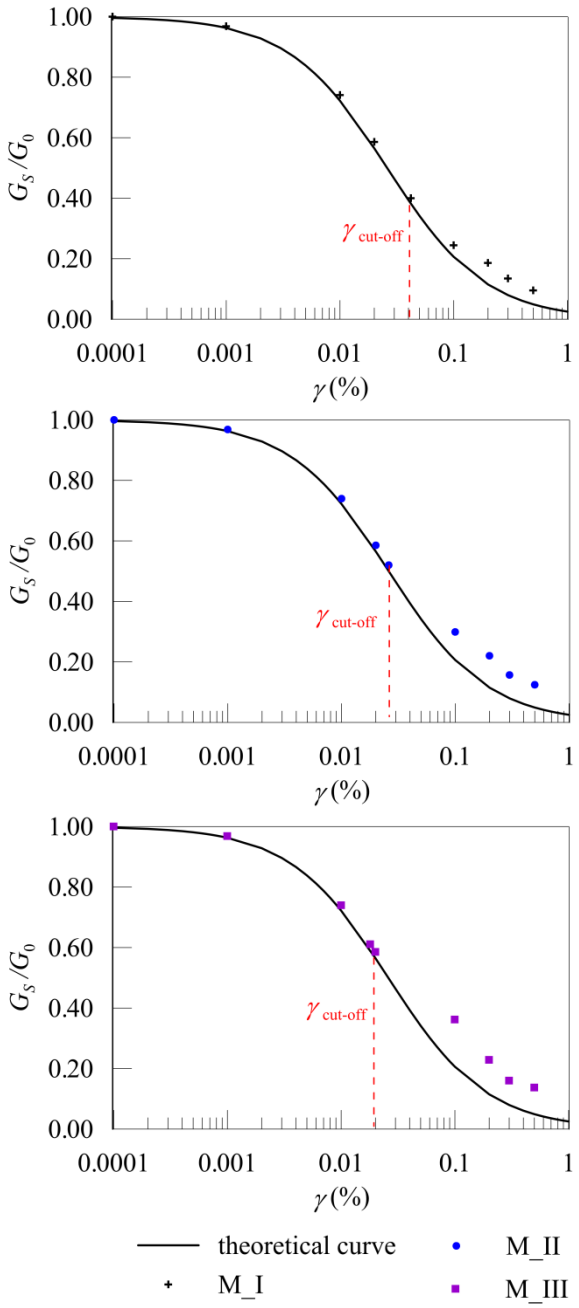

Figure 4.6. Comparison between theoretical and numerical G_s/G_0-γ curves for materials M_I, M_II and M_III.

4.2.3 Calibration of the soil constitutive model

In the numerical study presented in the next paragraphs, the soil stratigraphy refers to the ground conditions encountered at the sites *San Siro-Segesta* and *Lotto-Portello* of the Milan metro-line 5 (see Fig. 3.4 of Chap. 3) and the mechanical behaviour of the soils is described by the *Hardening Soil model with small-strain stiffness* (HSsmall, Benz, 2007), calibrated as discussed in the following.

A summary of all model parameters and their corresponding values for both sites is provided in Table 4.2.

Parameters	**Values**			
	San Siro-Segesta	*Lotto-Portello*		
	Gravelly-sand (0-30 m b.g.l.)	Gravelly-sand (0-20 m b.g.l.)	Sandy-silt (20-25 m b.g.l.)	Gravelly-sand (25-30 m b.g.l.)
γ (kN/m^3)	20	20	17.5	20
Failure parameters:				
c' (kPa)	0	0	5	0
ϕ' (°)	33	33	26	33
ψ (°)	0	0	0	0
Stiffness parameters:				
m (-)	0.4	0.4	0.85	0.4
$E'_{50}{}^{ref}$ (kPa)	48000	48000	54250	58944
$E'_{oed}{}^{ref}$ (kPa)	48000	48000	54250	58944
$E'_{ur}{}^{ref}$ (kPa)	144000	144000	162750	176832
ν_{ur} (-)	0.2	0.2	0.25	0.2
$G_0{}^{ref}$ (kPa)	250000	250000	155000	307000
$\gamma_{0.7}$ (-)	0.0001	0.0001	0.0002	0.0001
Other parameters:				
p^{ref} (kPa)	100	100	100	100
$K_0{}^{nc}$ (-)	0.455	0.455	0.562	0.455
R_f (-)	0.9	0.9	0.9	0.9
$\sigma_{tension}$	0	0	0	0
$c_{increment}$ (kPa/m)	0	0	0	0

Table 4.2. Soil parameters of the HSsmall constitutive model.

The strength parameters (c' and ϕ') were determined following what previously discussed in Section 3.3 of Chapter 3, while the same value for the total unit volume weight was assumed for the soils above and below the water table. The initial profile of the horizontal effective stress was calculated using K_0^{nc} values defined in Table 4.2.

The variation of the small strain stiffness with depth was obtained by calibrating the parameters G_0^{ref} and m against the down hole experimental results, as shown in Figure 4.7. The assumed shear stiffness decay curves for the gravelly-sand and sandy-silt layers follow the empirical ones proposed by Vucetic and Dobry (1991) for granular soils (I_P = 0) and for low plasticity silts (I_P = 15 %), respectively.

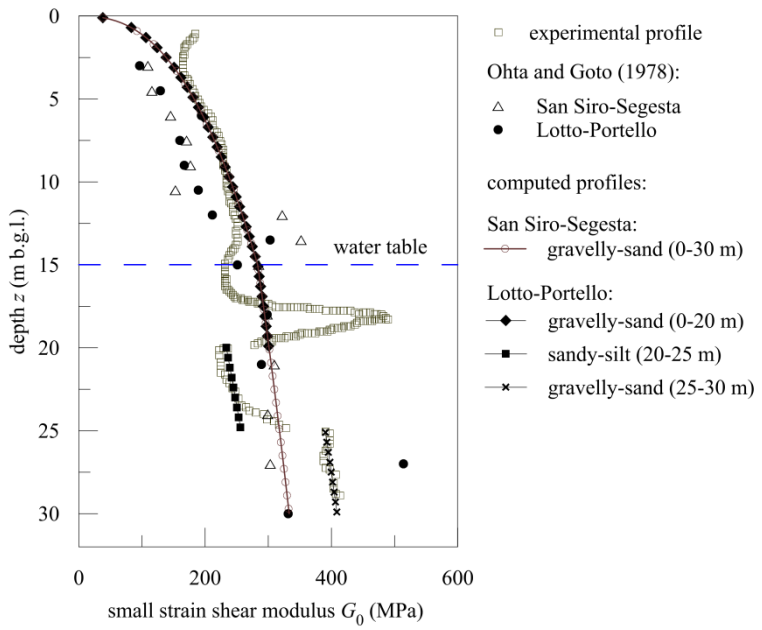

Figure 4.7. Computed and experimental profiles of the small strain shear modulus representative for the investigated segments of the route.

The reference value of the Young's modulus at small strains, $E'_0{}^{ref}$, is related to G_0^{ref} by the Poisson's ratio for unloading/reloading, υ_{ur}. This latter was set equal to 0.20 and 0.25 for the gravelly-sand and for the sandy-silt, respectively. Due to the lack of laboratory experimental data, the reference unloading/reloading stiffness, $E'_{ur}{}^{ref}$, was taken equal to 0.24 $E'_0{}^{ref}$ for the gravelly-sand and to 0.42 $E'_0{}^{ref}$ for the sandy-silt,

corresponding to the stiffness values observed along the decay curves at $\gamma = 0.1\%$. The other stiffness parameters, $E'_{50}{}^{ref}$ and $E'_{oed}{}^{ref}$, were assumed three times lower than $E'_{ur}{}^{ref}$. Finally, standard values were considered for the other parameters of Table 4.2.

For all soil layers the overconsolidation ratio was fictitiously imposed to be large enough to exclude the activation of the cap yield surface of the constitutive model.

4.2.4 Comparison of measured settlements and computed profiles: the role of the soil constitutive model

A first numerical analysis was conducted under plane strain conditions using the finite element code Plaxis 2D (Plaxis, 2012) in order to validate the performance of the HSsmall constitutive model for this class of problems. With this aim, the final settlements measured during the construction of the first tunnel of the metro-line along the initial portion of the route under free-field conditions (i.e. between *San Siro* and *Segesta* stations) were compared with the computed subsidence profile.

The numerical domain was discretised by linear strain 15-node triangular elements. Nodes at the bottom of the mesh were fixed in both vertical and horizontal directions, while the vertical boundaries were only fixed in the horizontal direction.

The size of the mesh employed in this study (Fig. 4.8), 80 m wide and 30 m high, minimises the influence of boundary conditions on the computed results. The domain was discretised in a total number of 7570 elements having an average dimension of about 1 m. The hydrostatic water table in the model was fixed at a depth of 15 m below the ground surface, according to the *in situ* observations.

The tunnel diameter is equal to $D = 6.7$ m and the depth of the tunnel axis, z_0, was set equal to 15 m.

The finite element analysis was performed in terms of effective stresses, modelling the coarse-grained soils as drained. The volumetric strain technique was used to simulate the tunnel excavation: a volume decrease was applied to the soil inside the tunnel in order to obtain at the surface a target volume loss value.

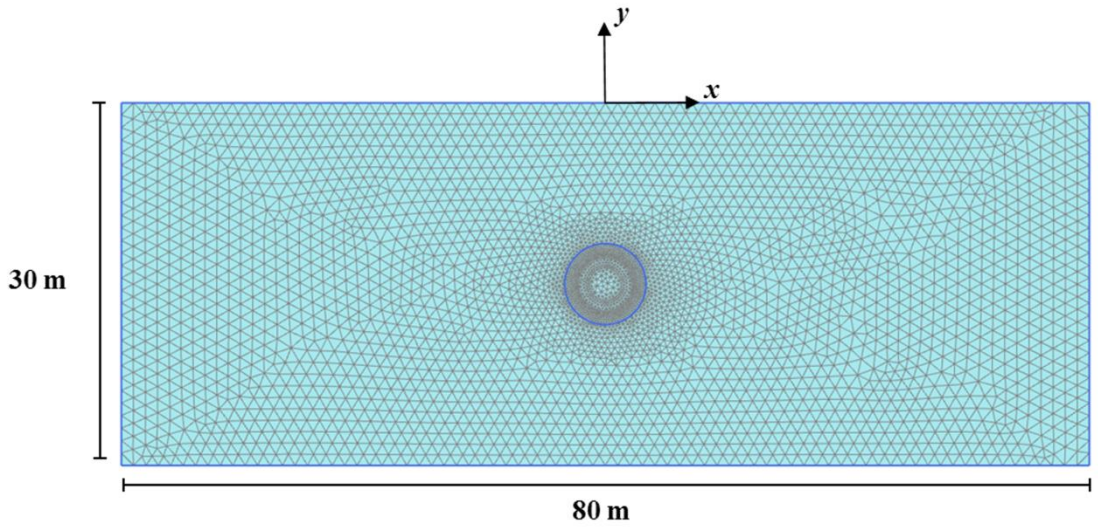

Figure 4.8. Sketch of the mesh employed in the 2D numerical study.

The soil behaviour was described using two different constitutive models for the soil: the simple linear elastic-perfectly plastic Mohr-Coulomb model (MC), which neglects many important aspect of soil behaviour (e.g. the marked non linearity of the stress-strain relationship at small strain and the early accumulation of plastic deformations) and the more advanced *Hardening Soil model with small strain stiffness* (HSsmall), previously described.

The soil parameters used for this latter model are summarised in Table 4.2 for the *San Siro-Segesta* segment of the route, while the MC model parameters were calibrated as in the following. A numerical drained triaxial test on an ideal soil sample, characterised by the HSsmall parameters (Tab. 4.2, *San Siro-Segesta* segment) was simulated: in the first phase of the test the sample, ideally retrieved at the tunnel crown

depth, was isotropically compressed up to a confining pressure p' of 150 kPa; subsequently, a prescribed displacement loading phase was defined in order to simulate the shearing phase in the test. The resulting stress-strain relationship is shown in Figure 4.9 by a dotted line.

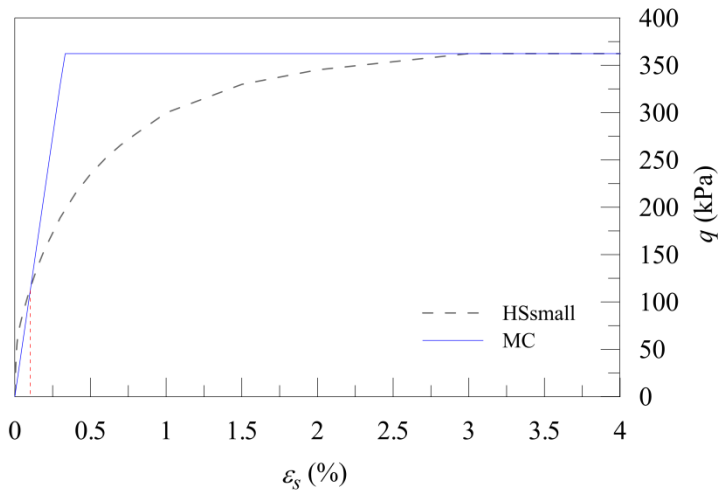

Figure 4.9. Computed stress-strain curves.

The secant Young's modulus for MC model was selected starting from the HSsmall stress-strain curve, at the point corresponding to 0.1% strain. Figure 4.9, which also shows the numerical q-ε_s curve obtained with the MC parameters summarised in Table 4.3, highlights the very high soil stiffness at very low strains and the stiffness reduction with the strain level as reproduced by the HSsmall model in comparison with the linear elastic-perfectly plastic response of the MC model.

Parameters	**Name**	**Value**
Failure parameters:		
c' (kPa)	effective cohesion	0
ϕ' (°)	effective friction angle	33
ψ (°)	dilatancy angle	0
Stiffness parameters:		
E' (kPa)	Young's modulus	110000
ν' (-)	Poisson's ratio	0.2

Table 4.3. MC model parameters.

The reference *in situ* measurements for the numerical analysis carried out in this study are the settlements recorded at the monitoring section S_{16} of the investigated metro-line segment, that is characterised by a typical value of the volume loss for a well-performing EPB excavation in coarse-grained soil, i.e. V_L = 0.4 %.

Such measurements are reported in Figure 4.10 in comparison with the Gaussian curve (K = 0.43) and the numerical back-predictions obtained by applying both MC and HSsmall constitutive models in the analysis.

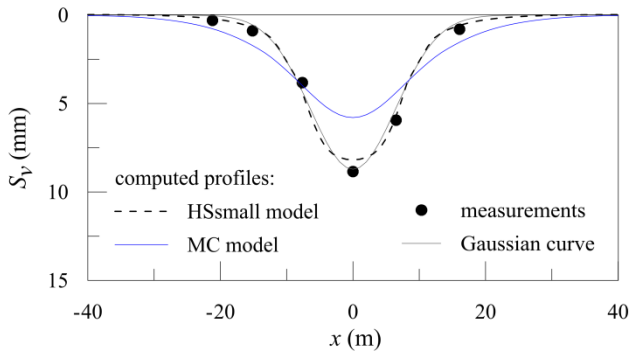

Figure 4.10. Comparison of monitored settlements, Gaussian curve and computed subsidence profiles for V_L=0.4% at the reference section S_{16} of the Milan metro-line 5.

As expected, the HSsmall subsidence profile is in agreement with the monitored data and with their Gaussian interpolation. This indicates, in particular, that the numerical model is capable of reproducing both maximum settlement and the extension of the subsidence curve, consistently with what discussed in similar studies proposed in the literature (e.g. Möller and Vermeer, 2008). Conversely, the MC model clearly overestimates the extension of the settlement profile, underpredicting its maximum vertical displacement.

The horizontal displacement $S_h(x)$ profile is presented in Figure 4.11. This figure illustrates a comparison with the empirical expression proposed by O'Reilly and New (1982), based on the assumption that the displacement vectors point towards the tunnel

axis; no *in situ* measurements of horizontal displacements were available along the examined route.

In general, it is possible to observe that the empirical profile is well replicated by the HSsmall computed trough, with the exception of the maximum value that results overestimated by the numerical analysis; conversely, the MC profile significantly diverges from the empirical curve, resulting in sufficient agreement with it only for the predicted maximum horizontal displacement. However, as reported in the literature (e.g. Grant, 1998), the displacement vector at the surface is more likely to be directed towards a point that is shallower than the tunnel axis. Therefore, the empirical prediction proposed by O'Reilly and New (1982) might underestimate the effective horizontal component of the displacement.

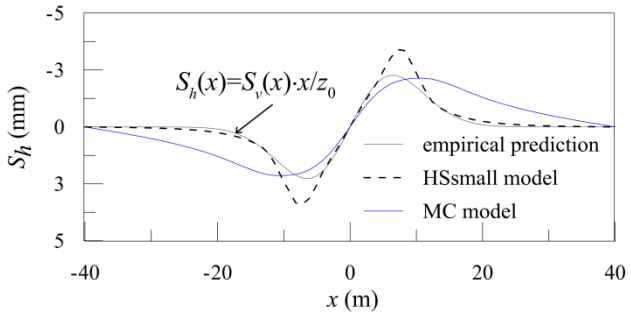

Figure 4.11. Horizontal displacements: comparison of empirical prediction and computed profiles for V_L=0.4%.

4.3 3D numerical schematisation of TBM-EPB tunnelling

4.3.1 Details of the excavation sequence

The simplified 3D numerical procedure adopted to model the construction of the two twin tunnels of the Milan metro-line 5 by TBM-EPB machines is illustrated in Figure 4.12.

The first portion of the tunnel cavity is lined by a steel shield, which extends for a total length of 9.8 m and it is connected to the soil via an interface characterised by the

strength parameters of the adjacent soil. In between the shield tail and the permanent lining, a 1.4 m length of soil is supported by a uniform pressure representing the action of grouting applied to back-fill the lining after the installation. According to the average monitored values (see Section 3.4.4 of Chap. 3), the grouting pressure was set equal to 150 kPa and 170 kPa for the first and the second tunnel, respectively.

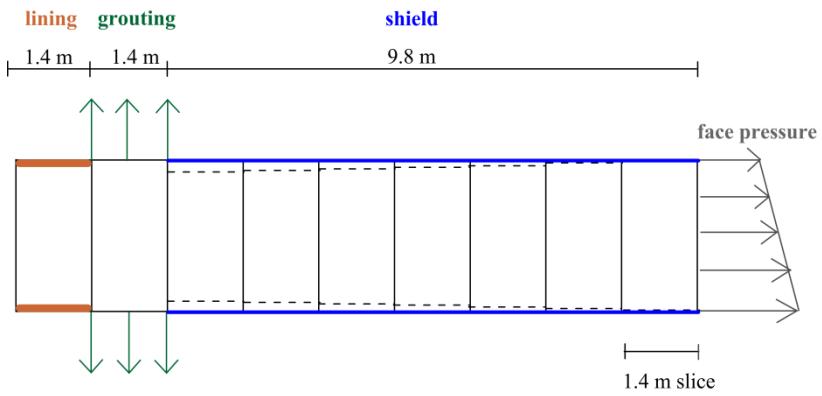

Figure 4.12. Numerical procedure adopted to simulate TBM-EPB tunnelling.

The shield and the lining were modelled by means of plate structural elements, characterised by isotropic linear-elastic behaviour, whose properties are listed in Table 4.4.

Parameter	Shield	Lining
thickness (m)	0.03	0.3
unit volume weight (kN/m^3)	75	25
Poisson's ratio (-)	0.25	0.15
Young's modulus (GPa)	210	35

Table 4.4. Shield and lining properties.

The excavation of each tunnel was simulated by a step-by-step procedure consisting in 43 advancements, each having the length of one concrete lining ring (1.4 m), from y = 9.8 m to y =70 m. The advancement consists in removing one slice of soil inside the tunnel and imposing dry conditions. The tunnel boundaries were considered as impervious. At each advancement, a pressure was applied at the new tunnel face,

corresponding to the theoretical total horizontal stress acting at rest σ_{h0} (z), which ranges from 106 kPa at the tunnel crown to 185 kPa at the invert.

In order to induce a subsidence volume at the ground surface, a fictitious contraction was applied along the shield, starting from the second slice. Such a contraction, which determines larger displacements at the top of the section and lower ones at the bottom, is characterised by a constant increment along each slice, aiming at reproducing in a simplified way the shield conical geometry. The application of a displacement field at the tunnel section, however, does not exclude the importance of the adopted constitutive model, especially for the low values of volume loss that characterise the case under study, as discussed in the previous Section 4.2.4.

4.3.2 Comparison of computed and measured tunnelling-induced settlements under free-field conditions

The ability of the numerical simulation of the excavation sequence to reproduce realistic surface settlement profiles was firstly checked with respect to free-field conditions (Fargnoli et al., 2015 *a*).

The numerical study, performed by the finite element code Plaxis 3D (Plaxis, 2012), refers to the segment of the route between *San Siro* and *Segesta* stations, for which free-field conditions were detected. In this case too, it was taken as an example the situation of the ground section S_{16} that is characterised by average values of maximum settlements and volume loss for the examined portion of the metro-line.

The dimensions of the model shown in Figure 4.13, set up to simulate the twin tunnel excavation, minimise the influence of the boundary conditions on the computed results.

Nodes at the bottom of the mesh were fixed in both vertical and horizontal directions, while the vertical boundaries were only fixed in the horizontal directions.

The soil domain was discretised by 10-node tetrahedral elements, while 6-node triangular plate elements were used to model the shield and lining of the tunnels.

According to the *in situ* stratigraphy, the soil profile is constituted by a single layer of gravelly-sand and its behaviour was described by the HSsmall constitutive model, using the parameters reported in Table 4.2 for the *San Siro-Segesta* segment. The water surface is located 15 m below the ground surface and it is characterised by a hydrostatic pore pressure distribution.

The numerical study was performed in terms of effective stresses, assuming for the soil drained conditions due to the relatively high permeability values measured during the geotechnical investigation (see Section 3.3 of Chap. 3).

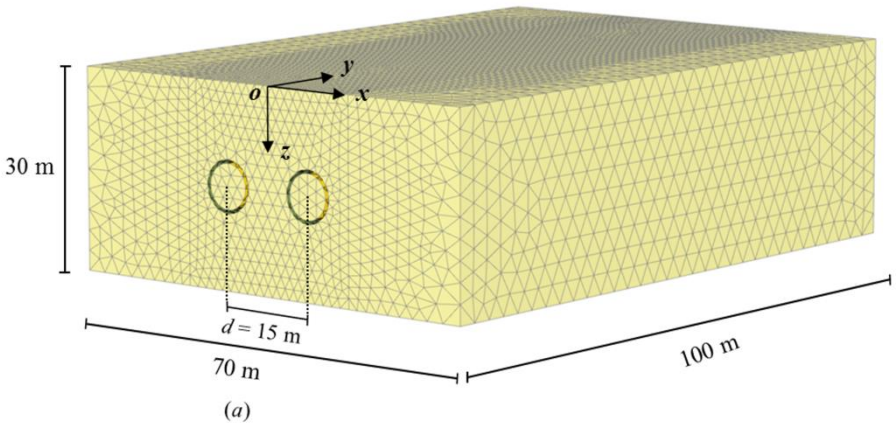

Figure 4.13. Sketch of the mesh for *San Siro-Segesta* segment of the metro-line 5 under free-field conditions.

The twin tunnels have a diameter $D = 6.7$ m and a depth of their axes $z_0 = 15$ m; the axis-to-axis tunnel horizontal distance, d, is equal to 15 m.

In the numerical analysis, after the initialisation of the stress field in the soil (i.e. lithostatic conditions), the excavation of each tunnel was simulated in several steps following the procedure described in the previous section.

The contraction applied at the shield of the first tunnel was initially calibrated in order to reproduce the volume loss due to the first excavation as observed at the ground section S_{16} ($V_L^{(I)}$ = 0.40%); then, the same procedure was repeated for the second tunnel, imposing a different amount of contraction in order to generate the final volume loss equal to $V_L^{(TOT)}$ = 0.95% (see Tabs. 3.3 and 3.6 of Chap. 3).

The computed surface settlements along the transversal and longitudinal directions, shown in Figure 4.14 and 4.15 (*a*, *b*) respectively, result in agreement with the measurements recorded at the reference section S_{16} after the complete excavation of the first and the second tunnel. The numerical results are also consistent with the corresponding empirical curves.

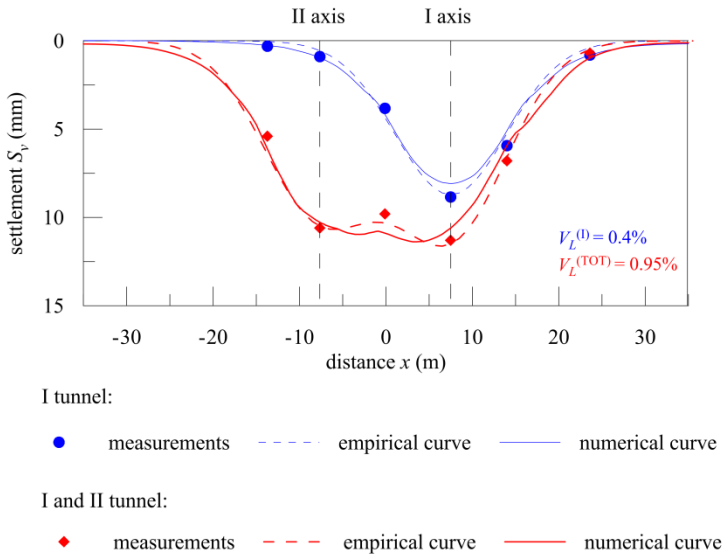

Figure 4.14. Comparison of measured, empirical and computed settlements along the transversal direction after the excavation of the first and the second tunnel under free-field conditions.

For both single and twin tunnel configurations, the computed curves along the transversal direction nicely replicate the maximum settlements observed above the two tunnel axes and the extension of the corresponding subsidence trough. The numerical analysis is also able to capture the interaction phenomena between the tunnels, resulting

in an increase in the maximum settlement above the first tunnel axis after the completion of the second excavation and in a non-symmetric final subsidence profile that, however, slightly overestimates the measured settlement between the tunnels.

The numerical longitudinal profiles (Fig. 4.15 *a* and *b*), though characterised by larger inflection distances with respect to the empirical ones, are in accordance with measurements recorded above the two tunnel axes in terms of face settlement (Fig. 4.15 *b*), settlement due to the shield passage (Fig. 4.15 *a*) and final values (Fig. 4.15 *a* and *b*).

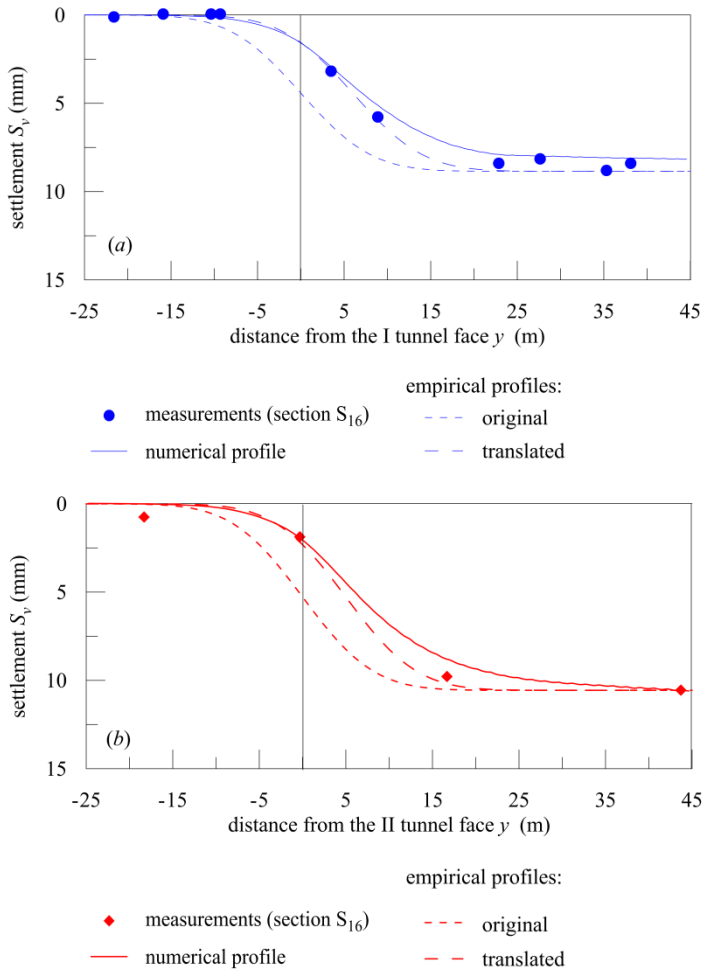

Figure 4.15. Comparison of measured, empirical and computed settlements along the longitudinal direction after the excavation of the first and the second tunnel under free-field conditions.

The distribution of the vertical strain, ε_z, in the soil at the end of the simulation of the first and the second tunnel construction is shown in Figure 4.16 (*a*, *b*) for the section at

y = 35 m (i.e. at a sufficient distance from the model boundaries and from the final position of the tunnel faces). The figure highlights that, as expected for the considered K_0 value, in both configurations the compressive strains (indicated with negative values in the figure) are localised at the tunnel lateral zones, while the tensile ones (associated to positive values) are concentrated at the crown and invert. In particular, after the first excavation the distribution of the compressive strains around the tunnel is rather symmetric and characterised by a maximum value of about -0.3%, while the tensile strains result more concentrated at the invert, with a maximum value equal to about 0.7%. After the second excavation, the soil subjected to compressive strains is not only localised at the lateral sides of the tunnel, but it extends towards the interaction zone between the two openings, with maximum values of about -0.5%. The maximum tensile strains, equal to about 1.5%, are reached in correspondence with the invert of the second tunnel, due to the larger volume loss imposed in this case.

Figure 4.16. Distribution of the vertical strain ε_z in the soil after the simulation of the first (*a*) and the second (*b*) excavation in correspondence with the tunnel middle-section (y = 35 m) (negative values indicate compression strains).

4.4 Comparison of the response of structural elements in Plaxis 3D and Sap 2000

The three-dimensional version of the finite element code Plaxis includes a wider choice of structural elements (such as *beams*, *plates* and *node-to-node anchors*), enhancing its modelling capability at the cost of a deeper structural competence required to the user. A number of structural models, where the different structural elements were employed,

is illustrated in this section in order to investigate and clarify their response under different loading conditions (Gragnano et al., 2014). These models range from simple single-bay spatial frame to multi-storey frame with cross-bracings simulating the presence of infilled panels. All the models were assumed to be fixed at the base, i.e. no foundation systems were considered, in order to focus the attention only on the structural response.

The observed behaviour was compared with that obtained by analysing the same structure by the finite element code Sap 2000 to highlight some differences in the formulation of the corresponding structural elements in the two codes.

4.4.1 Modelling a spatial frame with beams and columns: model M1

The reference structure shown in Figure 4.17 is a single-bay spatial frame fixed at the base and consisting only of beams and columns, all characterised by a section of 30 cm x 30 cm. The figure illustrates the dimension of the structural elements, the right-handed global reference system (*x*, *y*, *z*) and the local coordinate (*s*), this latter represented only for beam 2-6 for sake of simplicity.

In this example, named model M1, as in the following ones, beams and columns are modelled as one-dimensional elements of *frame*-type in Sap 2000 and *beam*-type in Plaxis 3D. This latter element, differently from the *frame* type, is not able to react to torsional actions. Both elements allow for deflections due to shearing as well as bending.

A linear-elastic constitutive law was adopted for these elements, whose parameters were selected consistently with the assumed reinforced concrete material: unit volume weight γ = 24 kN/m^3; Young's modulus E = 25 GPa; Poisson's ratio ν = 0.2.

All the six displacement components were restrained at the base of the model in Sap 2000. In an interaction problem, this condition simulates a rigid contact at the

soil-structure interface, thus being appropriate for the modelling of a soil-foundation system much stiffer than the superstructure.

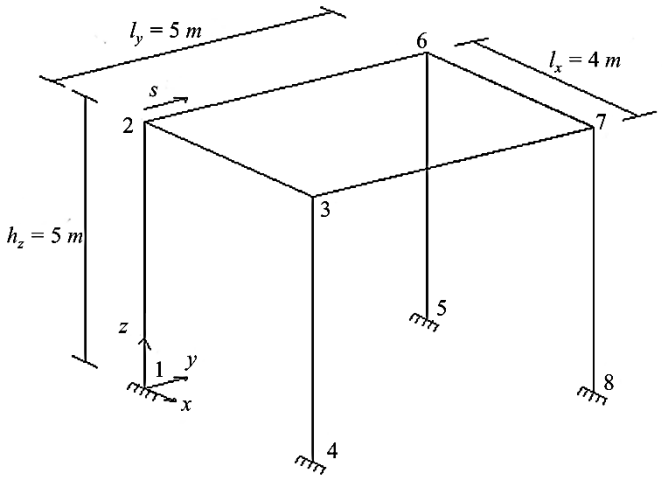

Figure 4.17. Spatial frame with beams and columns and global coordinate system.

On the contrary, a foundation plinth 1 m high and characterised by a square section (1 m x 1 m) was assumed at the base of each column in the Plaxis 3D analysis, modelled by a two-dimensional *plate* element. As this code does not allow to perform numerical analyses without including soil elements, a soil volume (12 m x 15 m x 15 m) was defined at the base of the frame, assuming for it a very rigid behaviour, characterised by a Young's modulus of 750 GPa and a Poisson's ratio equal to zero.

The response of the model was analysed considering the following loading conditions:

- C1 = gravity loads + uniformly distributed vertical loads equal to 10 kN/m acting on the beams (Fig. 4.18 *a*);

- C2 = gravity loads + concentrated vertical loads of 50 kN acting at nodes 3 and 6 (Fig. 4.18 *b*);

- C3 = gravity loads + concentrated horizontal loads of 50 kN acting at nodes 3 and 6 (Fig. 4.18 *c*).

Numerical analyses were carried out using a finite element mesh of medium density in Plaxis 3D (i.e. the average size of the finite element is equal to 1.3 m), while adopting the default option in Sap 2000.

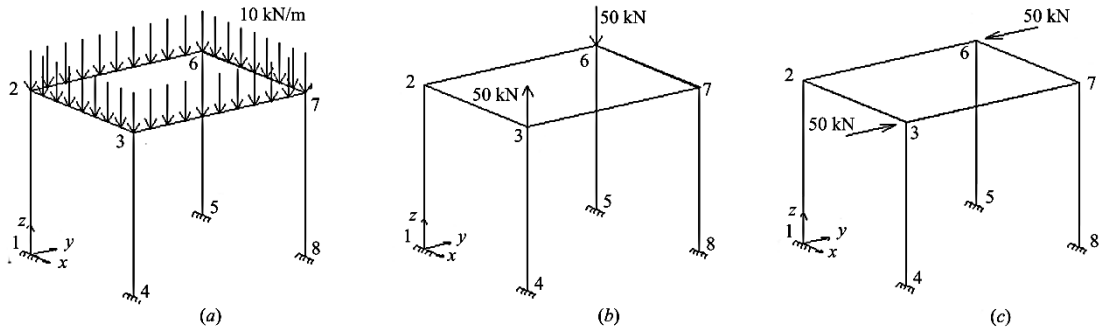

Figure 4.18. Three-dimensional view of model M1 under loading conditions C1 (*a*), C2 (*b*) and C3 (*c*).

Distributions of shear, bending moment and inflection for beams 6-7 (relative to loading conditions C1 and C3) and 3-7 (for loading condition C2), as calculated by the two codes, are shown in Figures 4.19, 4.20 and 4.21.

This latter figure also reports the horizontal displacements along *x* direction of column 1-2 under loading condition C3.

It is possible to note that the results calculated by Sap 2000 and Plaxis 3D are fairly coincident in terms of shear, bending moment and inflection, while the horizontal displacements evaluated for column 1-2 differ in a non-negligible way. Such difference is due to the characteristics of the *beam* element in Plaxis 3D which, as anticipated, does not sustain the torsional action induced by loading condition C3 (Fig. 4.21).

This is confirmed by the results of a further analysis, illustrated in Figure 4.22, identical to the previous one except for the torsional constraint at the column head which was removed in the Sap 2000 model: this modification leads to an almost coincident response as obtained by the two codes.

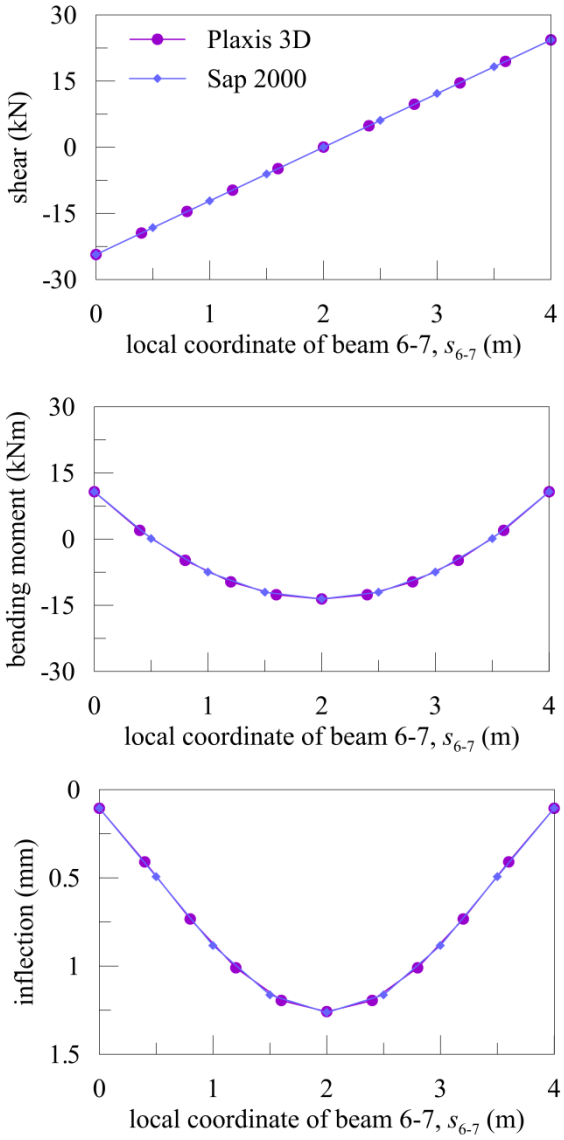

Figure 4.19. Model M1: response of beam 6-7 under loading condition C1 in Plaxis 3D and in Sap 2000.

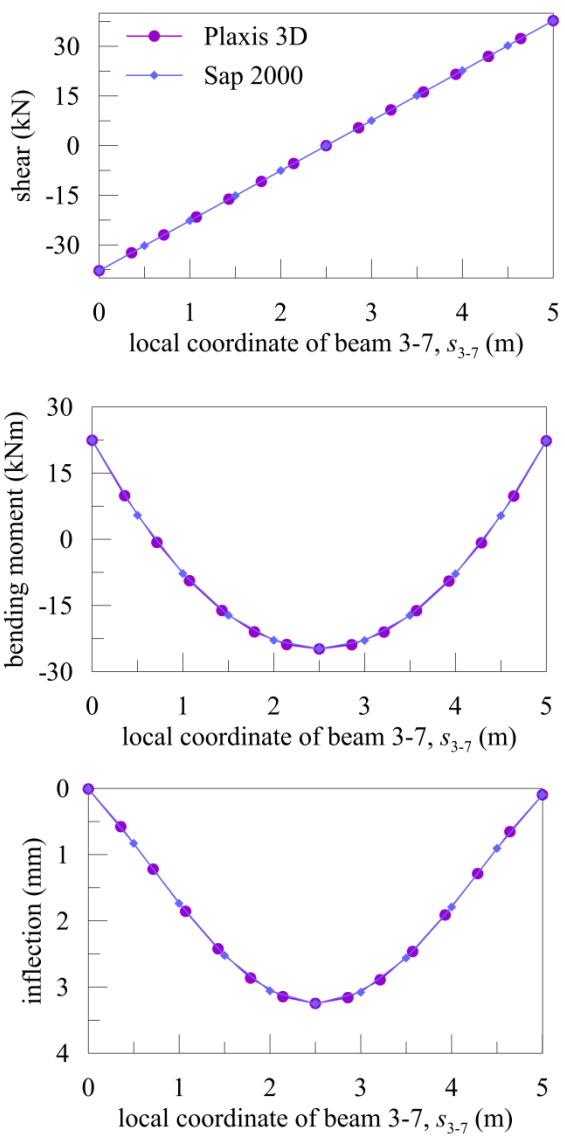

Figure 4.20. Model M1: response of beam 3-7 under loading condition C2 in Plaxis 3D and in Sap 2000.

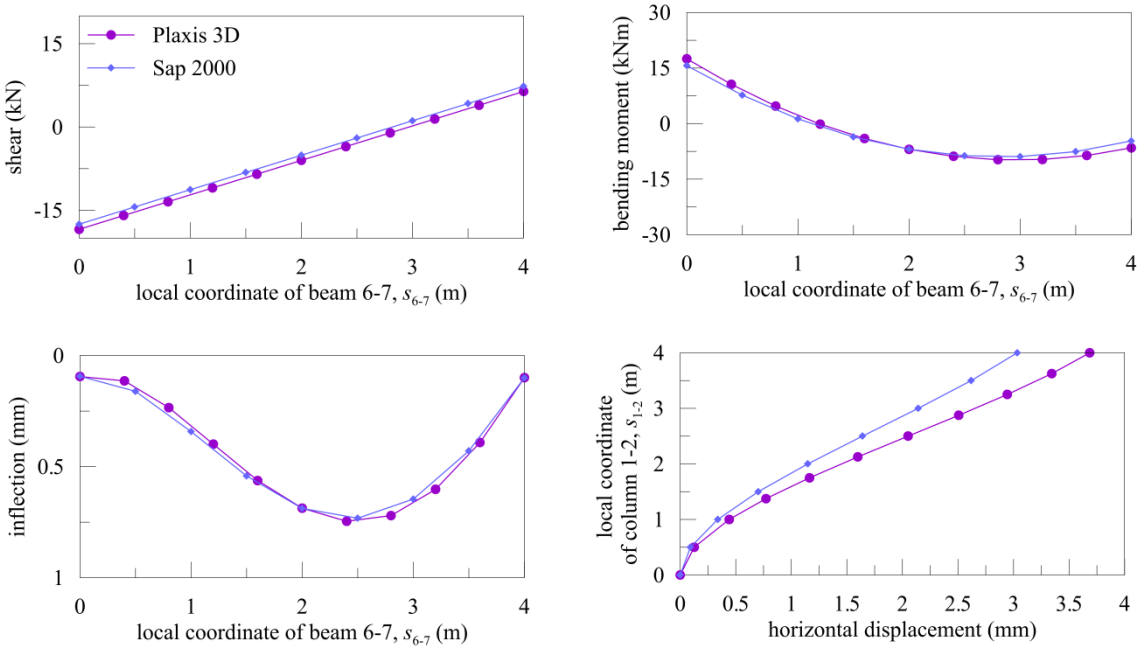

Figure 4.21. Model M1: response of beam 6-7 and column 1-2 under loading condition C3 in Plaxis 3D and in Sap 2000.

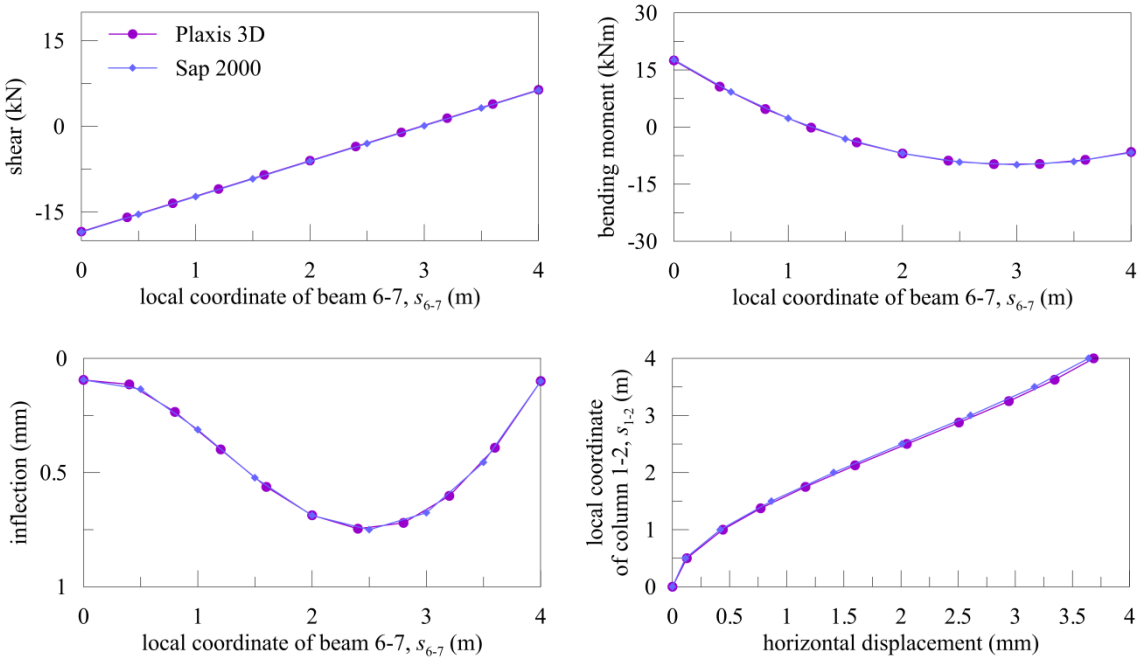

Figure 4.22. Model M1: response of beam 6-7 and column 1-2 under loading condition C3 in Plaxis 3D and in Sap 2000 without torsional constraints at column heads.

4.4.2 Modelling a floor slab in a simple spatial frame: model M2

Figure 4.23 shows a single-bay spatial frame differing from the simple structure of model M1 (see Fig. 4.17) for the presence of a floor slab at the top. A brick-reinforced concrete floor slab is a structural element having a heterogeneous composition (i.e. reinforced concrete and brick) and a different stiffness in both plane directions (i.e. higher stiffness in the warping direction). It is subjected to a plane stress condition and it is mainly loaded in its out-of-plane direction.

The numerical model of this structure (model M2) is coincident with model M1 in terms of beams, columns and constraint conditions at the base.

Concerning the floor slab, two different mechanical hypotheses were considered, namely isotropic and anisotropic. This latter allows to reproduce the main characteristic of a floor slab, that is a structural element rigid in its own plane and capable of differentiating the load transferred to the main beams as compared to the secondary ones.

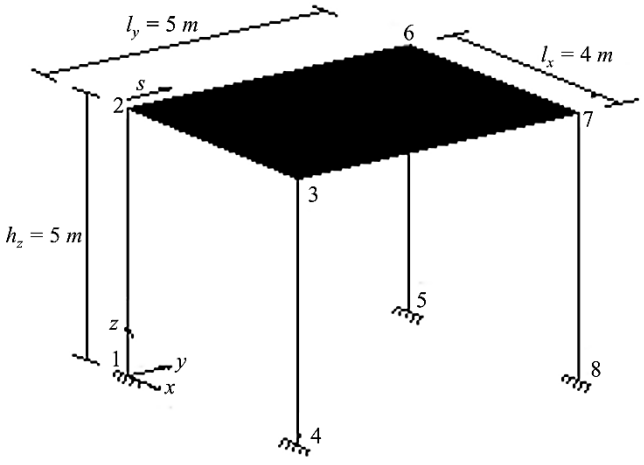

Figure 4.23. Spatial frame with beams, columns and a floor slab.

The isotropic behaviour was obtained in Plaxis 3D using a two-dimensional linear-elastic *plate* element of thickness equal to 25 cm with the following material

properties: unit volume weight γ = 32 kN/m^3; Young's modulus E = 10 GPa; Poisson's ratio ν = 0.2.

A two-dimensional *shell* element with the same geometrical and material properties was selected to model the isotropic floor slab in Sap 2000.

The presence of a floor slab with anisotropic behaviour was represented in Sap 2000 without simulating the structural element itself, but just applying the constraint *diaphragm* to nodes 2, 3, 6 and 7 of Figure 4.23. This constraint, generally used to model structural components with very high in-plane stiffness, forces the nodes belonging to the plane of the slab to move together in a rigid way. Assuming the warping direction of the floor slab along *x*-axis and according to the current design practice, the weight of the floor slab was accounted for by applying vertical forces to the main beams (in *y* direction) and to the secondary ones (in *x* direction) with reference to the influence areas: a load equal to 64.1 kN and 16.8 kN was attributed to the main and secondary beams, respectively. In particular, the first load is equal to half of the floor slab weight (80.9 kN, being the total weight equal to 161.8 kN), reduced of the load (16.8 kN) transferred to the adjacent secondary beams by a floor slab slice 50 cm wide.

When modelling the same slab in Plaxis 3D, an anisotropic elastic model was employed. More specifically, according to the warping direction along *x*-axis, the Young's modulus, E_y, and the shear modulus, G_{yz}, were reduced as compared to those adopted in the isotropic case. The amount of the necessary reduction of the moduli to match the reference results obtained by Sap 2000 is equal to 10%, as such the adopted parameters are E_y = 1 GPa and G_{yz}= 416.7 MPa.

The same loading conditions previously analysed for model M1 were considered, namely C1 (taking also into account the floor slab weight), C2 and C3.

The finite element mesh used for this model in Plaxis 3D is similar to that defined in model M1; in Sap 2000, on the contrary, the mesh of the model with isotropic slab was modified to make it roughly equivalent to that defined in Plaxis 3D. This expedient is related to the fact that in Sap 2000 the load of the floor slab is transferred to the beams in correspondence with the mesh nodes, therefore a similar finite element discretisation is required in order to obtain consistent results by the two different codes.

Figures 4.24, 4.25 and 4.26 show the comparison between models M1 and M2 in terms of shear, bending moment and inflection for beam 3-7 under loading conditions C1, C2 and C3, respectively. Figure 4.26 also shows the horizontal displacements of column 1-2 along *x*-axis.

Results demonstrate the good agreement between the structural responses obtained by the two different numerical codes. In general, it is possible to observe an equivalent response of beam 3-7 under loading conditions C1 and C2 for model M2 too.

As expected, the different assumption concerning the behaviour of the floor slab (i.e. isotropic or anisotropic) plays an essential role in the intensity and distribution of shear, bending moment and inflection.

In the anisotropic case, the structural element 3-7 is one of two main beams of the floor slab and it results to be more heavily loaded as compared to what observed in the isotropic model, where all the beams were equally loaded per unit of length.

On the contrary, the different mechanical hypotheses seem to have a barely relevant influence on the horizontal displacement of the column: this should be due to the fact that in both isotropic and anisotropic cases the relevant shear stiffness G_{xy} assumes the same value, leading to a similar head restrain acting on the column, therefore resulting in a correspondingly similar displacement pattern.

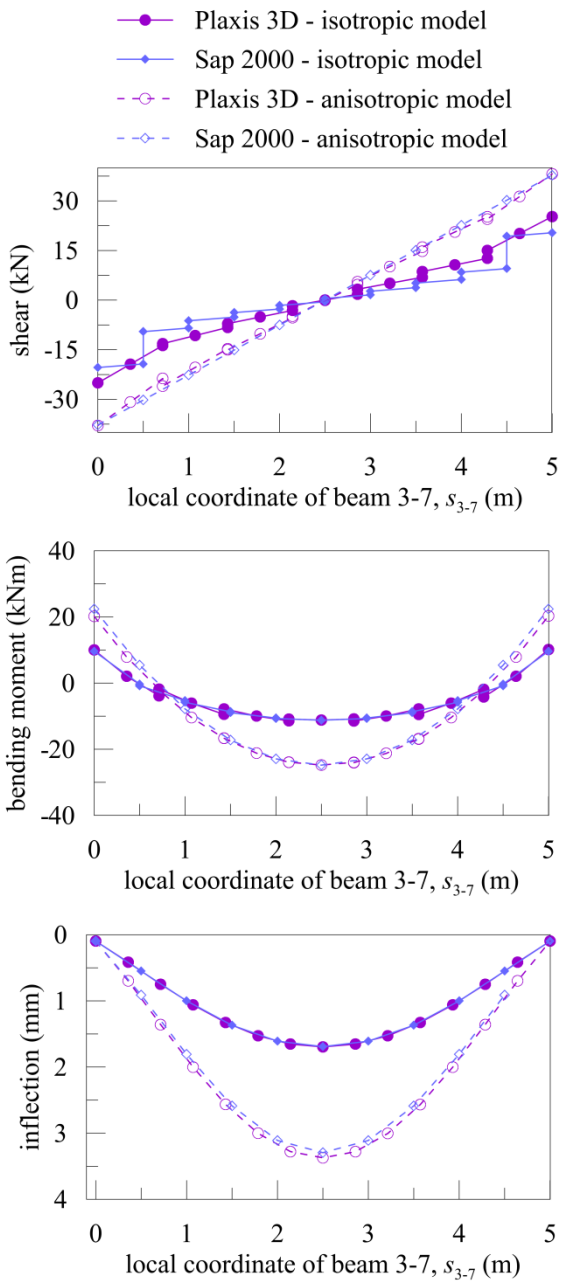

Figure 4.24. Model M2: response of beam 3-7 under loading condition C1 in Plaxis 3D and in Sap 2000.

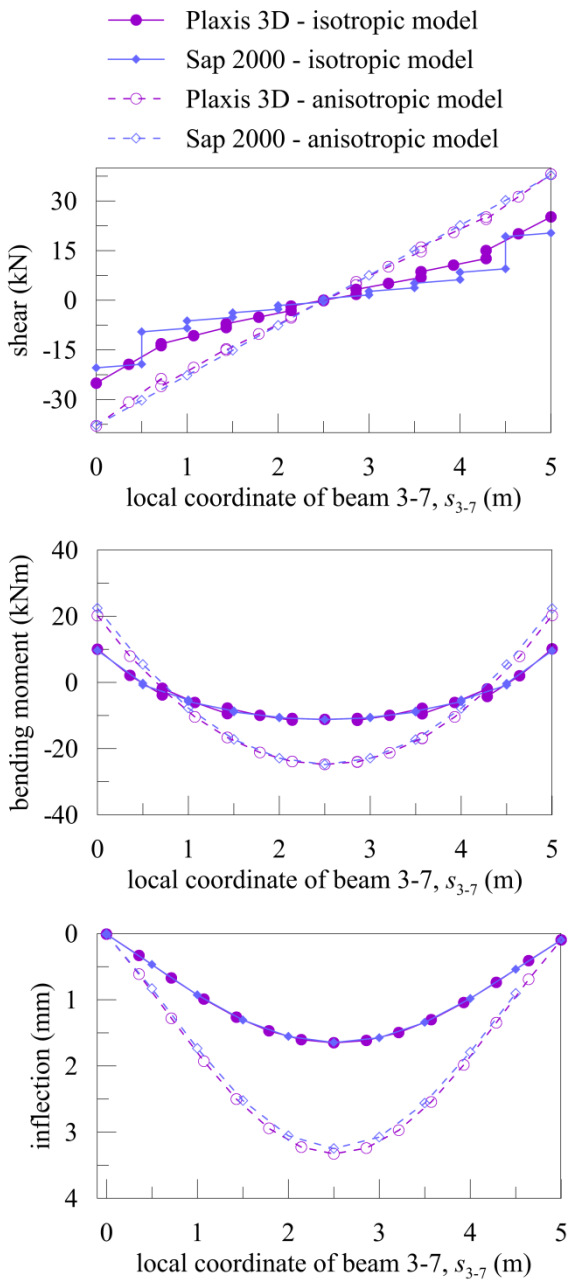

Figure 4.25. Model M2: response of beam 3-7 under loading condition C2 in Plaxis 3D and in Sap 2000.

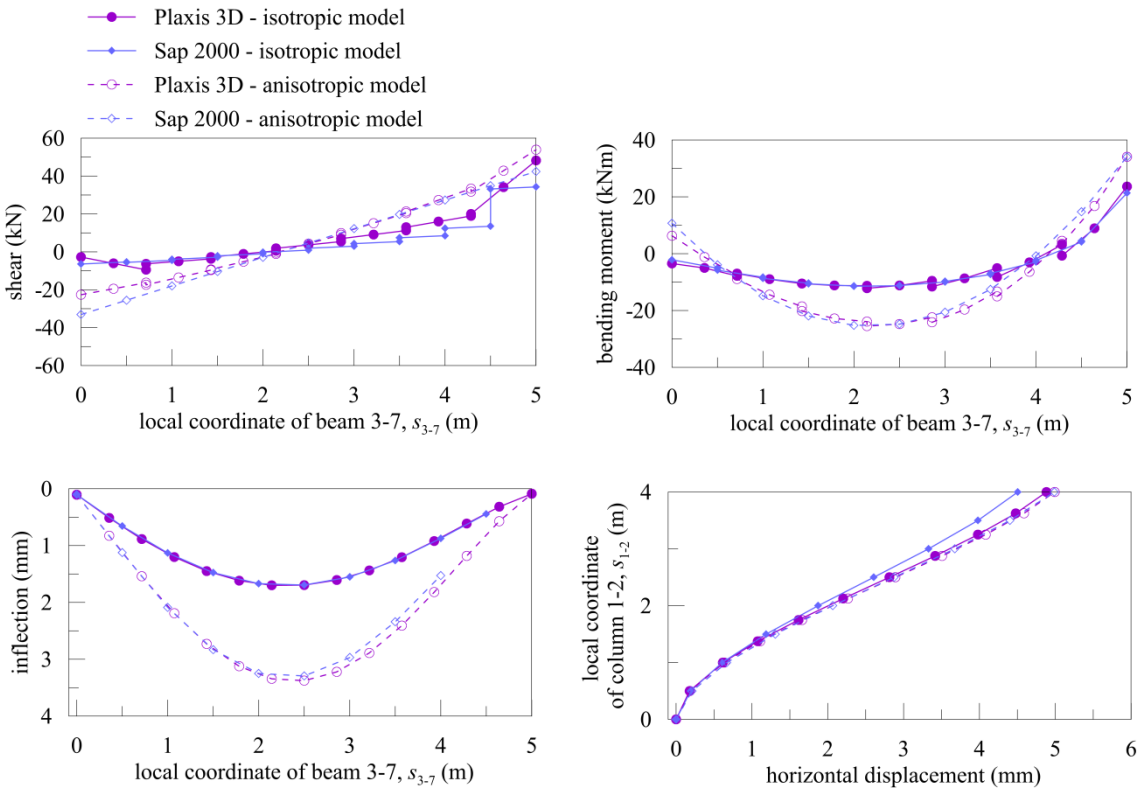

Figure 4.26. Model M2: response of beam 3-7 and column 1-2 under loading condition C3 in Plaxis 3D and in Sap 2000.

4.4.3 Modelling a 2D-frame with diagonal elements: model M3

The simple structure shown in Figure 4.27 is a single-bay plane frame with cross bracings. These elements are commonly adopted in numerical studies to account for infill panels (e.g.: Panagiotakos and Fardis, 1996). Those latter, although being non-structural components, significantly contribute to the overall structural response in the in-plane horizontal direction, leading to a generally stiffer behaviour as compared to open-frame ones.

In the corresponding numerical model, defined as model M3, the structural elements (i.e. beam and columns) are represented by *frames* and *beams* in Sap 2000 and Plaxis 3D respectively, and they are characterised by the following material properties: unit volume weight γ = 24 kN/m^3; Young's modulus E = 25 GPa; Poisson's ratio ν = 0.2.

The base of the frame is constrained as in all the other models.

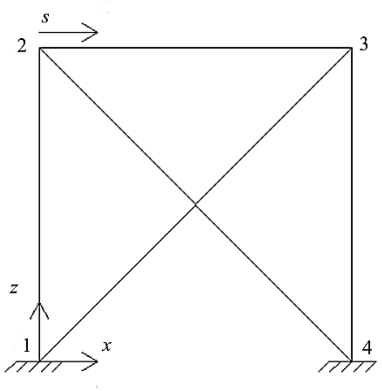

Figure 4.27. 2D frame with cross-bracings.

The diagonal elements of the frame were modelled in order to make them equivalent to a building infill panel, adopting a simplified version of a formulation proposed in the literature (Panagiotakos and Fardis, 1996; Fardis, 1997). The width of the cross bracings, b_w, was defined with reference to the expression of Mainstone (1971):

$$b_w = 0.175 \cdot (\lambda_h \cdot h_w)^{-0.4} \cdot d_w \tag{4.11}$$

where: d_w is the diagonal length of the panel, h_w is the panel height and the parameter λ_h is equal to:

$$\lambda_h = \sqrt[4]{\frac{E_w \cdot t_w \cdot \sin(2\theta)}{4 \cdot E_c \cdot I_c \cdot h_w}} \tag{4.12}$$

where E_w and E_c are the Young's moduli of the infill panel and of the reinforced concrete structural elements surrounding the panel, respectively; θ is the angle formed by the diagonal of the infill panel with respect to the horizontal axis; t_w is the panel thickness; I_c is the moment of inertia of the columns adjacent to the infill panel.

The values of these parameters are summarised in Table 4.5.

Parameter	Value
t_w (m)	0.3
h_w (m)	4
E_w (GPa)	3
E_c (GPa)	25
I_c (m^4)	0.000675
θ (°)	45
λ_w (1/m)	1.3
d_w (m)	5.6
b_w (m)	0.5

Table 4.5: Values of the parameters for estimating the equivalent diagonal width, b_w.

The cross bracings were modelled as weightless one-dimensional elements reacting only to axial stress (denoted as *truss* elements in Sap 2000 and *node-to-node anchor* elements in Plaxis 3D), characterised by an axial stiffness equal to $K = E_w \text{ x } b_w \text{ x } t_w$. An elasto-plastic constitutive law was selected for such elements to introduce a limit value of the tensile strength equal to zero. Furthermore, the maximum value of the compression strength was evaluated according to the following expression:

$$F_{lim} = 1.30 \cdot \tau_{cr} \cdot A_w \tag{4.13}$$

where: τ_{cr} is the shear cracking stress of the panel, assumed equal to 0.2 MPa, and A_w is its transversal area, evaluated as the product of the panel length, l_w per its thickness, t_w.

The response of model M3 was assessed by considering the structural elements weight (beams and columns) and a force of 20 kN applied at node 2 along the *x*-axis (loading condition C4).

Figure 4.28 shows a perfect match among the results of the two models in terms of normal stress acting in column 3-4 and diagonal element 2-4; shear, bending moment and inflection in beam 2-3; horizontal displacement in column 3-4.

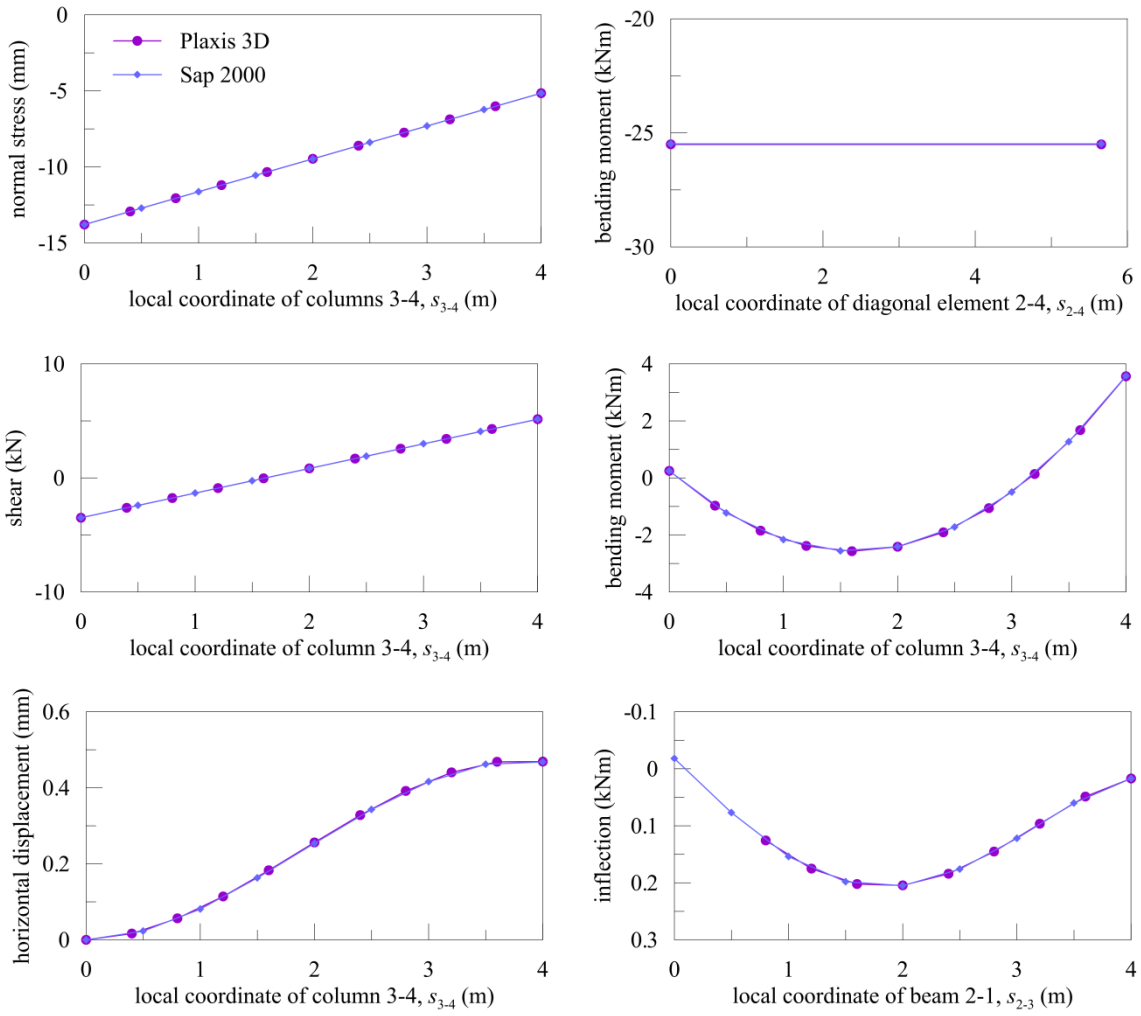

Figure 4.28. Model M3: responses of column 3-4, beam 2-3 and diagonal element 2-4 under C4 load condition in Plaxis 3D and in Sap 2000.

4.4.4 Modelling a spatial 3-storey frame with and without cross bracings: models M4 (I) and M4 (II)

In this section the responses of two 3-storey framed structures subjected to horizontal loads are compared, the structures differing only for the presence of cross bracings (Fig. 4.29). The inter-storey height is 4 m and the beams length is equal to 4 m in *x* direction and 5 m in *y* direction.

The numerical models of the open-frame structure and that of the structure with diagonal elements are denoted as $M4^{(I)}$ and $M4^{(II)}$. In the models beams and columns were represented by one-dimensional elements (*frames* and *beams* in the two codes)

and, for sake of simplicity, the floor slabs were modelled as linear-elastic-isotropic elements of *shell*-type in Sap 2000 and *plate*-type in Plaxis 3D. For both models the mechanical properties of columns and beams are γ = 24 kN/m^3 and E = 25 GPa, while for the floor slabs these parameters are equal to 32 kN/m^3 and 10 GPa. For all the structural elements the Poisson's ratio v is equal to 0.2; the usual rigid constraint conditions were assumed at the base of the frames.

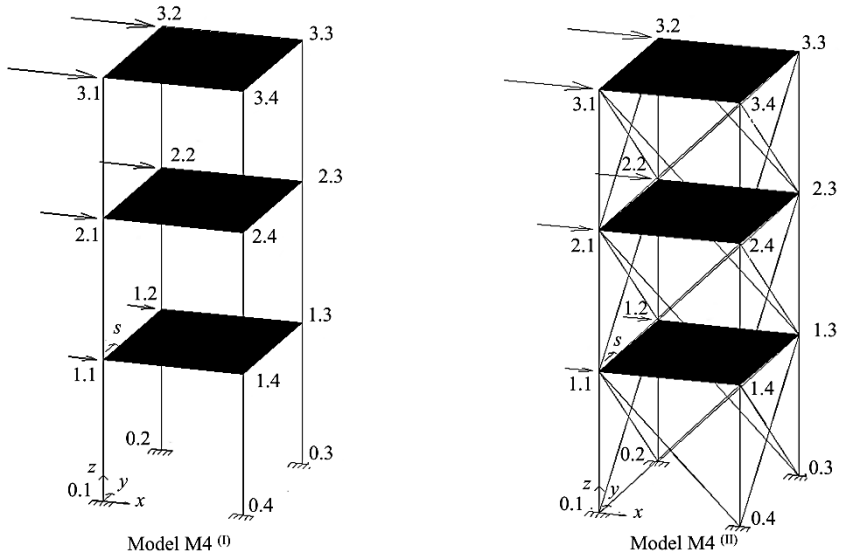

Figure 4.29. Three-dimensional view of models M4 (I) (on the left) and M4 (II) (on the right). Each node of the frame is defined through a double number: the first indicates the level it belongs to, while the second is a sequential number.

The equivalent width b_w of the cross bracings, modelled as *node-to-node anchor* and *truss* elements in Plaxis 3D and Sap 2000 respectively, was defined using Equation (4.11) and the same elastic-plastic constitutive law assumed for model M3 was selected in this case.

Both models were analysed under gravity loading and horizontal ones acting along *x*-axis, those latter equal to 20 kN, 40 kN and 60 kN at the first, the second and the third frame level, respectively (loading condition C5) (Fig. 4.29). A control point position

was selected at the top level (node 3.4) as representative of the horizontal displacement of the structure.

The horizontal displacement distributions in columns 0.4-1.4, 1.4-2.4, 2.4-3.4 are reported in Figure 4.30 for both models.

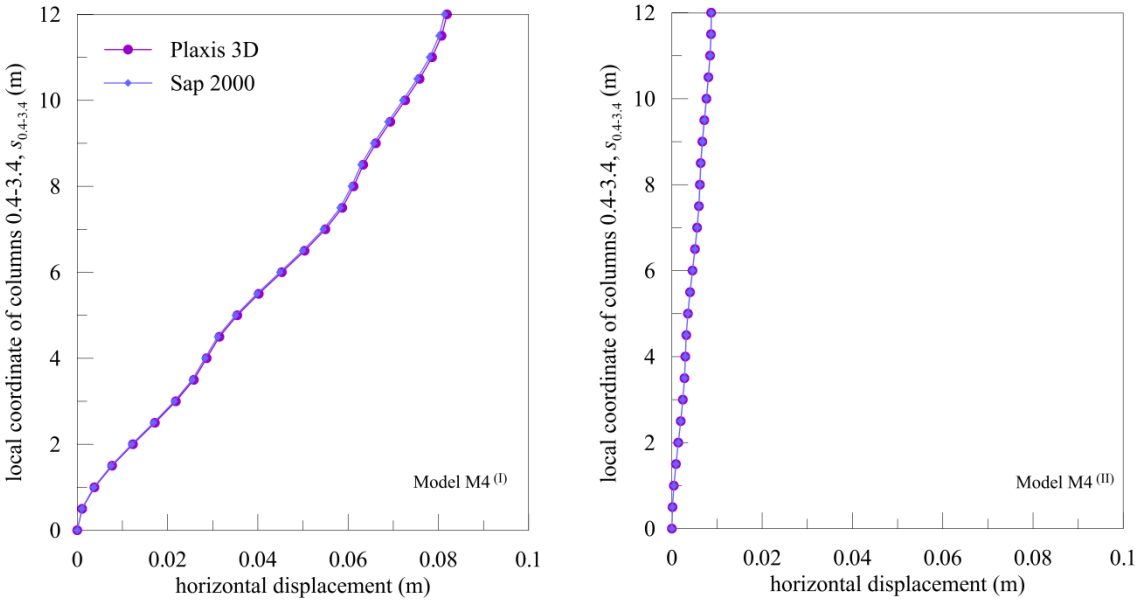

Figure 4.30. Models M4$^{(I)}$ and M4$^{(II)}$: comparison between horizontal displacements obtained in Plaxis 3D and in Sap 2000 with (on the right) and without (on the left) cross-bracings.

It is worth noting that both codes provide the same results: the maximum horizontal displacement is equal to 8 cm for model M4$^{(I)}$ and about 0.8 cm for model M4$^{(II)}$. The outcome of the analyses clearly highlights the effect of claddings on the overall structural stiffness, although simply accounted for by means of equivalent diagonal elements: in fact, the presence of cross bracings produces a horizontal displacement reduction of an order of magnitude as compared to the reference case where they are not included.

The study presented in this last section should be considered as a preliminary step towards more complex soil-structure interaction problems, which indeed require a good level of confidence in the use of structural elements in 3D analyses with Plaxis.

The main outcomes resulting from the comparison between the two codes, carried out in terms of stress and displacements, can be summarised as follows:

- beams and columns can be modelled by *frame* elements in Sap 2000 and *beam* elements in Plaxis 3D. The main difference in the element formulations resides in the inability of *beam* elements to react to torsional actions. In fact, the release of torsional constrains in Sap 2000 produces perfectly matching results;

- the floor slab can be modelled in Sap 2000 by a *shell* element or using a *diaphragm* constraint combined with some additional vertical forces at the top of the columns to simulate the effect of the slab weight. In the first case an isotropic behaviour is obtained, while in the latter a more realistic response is reproduced, as it allows to account for the higher stiffness observed in the warping direction. A *plate* element is instead available in Plaxis 3D. The use of an isotropic formulation allows to nicely reproduce the response of the *shell* element, while an anisotropic model should be selected to fit, after a careful calibration of its elastic parameters, the response of the more advanced scheme of Sap 2000;

- infill panels can be modelled in a simplified manner as cross bracings, whose characteristics were obtained using the formulation proposed by Mainstone (1971). *Truss* and *node-to-node anchor* elements were used respectively in Sap 2000 and Plaxis 3D, leading to perfectly consistent structural responses.

5. 3D numerical modelling of soil-structure interaction during EPB-tunnelling: an integrated geotechnical and structural approach

5.1 Purpose of Chapter 5

In this chapter the interaction between the ground and multi-storey reinforced concrete framed structures during tunnelling is investigated by a fully coupled three-dimensional (3D) approach using the finite element code Plaxis.

The first part of the work is devoted to analyse the response of a number of ideal 2, 4 and 8-storey buildings, with real geometrical and material properties, located in a symmetric position with respect to a single tunnel. Soil conditions as well as tunnel characteristics were selected referring to the real case-history of the Milan metro-line 5.

This preliminary interaction analysis is aimed at investigating the modification of the free-field subsidence troughs, in the transversal and longitudinal directions to the tunnel, due to the presence of surface structures, specifically evaluating the role of their stiffness and weight on the absolute and differential settlements.

In the second part of the chapter, the integrated, geotechnical and structural, 3D numerical study is extended to investigate the response of a real 9-storey reinforced concrete framed building affected by the settlements induced by the construction of the Milan metro-line 5. The surface structure is first introduced in the numerical scheme in detail, taking into account not only its main structural components, but also its secondary elements (e.g. the external infill-panels). The outcomes of the finite-element computation, carried out simulating the excavation of both twin tunnels of the line, are presented and compared with those obtained under free-field conditions and with monitoring settlement data.

Then, the role of the different structural components on the overall behaviour of the soil-structure system is specifically evaluated, performing additional numerical analyses with simplified building models, including the equivalent plate schematisation and a structural model only consisting in the buried portion of the building, properly loaded, together with its foundation elements. The computed results are finally illustrated and critically discussed.

5.2 Analysis of ideal multi-storey building response to tunnelling

5.2.1 Finite element model

The different numerical models set up in the present study to simulate an ideal interaction problem (Boldini et al., 2014) are represented in Figure 5.1 (*a*-*c*). In each scheme the size of the mesh (68 m x 100 m x 30 m) is sufficient to minimise the influence of boundary conditions on the computed results. As for the scheme of the free-field numerical analysis previously presented in Section 4.3.2 of Chapter 4, in these models too the nodes at the bottom of the mesh are fixed in both vertical and horizontal directions, while the vertical boundaries are only fixed in the horizontal direction.

The soil domain was discretised by 10-node tetrahedral elements. In each model the soil stratigraphy was defined taking as reference that encountered *in situ* between the stations of *Lotto* and *Portello* of the line 5 (see Fig. 3.4 of Chap. 3). It is constituted by two layers of gravelly-sand (between 0-20 m and 25-30 m) and one layer of sandy-silt (between 20-25 m); the water table was imposed at 15 m below the ground surface. The soil behaviour was described by the *Hardening Soil model with small-strain stiffness* (HSsmall, Benz, 2007), using the calibration reported in Table 4.2 of Chapter 4 for the reference segment of the route.

The tunnel (D = 6.7 m) is located at a depth of z_0 = 15 m and the excavation sequence follows the steps previously described in Section 4.3.1 of Chapter 4.

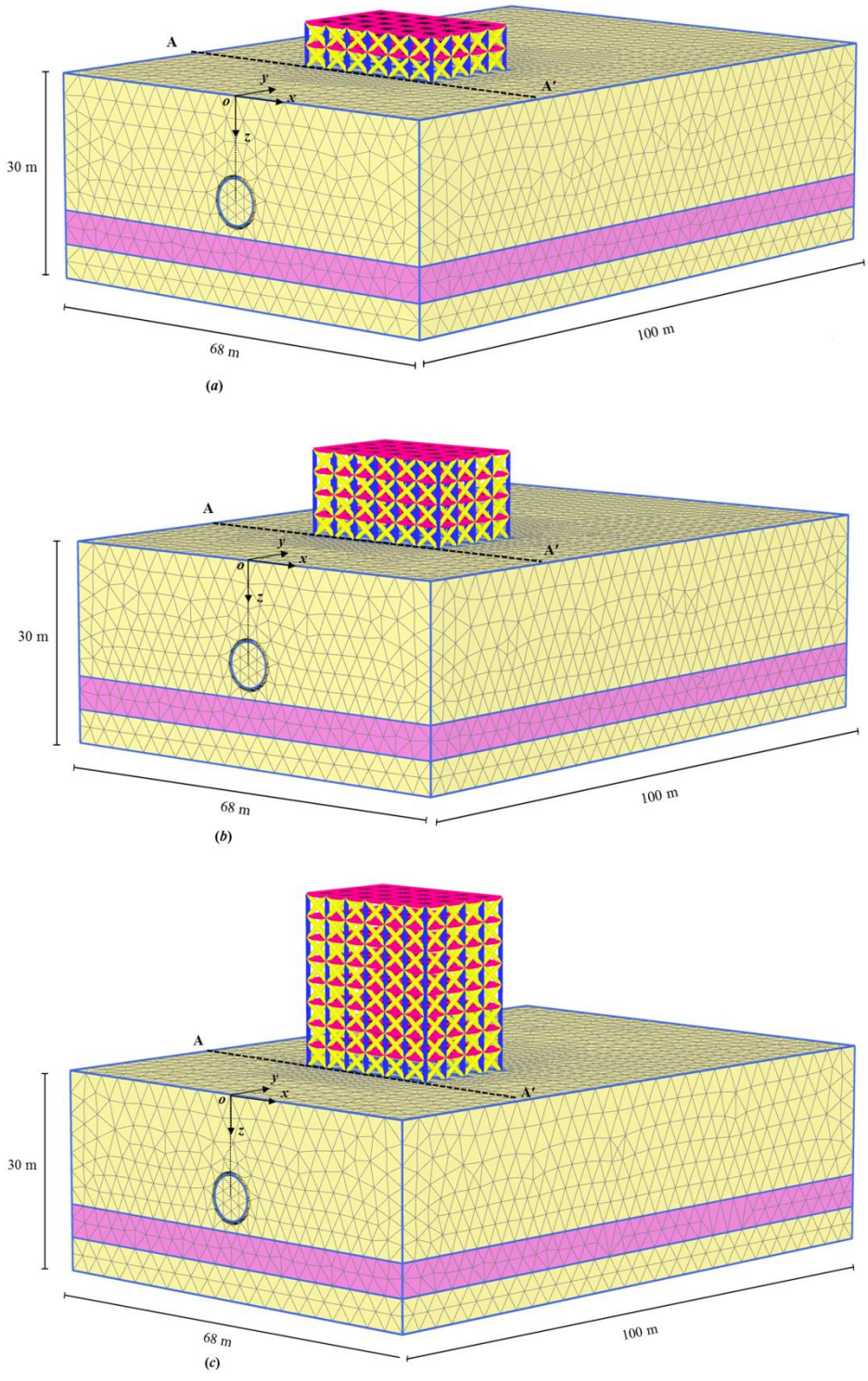

Figure 5.1. Sketch of the analysed numerical models with ideal multi-storey buildings.

The structural models underpassed by the tunnel are 2, 4 and 8-storey reinforced concrete framed buildings having a dimension of 24 m x 16 m in plan, an inter-storey height of 3.2 m and 4 m long bays in both *x* and *y* directions. Each structure

is founded on 5 strip footings (25.2 m x 1.2 m x 1 m) situated 1 m below the ground surface and warped along the *x*-axis; it is composed by beams and columns, both with a section of 30 cm x 30 cm, and of 22 cm thick floor slabs.

The main structural components were modelled as follows:

- 3-node line beam elements were used for beams and columns;
- 6-node triangular plate elements with isotropic behaviour were used for floor slabs;
- the foundations were modelled by 10 node tetrahedral volume elements constituted by a non-porous material.

A linear-elastic constitutive law was adopted for these structural components, whose parameters were selected consistently with the reinforced concrete material properties: unit volume weight $\gamma_c = 24$ kN/m^3, Young's modulus $E_c = 25$ GPa and Poisson's ratio $\nu_c = 0.2$.

The 40 cm thick infill panels, uniformly distributed along the external frames, were modelled in a simplified way as equivalent cross-bracings (Mainstone, 1971), following the approach described in Section 4.4.3 of Chapter 4. In this case, however, a reduced value of $E_w = 3$ GPa was entered in Equation (4.12) instead of the effective Young's modulus of the infill panels (equal to about 6 GPa) in order to take into account the generally diffuse presence of voids (doors or windows) on the building façades, which contributes in reducing the overall stiffness of the structures (Melis and Ortiz, 2003).

An interface with a strength controlled by the soil parameters was introduced in the model solely between the tunnel shield and the soil, while no interfaces were defined at the soil-lining and soil-building contacts.

5.2.2 Numerical analyses and results

All the numerical analyses were performed in terms of effective stresses, assuming drained conditions for the soils due to the relatively high permeability detected during the geotechnical investigation.

The finite-element simulations were carried out according to the following steps:

- initialisation of the stress field in the soil (lithostatic conditions);
- activation of the structure in a single step;
- excavation of the first tunnel in several steps (in the first step the displacement field due to the weight of the building was reset to zero).

In order to calibrate the contraction to be applied at the tunnel profile to reproduce a target volume loss equal to about 0.3%, a free-field numerical analysis was firstly performed under free-field conditions (FF analysis) using the procedure previously validated against measured settlements in Chapter 4 (see Section 4.3). The reference value of the volume loss corresponds to that observed on average at the Milan construction site along the *Lotto-Portello* segment after the excavation of the first tunnel of the metro-line.

The computed transversal (Fig. 5.2 *a*) and longitudinal (Fig. 5.2 *b*) surface profiles are in fair agreement, respectively, with the Gaussian distribution (Peck, 1969) and the cumulative Gaussian curve (Mair and Taylor, 1997), this latter translated in order to take into account the effect of the support pressure acting at the tunnel face. The comparison between the steady-state computed profiles and the empirical ones, obtained with $K = 0.45$ and assuming $i_x = i_y = 6.75$ m, although generally satisfactory, highlights that the transversal and longitudinal inflection distances of the numerical troughs are slightly larger than the empirical ones (defined by the parameters i_x and i_y, respectively) and this comports that the final maximum settlement results rather underestimated.

This preliminary FF analysis was followed by the simulations including the structural models of 2, 4 and 8-storey buildings (STR interaction analyses), all carried out by imposing the same excavation sequence and amount of contraction defined above.

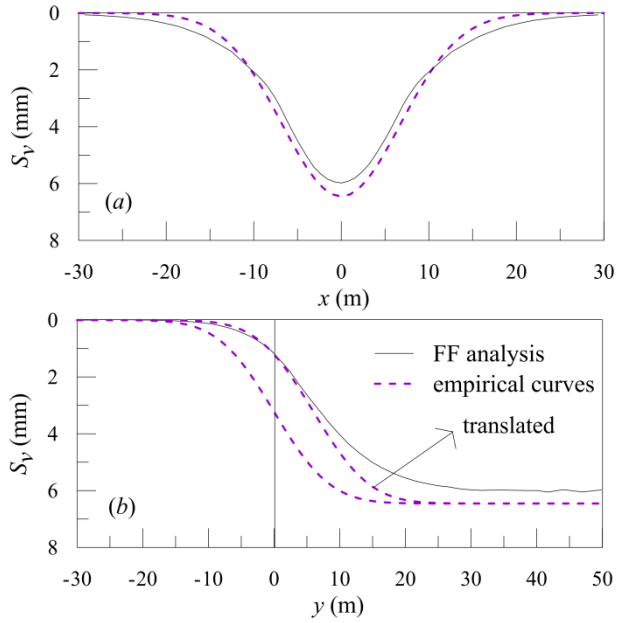

Figure 5.2. Comparison between numerical and empirical free-field subsidence profiles along transversal (*a*) and longitudinal (*b*) directions for V_L=0.31%.

Each structure is characterised by appropriate properties of weight and stiffness, these latter also enhanced by the inclusion in the structural models of the external cross-bracings.

The transversal and longitudinal settlement profiles computed by the STR analyses at the foundation level (i.e. 1 m below the ground surface) are compared in Figure 5.3 (*a*) and (*b*), where the free-field numerical curves (FF) are also shown. In particular, the proposed transversal troughs are those resulting along section A-A′ of the models (see Fig. 5.1), i.e. in correspondence with the main building façade.

In general, it is possible to observe that the taller the structure, the larger the maximum settlement and the extension of the curve as compared to the free-field one, and the greater the computed V_L. This latter feature has to be related to the dependency of the

adopted constitutive model on the effective stress state, leading to the non-negligible role of the weight of the structure.

Figure 5.3 (*a*) points out that the profiles of the analyses including the structure are characterised by lower differential settlements with respect to the free-field one, while they exhibit larger vertical displacements at the building edges, which indicate their embedment into the soil. Such a result, more evident for the 8-storey structure, is consistent with observations of centrifuge experiments discussed in the literature (e.g. Farrell and Mair, 2011).

Figure 5.3 (*b*) clearly highlights the stiffer response observed in correspondence with the foundation elements, whose position is reported by dashed lines. It also shows the non-uniform subsidence profiles under the buildings, to be related to the effect of the weight distribution.

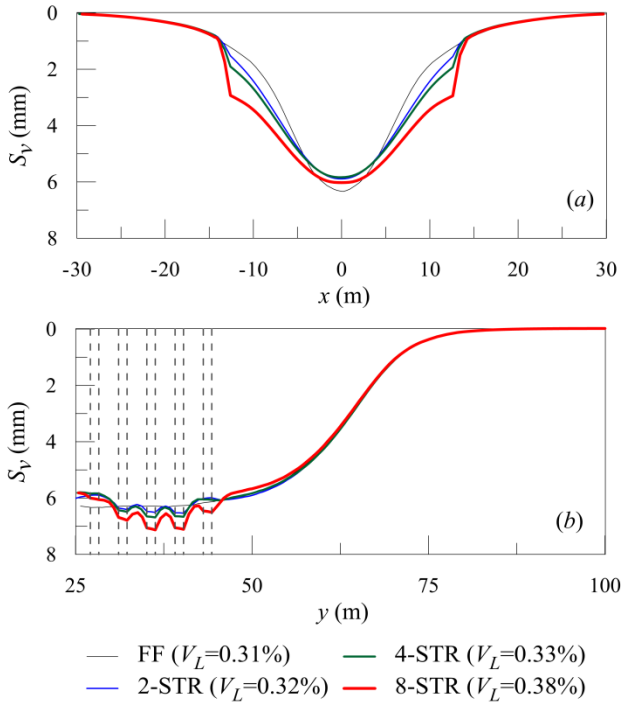

Figure 5.3. Computed transversal (*a*) and longitudinal (*b*) settlement profiles of free-field (FF) and interaction (STR) analyses with buildings of different height.

The role of the foundation warping direction was explored in an additional analysis (4-STR*), where the foundation beams of the 4-storey building were oriented along the *y*-axis, instead of along the *x*-axis (4-STR analysis). Such a comparison is shown in Figure 5.4, where the position of the foundation elements is reported by dashed lines. The figure highlights that, as expected, the 4-STR* transversal settlement profile is more discontinuous than the 4-STR one, although characterised by rather similar values of the vertical displacements computed in correspondence with the strip footings.

The contribution of the cross-bracings and the influence of the weight of the structure were specifically investigated for the 8-storey building in the analyses denoted as 8-STR$_{wcb}$ and 8-STR$_{w,}$ respectively.

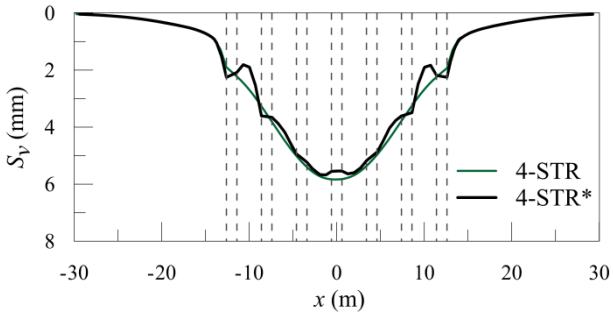

Figure 5.4. 4-storey building: comparison between 4-STR* and 4-STR subsidence profiles.

In particular, the building was modelled without cross-bracings in the 8-STR$_{wcb}$ analysis, while the structure was reduced to its corresponding non-uniform stress distribution acting at the strip footings levels, 1 m below the ground surface, in the 8-STR$_{w}$ analysis. The numerical outcomes are compared in Figure 5.5 (*a*) and (*b*). As displayed in Figure 5.5 (*a*), all the settlement troughs approximately intersect at i_x and overlap for *x* values located outside the building area. In particular, the figure highlights the stiffening role of the cross-bracings, which leads to a modification of the subsidence profile along both directions: an increasing in maximum and differential settlements is observed as the structural stiffness decreases. In Figure 5.5 (*b*) it appears that such an

effect is more evident in correspondence with the less loaded foundation elements (i.e. the external strip footings). As expected, the largest maximum and differential settlements are obtained by neglecting the overall stiffness of the structure, i.e. only considering its own weight (in STR_w analysis), despite the small variation in terms of volume loss.

The analysis of the results was also extended to compare the evolving response shown during the tunnelling process by the columns composing the main façade of the structure. Due to symmetry, the sole response of the columns located on the right side of the building was examined.

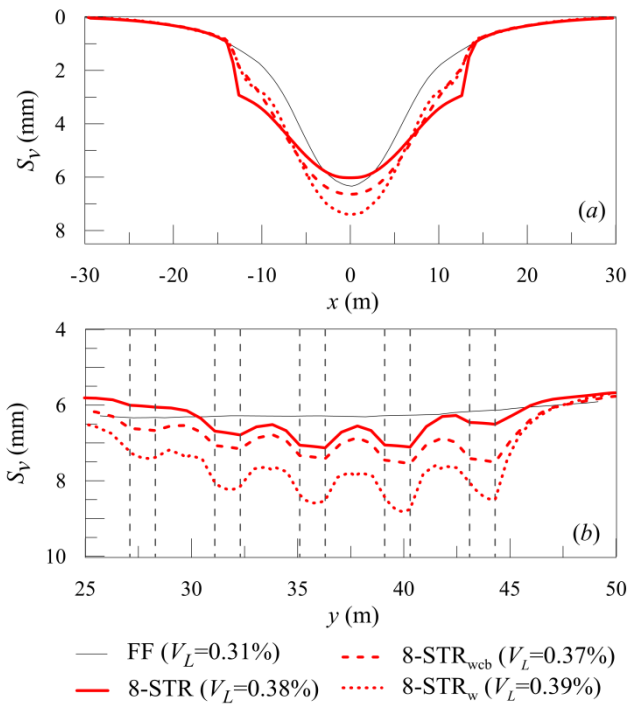

Figure 5.5. Comparison of computed settlement profiles of 8-storey building along transversal (*a*) and longitudinal (*b*) directions: the effect of the structural stiffness and weight.

In particular, the normal compressive forces (N) acting at the columns base (z = 0 m and x = 0 m, x = 4 m, x = 8 m and x = 12 m) are shown in Figure 5.6 (*a*) and (*b*) for different tunnel face positions (indicated by arrows in the figure). It is possible to observe (Fig. 5.6 *a*) that as the tunnel face is far from to the examined section (e.g. 16.5 m before the

section), the columns at x = 0 m, x = 4 m and x = 8 m are characterised by the same N value. This latter coincides with that due to the building self-weight and it is larger than that acting in the outer column (x = 12 m).

During tunnel advancement, the normal force decreases in the inner columns (i.e. those at x = 0 m and x = 4 m), while in the outer ones, affected by lower settlements, it exhibits an opposite trend. At the end of the excavation sequence, N reaches its maximum value in the column at x = 12 m, which experiences the lowest vertical displacement.

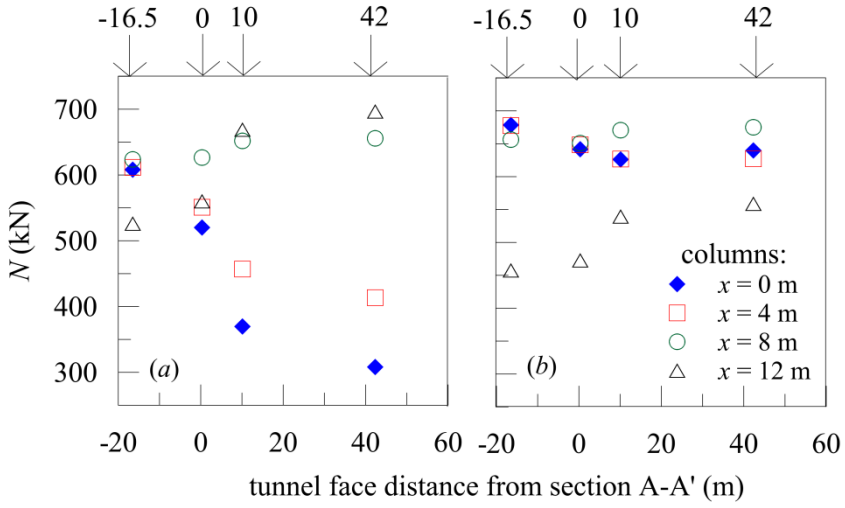

Figure 5.6. 8-STR (*a*) and 8-STR$_{wcb}$ (*b*) analyses: *N* values acting in the columns of the 8-storey building at the excavation progress.

This behaviour is due to the process of force redistribution within the structure, which is enhanced by the presence of the cross-bracings. The absence of these latter elements in the numerical model (8-STR$_{wcb}$ analysis) inhibits the load transfer within the structure: in fact in this case, illustrated in Figure 5.6 (*b*), N values in the inner columns are rather constant during tunnelling, while the normal stress evolution in the outer one is similar to that of Figure 5.6 (*a*), but for lower values of normal compressive forces.

5.3 Numerical simulation of the interaction process between a 9-storey reinforced concrete framed building and the Milan metro-line 5

5.3.1 Finite element scheme with a detailed structural model

The numerical model (80 m x 100 m x 30 m) set up to simulate the interaction between the twin tunnels of the metro-line 5 and the investigated multi-storey reinforced concrete framed building undercrossed by the first tunnel (Fargnoli et al., 2015 *a*) is shown in Figure 5.7. It neglects, for sake of simplicity, the presence of other nearby constructions and its dimension minimises the influence of boundary conditions on the computed results.

The soil profile refers to the subsoil conditions encountered between *Lotto* and *Portello* stations (the segment of the route where the building is located) and it was defined according to the *in situ* stratigraphy. As for the previous numerical analyses, in this case too the mechanical behaviour of the soils was described by the *Hardening soil model with small strain stiffness* using the parameters summarised in Table 4.2 of the previous chapter.

The tunnels have a diameter D = 6.7 m and their axes, having a horizontal distance d equal to 16.7 m, are located at a depth of z_0 = 15 m, as in the reference case of study in correspondence with the ground section S_{35} nearby the building (see Fig. 3.30 of Chap. 3), also represented in Figure 5.7.

The simulation of each tunnel excavation was performed by the step-by-step numerical procedure already described in detail and validated in Section 4.3.2 (see Chap. 4), using the same values of the face and grouting pressures.

In the model of Figure 5.7, the first tunnel underpasses the building according to the real tunnel-structure relative position. In particular, the rotation angle of the longitudinal sides of the building with respect to the tunnel axes is set equal to 25.14° and the x and y

coordinates of the structure's middle point *C* (see Fig. 3.30 of Chap. 3) are equal to 0 m and 35 m, respectively.

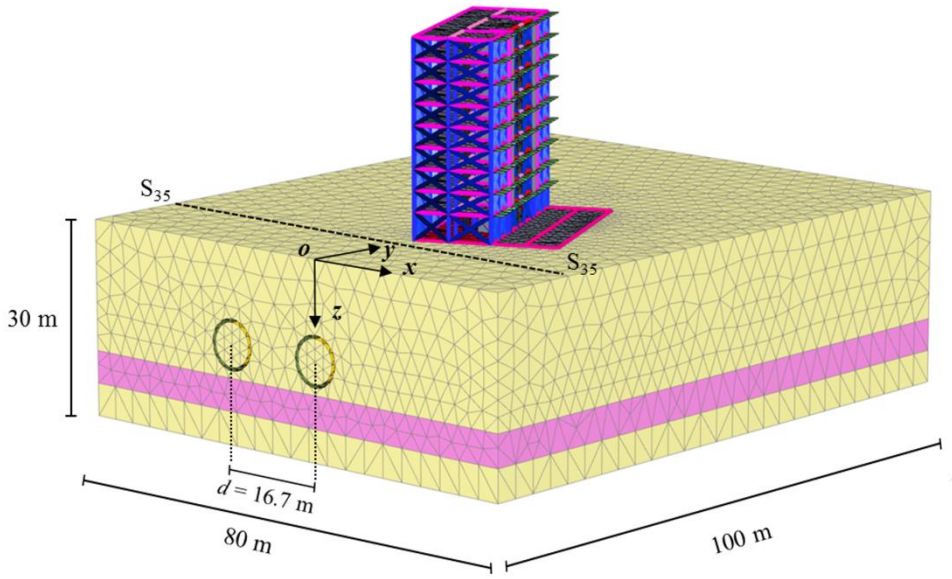

Figure 5.7. Detail of the mesh used in the numerical model with the building and the twin tunnels.

In the structural model of the building:

- beams and columns were modelled by beam elements;

- floor-slabs, reinforced concrete interior panels, elevator shafts, stairwell and retaining walls were modelled using plate elements;

- foundations were modelled using volume elements constituted by non-porous material.

A linear-elastic constitutive law was selected for all the structural components, considering material properties appropriate for the reinforced concrete (i.e. γ_c = 24 kN/m^3; E_c = 25 GPa; ν_c = 0.2).

The building is characterised by the presence of infill panels, uniformly distributed along the external frames, which were modelled, in this case too, in a simplified way by means of equivalent cross-bracings following Mainstone (1971) (see Section 5.2). In this model, however, in order to introduce a more realistic value of the maximum tensile strength, F^{T}_{lim}, it was assumed to be equal to 0.1 F^{C}_{lim}.

The pressure distribution of this structure at the foundation level is shown in Figure 5.8. It is possible to observe, in particular, higher pressure values in correspondence with the elevator shafts (F_{VI} and F_{VIII}) and the stairwell (F_{VII}), i.e. the heavier components of the building.

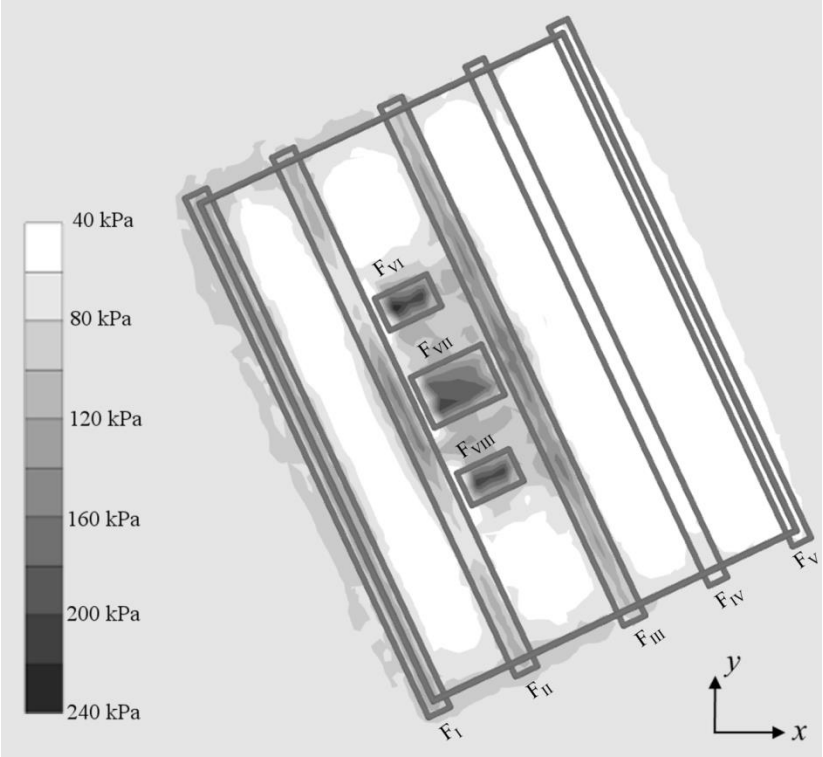

Figure 5.8. Pressure distribution at the foundation level of the building.

5.3.2 Results of the numerical analysis with a detailed structural model

The first part of the finite element study was devoted to simulate the excavation of the first tunnel which directly interacts with the reference building.

Such simulation was firstly performed without activating the surface structure in the model (under free-field conditions, i.e. numerical analysis defines as FF) in order to calibrate the contraction to be applied at the tunnel shield to reproduce a volume loss $V_L^{(I)}$ equal to 0.34%, which corresponds to that observed at the monitoring ground section nearby the building (i.e. section S_{35}, see Tab. 3.5 of Chap. 3). In particular, such

a contraction was calibrated verifying that the induced maximum vertical displacement at the tunnel crown in correspondence with the shield tail (equal to about 10 mm for the reference volume loss) was compatible with the available gap of the adopted EPB machine.

The computed transversal and longitudinal surface settlement profiles were compared with the measurements recorded at section S_{35}, as shown in Figure 5.9 (*a* and *b*) which also illustrates the Gaussian empirical curves.

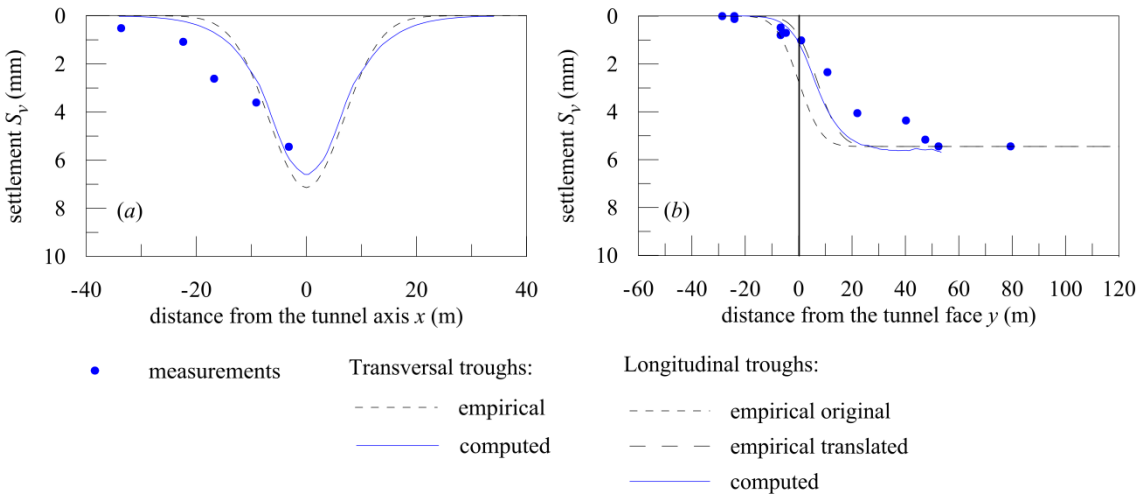

Figure 5.9. Comparison of measured settlements with empirical and computed (analysis FF) subsidence profiles along transversal and longitudinal directions due to the first tunnel excavation.

In general, the comparison is satisfactory. The computed transversal profile (Fig. 5.9 *a*) results in fair agreement with the Gaussian distribution; however, the accordance with the experimental measurements decreases as the distance from the tunnel axis increases, so that settlements measured at x lower than -16.7 m result underestimated.

The numerical longitudinal subsidence trough (Fig. 5.9 *b*), quite similar in shape to the translated one, is able to capture the face and final recorded settlements; nonetheless, it predicts the attainment of steady-state conditions at a shorter distance from the face as compared to what measured.

The overall consistency of the computed profiles with the empirical solutions and with available measurements indicates that the adopted numerical model is amenable to be adopted for more complex interaction analyses, as illustrated in the following.

With the aim to investigate the interaction between the first tunnel and the building, this latter was included in the numerical model and the computation was repeated imposing the same excavation sequence adopted in FF analysis, thus assuming that no relevant changes in volume losses occurred between the ground section S_{35} and the structure. This interaction analysis, defined as STR, was performed accounting for the appropriate weight and stiffness of the structural elements, including in the model the external cross-bracings.

The numerical final settlement troughs, as computed along the transversal and longitudinal directions to the tunnel axis at the foundation level (i.e. 4 m below the ground surface), are compared to the corresponding free-field predictions in Figure 5.10 (*a*) and (*b*). The plant position of the foundation elements is also shown by dashed lines. In particular, the figure refers to the subsidence profiles computed at the barycentre of the building (point C in Fig. 3.30 of Chap. 3).

As expected, the presence of the building influences the settlement profiles which deviate from the free-field ones along both directions, highlighting the stiffer response observed in correspondence with the discrete foundation elements. The two profiles only overlap outside the building area. It is worth noting that the maximum vertical displacement and volume loss of the interaction analysis are larger than the free-field one, due to the effect of the building weight. Such an observation is particularly evident at the stairwell (F_{VII} in Fig. 5.10 *a*) and at the elevator shaft (F_{VI} in the same figure), i.e. in correspondence with the heavier components of the building.

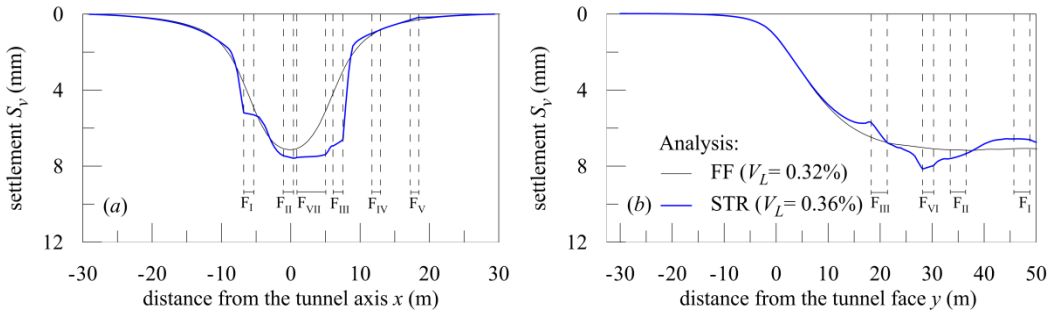

Figure 5.10. Comparison between computed settlement profiles of FF and STR analyses as evaluated along the middle section of the building along the transversal (*a*) and longitudinal (*b*) directions to the tunnel axis at the end of the first tunnel excavation (the corresponding volume loss values are also reported in the legend).

In order to explore the influence of the second excavation, the construction of the other tunnel of the metro-line was subsequently simulated in the STR analysis. In this case too, the value of the contraction to be applied at the second shield was calibrated to achieve the observed final volume loss $V_L^{(TOT)} = 0.84\%$ as evaluated in the ground section S_{35} (see Tab. 3.6 of Chap. 3) .

The comparison shown at the transversal section S_{35} in Figure 5.11 confirms the accordance between the computed profiles, the empirical relationship and the monitoring data. The numerical profile is capable of capturing the final settlements above the tunnel axes and the increase in the maximum vertical displacement above the first axis after the second excavation (as highlighted from the comparison with the computed and measured settlements due to the first excavation, also reported in the same figure for sake of clarity). In particular, it is possible to note that the numerical curve obtained after the simulation of the second tunnel construction well reproduces the corresponding measurements, irrespectively of the fact that the same comparison was not very satisfactory after the first tunnel excavation.

In Figure 5.12 (*a*-*c*) the structural vertical displacements measured at selected stages of the excavation process are compared with the computed profiles along the left and right

longitudinal façades of the building and along its transversal side. In particular, reference is made to the observations carried out for a position of the first tunnel face at the middle of the structure (point *C* in Fig. 3.30 of Chap. 3) and at the end of the first and the second excavation, respectively.

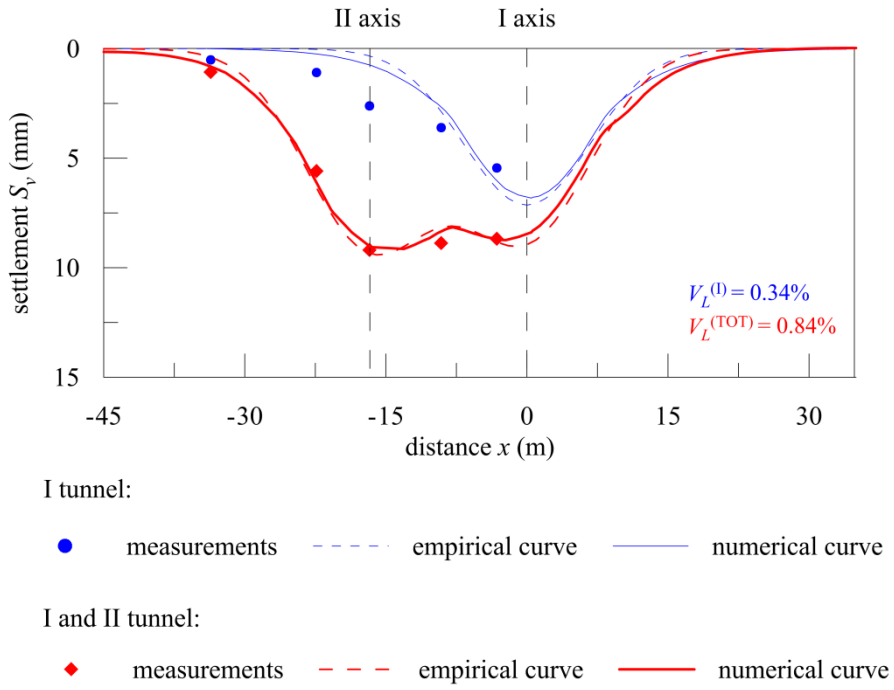

Figure 5.11. Comparison of measured settlements induced by the first and the second tunnel at ground transversal section S_{35} with numerical curves (the Gaussian empirical curves are also shown in the plot).

The numerical analysis, properly taking into account the geometry, the stiffness and the weight of the building, provides subsidence profiles along each building façade that well reproduce the measured vertical displacements in terms of both shape and single values. In general, the finite element computation accurately predicts the deformative pattern of the building, realistically capturing the evolution from hogging to sagging configurations during the different phases of tunnelling. In fact, the hogging and sagging zones are highlighted along the left and right longitudinal building façades (Fig. 5.12 *a* and *b*), where the settlement troughs are more continuous than that observed

along the transversal side (Fig. 5.12 *c*), as they are computed under the strip footings F_I and F_{III}, respectively (see Fig. 3.31 of Chap. 3). In particular, in order to define in detail the position of the inflection point along each façade, the computed subsidence profiles were interpolated by a polynomial function (a fourth order one provides in all cases a regression coefficient $R^2 > 0.99$) and the inflection point was numerically determined as the zero of its second derivative.

In general, it is possible to observe that when the tunnel face is located at the middle of the structure, the numerical settlement profiles mainly show a hogging-type deformative mode along both the longitudinal sides, while the transversal one is interested by null settlements. After the first and the second excavation, a sagging configuration mainly characterises the right longitudinal side, while both sagging and hogging modes can be detected along the left one, where the inflection point translates from x = 16 m (at the end of the first tunnel construction) to x = 14 m (after the second tunnel excavation), as indicated in Figure 5.12 *a*. In particular, along the left side the second excavation induces a slight reduction of the maximum deflection ratios (Δ_{max}/L) (%) with respect to the previous deformative configuration (i.e. the end of the first tunnel excavation), from 2.75×10^{-3} to 1.41×10^{-3} in the sagging zone and from 1.70×10^{-3} to 1.53×10^{-3} in the hogging one. A negligible decrease in $(\Delta_{max}/L)_{sag}$ (%) from 1.13×10^{-2} to 1.01×10^{-2} is also observed along the right side, characterised by larger values of this parameter as compared to the left one.

Analysing in detail Figure 5.12 (*c*), it emerges that the final displacement profile obtained along the transversal side is characterised, as expected, by a stiffer response in correspondence with the discrete foundation elements. In particular, a hogging deformative mode affects the portion between the strip footings F_I and F_{II}, while the settlement profile appears to be more regular between the foundation elements F_{II} and

F_{III}, where the final deformative pattern corresponds to an almost rigid rotation if evaluated with respect to the previous configuration (i.e. that at the end of the first excavation).

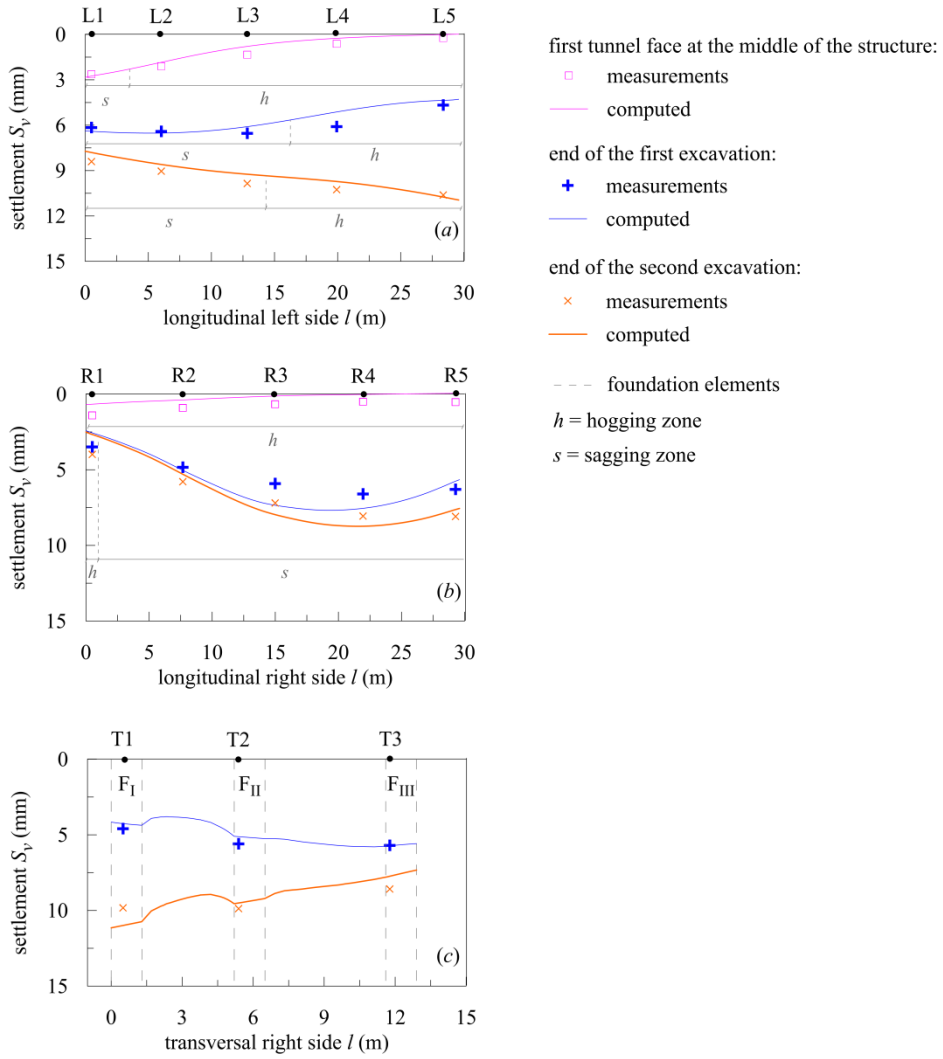

Figure 5.12. Comparison of settlements measured along the left (*a*) and right (*b*) longitudinal sides of the building and along its transversal one (*c*) at different phases of twin tunnel excavation (on the transversal side the position of the foundation beams is also indicated by dashed lines).

Field observations demonstrate that typically structures are more vulnerable to hogging deformative modes as compared to sagging ones (e.g. Burland et al., 2001), as settlements may induce cracks in the upper portions where the constructions are not constrained by ground and foundation elements and, as such, they are more prone to

deform. However, differently from masonry structures, the presence of closed frames in reinforced concrete buildings confines the crack propagation, generally preventing severe damages to occur (Son and Cording, 2011).

Figure 5.13 presents an attempt to investigate this aspect of the structural response, by plotting the normal stresses acting within the cross-bracings of the longitudinal façades while the building experiences a predominantly hogging-type mode of deformation, i.e. when the first tunnel face is located at the middle of the structure. The figure also includes the corresponding computed subsidence profiles and the relative values of the deflection ratio $(\Delta_{max}/L)_{hog}$ (Burland and Wroth, 1974; Burland et al., 2004).

Larger normal compressive stresses (σ_c) are observed at the lower floors, due to the effect of the structure's weight. According to the deformative mechanism, the cross-bracings subjected to normal tensile stresses (σ_t), represented by dashed lines in the figure, are located in the upper levels of the structure. They tend to concentrate along the left longitudinal side, which is characterised by larger total and differential settlements and, consequently, by the highest value of the maximum deflection ratio. The computed maximum value of the tensile strain, detected on this side and equal to about 0.004 %, is much lower than the limit value proposed by Boscardin and Cording (1989) to identify the upper bound of the "negligible" damage category (i.e. 0.05 %); this is consistent with the absence of damage observed *in situ* on this structure.

The structural response was also analysed in terms of normal compressive forces (N) acting at the base ($z = 0$) of the columns located along the longitudinal façades of the building at the end of the first tunnel excavation. These values are reported in Figure 5.14 (*a*) and (*b*) together with the settlements computed at the columns' base at such selected tunnelling stage.

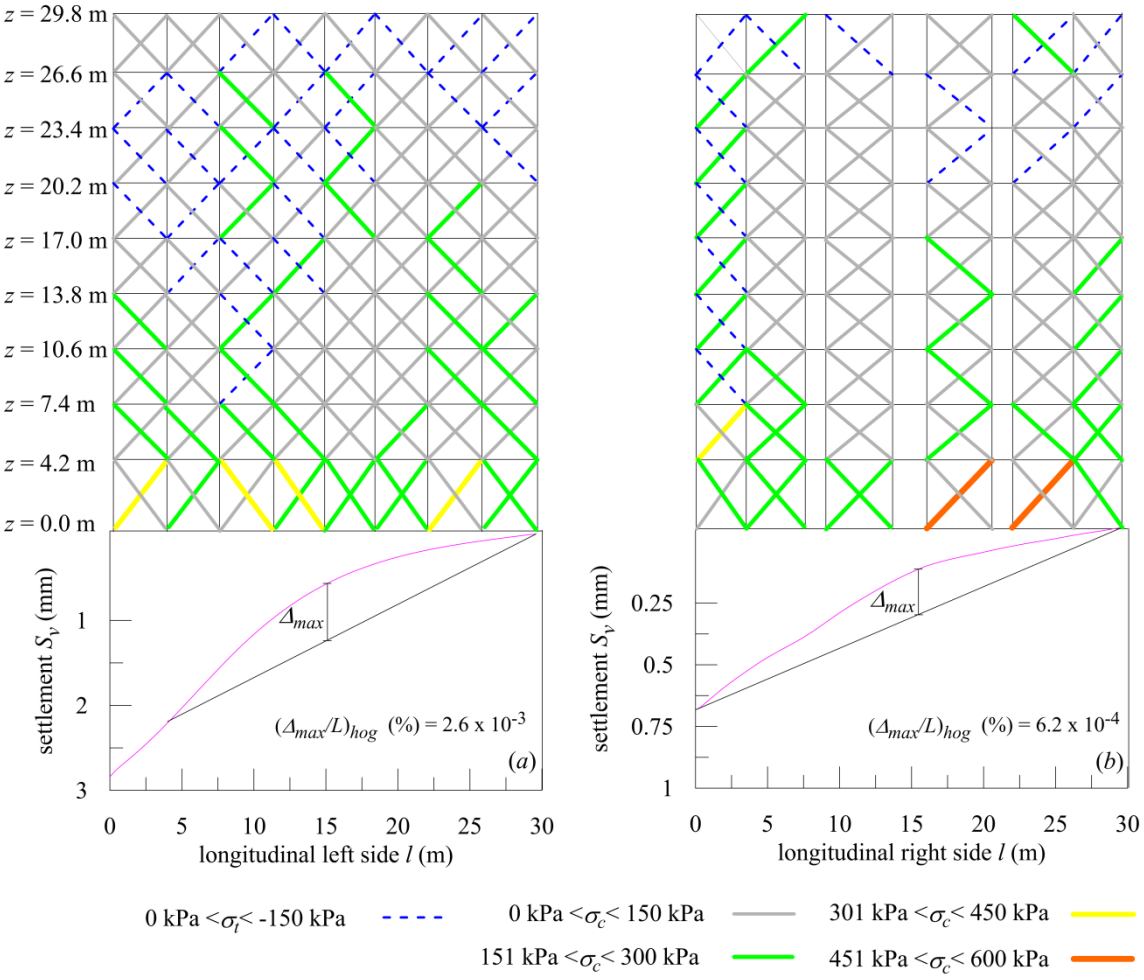

Figure 5.13. Distribution of the normal compressive and tensile stresses in the cross bracings of the left and right longitudinal façades of the building associated to a hogging-type mode of deformation (i.e. when the first tunnel face is located at the middle of the building).

The *N* values predicted before tunnelling are approximately constant, their distribution being more regular along the left side of the building due to the corresponding more regular column distribution. Once the excavation process has been completed, the distribution of *N* results as modified: in general, *N* decreases for the columns that experience larger settlements, while it increases for those which settle the less. This expected pattern, more evident for the left façade, should be ascribed to the force-transfer mechanism which is enhanced by the presence of the cross-bracings, as already discussed in the previous paragraph concerning the ideal 8-storey building.

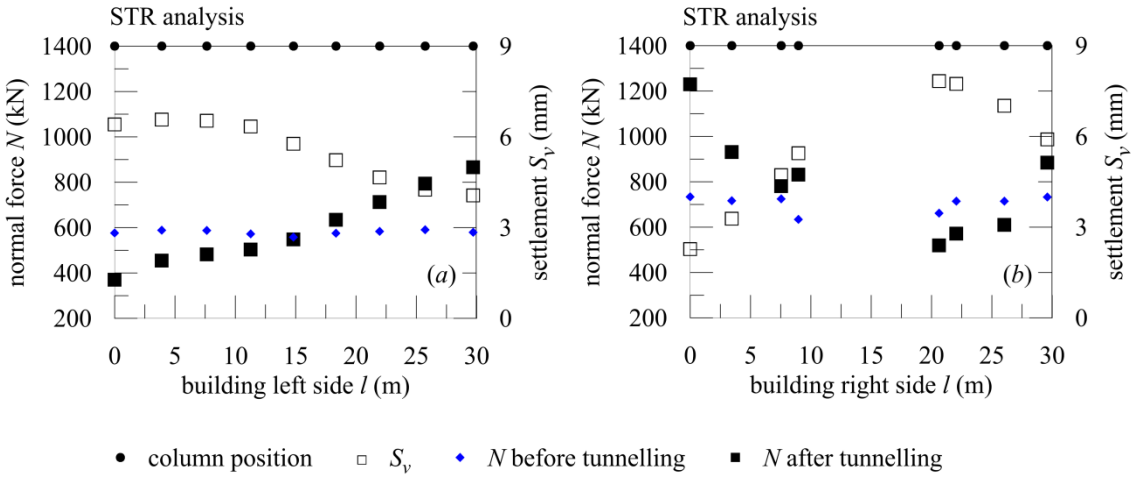

Figure 5.14. STR analysis: normal compressive force and settlement values at the base of the columns on the left (*a*) and right (*b*) longitudinal sides of the building before tunnelling and at the end of the first tunnel construction.

5.3.3 Finite element schemes with simplified structural models

Additional numerical schemes were also set up adopting different levels of detail in the structural modelling (Fargnoli et al., 2015 *b*). The analysis was limited to the interaction with the first tunnel of the metro-line and, in order to reduce the computational effort, the width of the mesh was reduced from 80 m (see Fig. 5.7) to 68 m, as shown in Figure 5.15.

The simplified structural schemes considered in the numerical study are described in the following:

- the building was first modelled without cross-bracings (Fig. 5.15 *a*) in order to investigate the stiffening role of these components (analysis STR_{wcb});

- the building was limited to its buried portion (Fig. 5.15 *b*) in order to evaluate its stiffening contribution (analysis STR_w). This model also includes the foundation elements and the retaining walls, those latter 0.4 m thick and 3.5 m high, connecting the foundation level to the ground floor. The upper portion was reduced to an equivalent load distribution; these loads were evaluated with reference to their influence area and

they were applied at the ground floor in correspondence with the columns' head, the stairwell and the elevator shafts;

- the structure was strongly simplified and schematised as an equivalent plate (L = 30 m and B = 12 m) in terms of stiffness and weight (Fig. 5.15 *c*), placed at the foundation level (analysis STR*). In this model the retaining walls were also introduced. The input parameters of the equivalent plate were derived adapting the approach proposed by Franzius et al. (2006), as discussed in the following.

The axial $(E_cA)_{building}$ and bending $(E_cJ)_{building}$ stiffness of the building were calculated considering the structure to consist only of floor slabs and to be oriented with the longitudinal sides parallel to the tunnel axis (such hypothesis does not significantly influence the second moment of area of the slab):

$$(E_cA)_{building} = \sum_{1}^{n} (E_cA)_{slab} \tag{5.1}$$

$$(E_cJ)_{building} = \sum_{1}^{n} (E_cJ)_{slab} = E_c \sum_{1}^{n} (J_{slab} + A_{slab} H_m{}^2) \tag{5.2}$$

were:

- n is the reference level of the building;

- A_{slab} and J_{slab} are the cross-sectional area and the second moment of area of the slab at each level, respectively;

- H_m is the vertical distance between the slab's and the structure's neutral axis (this latter assumed to be located in correspondence with the structure's centroid).

The building foundation system was neglected in this simplified approach (Franzius et al., 2006).

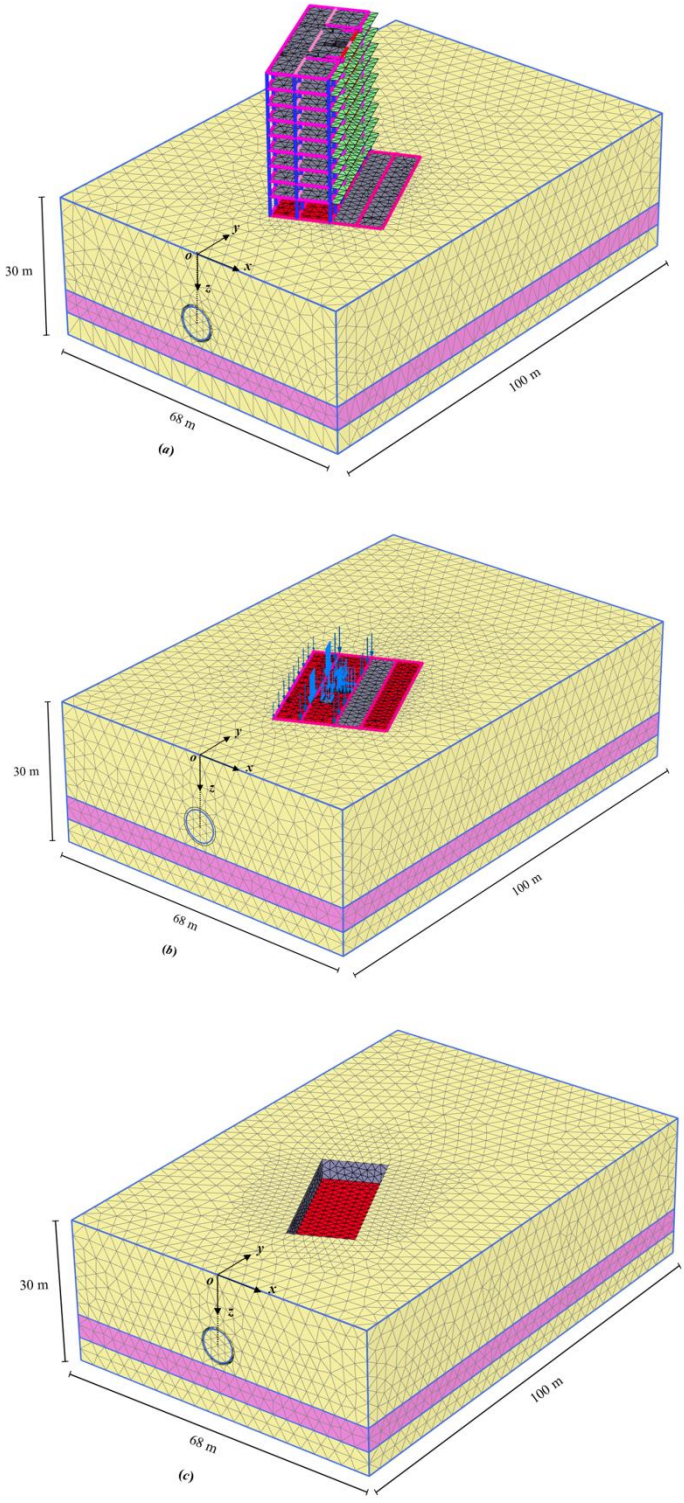

Figure 5.15. Sketch of the finite element models with simplified structural schemes: building without cross-bracings (*a*); building reduced to its buried portion (*b*); building reduced to an equivalent plate (*c*).

The computed axial and bending stiffness for each slab are reported in Table 5.1 together with the thickness and H_m values.

level, n	slab thickness (m)	H_m (m)	$E_c A_{slab}$ (kN)	$E_c J_{slab}$ (kNm^2)
basement floor	0.26	15.70	1.95E+0.8	1.10E+06
ground floor	0.26	13.20	1.95E+08	1.10E+06
1st floor	0.22	9.00	1.65E+08	6.66E+05
2nd floor	0.22	5.80	1.65E+08	6.66E+05
3rd floor	0.22	2.60	1.65E+08	6.66E+05
4th floor	0.22	0.60	1.65E+08	6.66E+05
5th floor	0.22	3.80	1.65E+08	6.66E+05
6th floor	0.22	7.00	1.65E+08	6.66E+05
7th floor	0.22	10.20	1.65E+08	6.66E+05
8th floor	0.22	13.40	1.65E+08	6.66E+05
9th floor	0.22	16.60	1.65E+08	6.66E+05

Table 5.1. Stiffness properties of the slabs at each level.

The input parameters of the plate element used in the FE analyses were then evaluated as:

$$t_{fe} = \sqrt{\frac{12(E_c J)_{building}}{(E_c A)_{building}}} \tag{5.3}$$

$$E_{fe} = \frac{(E_c A)_{building}}{t_{fe}} \tag{5.4}$$

being t_{fe} (equal to 36 m) and E_{fe} (equal to 51.8 GPa) the equivalent thickness and Young's modulus, respectively.

The unit volume weight of the plate element, equal to 2.92 kN/m^3, was calculated as the ratio between the total building weight (excluding the weight of the retaining walls modelled in the analysis, equal to about 2500 kN) and the plate volume (B x L x t_{fe}).

5.3.4 Results of the numerical analyses with simplified structural models

The additional analyses carried out adopting simplified schematisations of the building aim at highlighting the role of different structural components on the overall stiffness of the system and, thus, on the computed displacement field.

Figure 5.16 summarises all the monitored and computed settlement profiles as observed and back-predicted along the longitudinal and transversal sides of the building.

The comparison between the STR_{wcb} and STR results proves that the absence of the cross-bracings does not significantly affect the overall displacement pattern (Fig. 5.16), while it can play a non-negligible role on the structural forces.

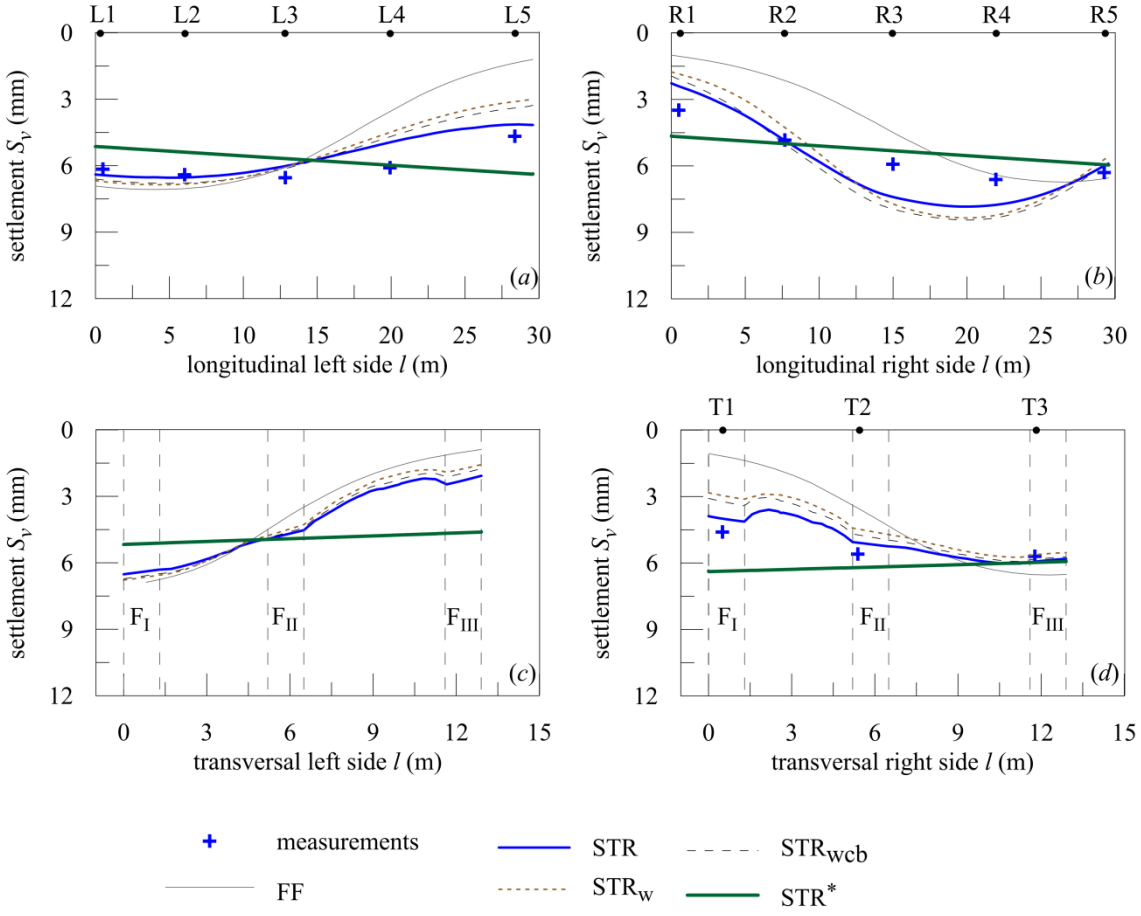

Figure 5.16. Comparison of monitored, empirical and computed settlements at the end of the first tunnel excavation on the longitudinal left (*a*) and right (*b*) sides and on the transversal right side of the building (*d*). Empirical and computed settlement profiles on the transversal left side of the structure, where measurements were not available, are also compared (*c*).

As shown in Figure 5.17 (*a* and *b*), in fact, the absence of these elements reduces the force redistribution process within the structure: at the end of excavation, the *N* distribution is characterised by a different pattern as compared to analysis STR (see Fig. 5.14 *a* and *b*), with relatively higher values in the inner columns for the left side of the

building (Fig. 5.17 *a*) and less intense actions on the external columns along the right side (Fig. 5.17 *b*).

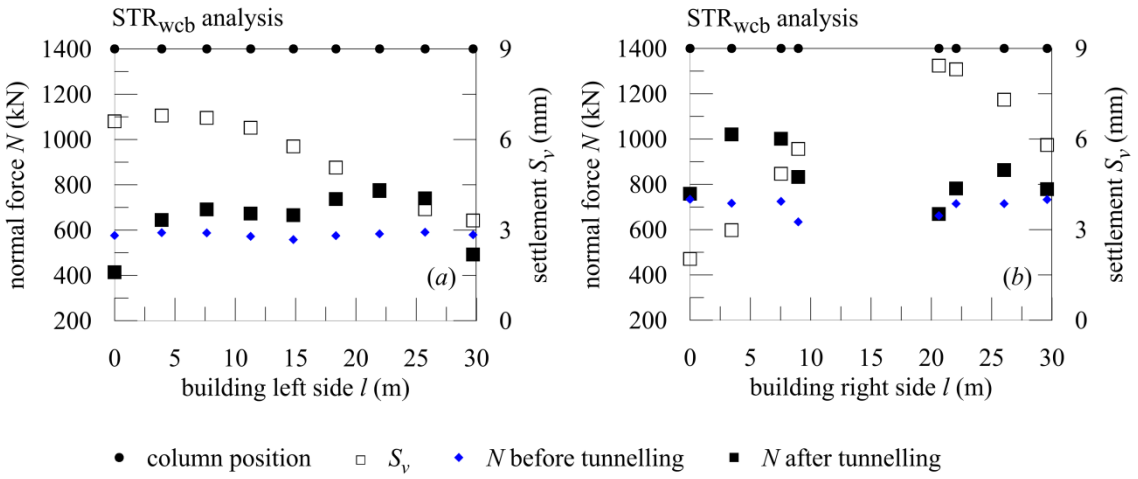

Figure 5.17. STR analysis: normal compressive force and settlement values at the base of the columns on the left (*a*) and right (*b*) longitudinal sides of the building before tunnelling and at the end of the first tunnel construction.

The displacement curves obtained by the analysis STR$_w$, carried out disregarding the above-ground portion of the building, are very similar to the STR ones, thus indicating that, in this particular case, the buried portion of the structure provides the most relevant contribute to the overall stiffness. In particular, the differential settlements along the transversal sides of the building, in correspondence with the foundational elements, are practically coincident with those computed by the complete structural model.

The free-field results, reported for comparison in Figure 5.16, in each case lead to less intense settlements with respect to the interaction analyses and rather overestimated differential ones.

Finally, the results obtained using the equivalent plate schematisation (STR* analysis) are highly unsatisfactory for this specific framed building which rests on a discrete foundation system. The outcomes provided by this simplified structural scheme are also on the unsafe side, since the building stiffness results to be largely overestimated and

the displacement field at the foundation level appears to be characterised by almost rigid rotations along the four sides of the structure, without indicating any sagging or hogging deformative modes.

6. Conclusions

This research is mainly devoted to analyse the interaction mechanism between a reinforced concrete framed building and the twin tunnels of an urban metro-line. Reference is made to *in situ* settlement monitoring data and results of three-dimensional (3D) finite element computations performed by a fully-coupled approach, i.e. incorporating in a unique numerical model the soil, the tunnel and the structure. This integrated solution, sometimes adopted in the past by other researchers to evaluate the effects on masonry buildings due to tunnel excavation, has not yet been extended to date to framed structures schematised with accuracy. As such, one element of novelty of this study is the detail adopted in modelling an existing multi-storey reinforced concrete building influenced by tunnelling activities. This topic is nowadays of great relevance for metro-line construction in urban areas, where structures frequently interact with underground excavations and, as such, might be damaged.

As discussed in Chapter 2, the empirical approach proposed in the past to predict the surface subsidence in absence of existing structures on the ground (i.e. under free-field conditions), considers Gaussian distributions for the settlement profiles induced by tunnelling in the transversal and longitudinal directions to the tunnel axis. Interaction phenomena affect the settlements experienced by existing buildings, which differ from those predicted under free-field conditions by the empirical solutions. These latter, in fact, neglect the modification of the subsidence profile due to the stiffness and weight of the structures, often leading to an unrealistic scenario, characterised by a far too cautious estimation of their structural damage.

The more recent development of numerical methods to analyse this class of soil-structure interaction problems represents a valuable opportunity to properly

estimate the unavoidable impacts of tunnelling on nearby constructions, especially when a three-dimensional scheme is set up in the analysis.

The case study of the new metro-line 5, recently built in Milan (Italy), is taken as reference in this work and introduced in Chapter 3. The twin tunnels of the line, characterised by a diameter of 6.7 m, were excavated by earth pressure balance (EPB) machines in sandy soils partially under the water table; their axes have an average distance equal to 15 m and a mean depth of 15 m.

Measurements of the surface subsidence collected along several ground sections under free-field conditions are analysed and typical settlement values due to the first and the second tunnel excavation are defined, representing a very large database to infer the performance of EPB tunnelling in these specific geotechnical conditions. It is found, in particular, that settlement measured above the first tunnel axis after the first excavation varies between 5.1 mm and 21.4 mm, with an average value of about 11.0 mm, while it ranges from 6.0 mm to 24.8 mm, with an average value equal to about 15.0 mm, after the second excavation. The settlement measured above the second tunnel after its construction varies from 8.0 mm to 27.8 mm, with an average value of about 12.0 mm.

It is observed that the excavation of the second tunnel systematically induces an increase in the settlement above the first tunnel axis. This latter is, most of the times, the largest one.

Surface ground settlements are analysed and interpreted using the well-known empirical solutions to obtain a complete description of the subsidence profile in the transversal and longitudinal directions to tunnels.

In the transversal direction, settlements due to the first tunnel construction result to be well fitted by a Gaussian distribution curve (Peck, 1969) characterised by back-calculated trough width parameters, K, appropriate to coarse-grained soils, thus in

the range 0.3-0.45, and by volume loss values varying from 0.27 % to 0.82 %, with an average value of about 0.5 %. Consistently with other studies reported in the literature, the monitoring data highlight the dependency of the width of the subsidence profile on the corresponding settlement magnitude: in general, the width decreases as the maximum settlement increases.

The observed transversal subsidence trough due to twin-tunnelling is characterised by a volume loss value in the range 0.62-1.89 % and on average equal to 1 %. It is demonstrated that this final profile cannot be simply reproduced by superimposing two single identical Gaussian curves, being in general unsymmetrical with different maximum values of settlement above the tunnel axes. As such, the specific empirical equation proposed by New and O'Reilly (1991) for the description of the subsidence profile in the transversal direction, always using K parameters in the typical range of this class of geotechnical conditions, results as adequate only if two different values of the vertical settlements above the two axes are selected.

The subsidence induced solely by the second excavation is found to be not symmetric with respect to the second tunnel axis, being the displacements larger on the side towards the first tunnel. This effect should be related to the reduced stiffness of the soil in this area due to the former accumulation of strains as a consequence of the excavation of the first tunnel.

Concerning the longitudinal direction, the evolution of settlements above the tunnel axes is adequately interpolated by a Gaussian cumulative curve (Attewell and Woodman, 1982) if the face settlement is set equal to the measured one. This curve is characterised by the same value of the inflexion point as observed in the transversal direction and by a face settlement generally lower than 0.5 times the steady-state value. This ''translated'' pattern of the subsidence curve along the longitudinal direction has to

be related to the limited volume loss guaranteed by the pressure applied at the tunnel face.

Different excavation parameters are analysed in the study to highlight possible correlations with settlement data. It is found that only the face and the back-filling grouting pressures seem to a have a not negligible influence on the subsidence due to the first tunnel construction, showing an inverse linear correlation with the volume losses computed at the end of this stage of the excavation process. Conversely, the settlement values measured above the tunnel axes after the second excavation do not show any apparent correlation with the same excavation parameters.

Vertical displacements were also monitored along three sides of a 30 m high reinforced concrete framed building diagonally undercrossed by one of the two tunnels. This structure is founded on five strip footings and on three raft foundations located at a depth of 4 m below the ground surface. Reinforced concrete retaining walls surround its buried portion along three sides, significantly contributing to the overall stiffness of the building. Measurement analysis allows to better understand the modification of the structural deformative pattern during the tunnelling activities. In particular, the response of the building changes from a hogging-type to a prevailing sagging-type mechanism during the construction of the first tunnel, while the second excavation determines an increase in the absolute settlements along each building side and a translation of the inflection point along the longitudinal façade closer to the second tunnel (i.e. the left one). No damage induced by the construction of the metro-tunnels was detected on this structure, due to the relatively low values of the absolute settlements, always lower than 11.0 mm.

The advanced 3D numerical analysis of the investigated problem was preceded by a preliminary finite element study, presented in Chapter 4. In particular, the attention is

first devoted to the constitutive hypothesis adopted to describe the soil mechanical response. Thus, two-dimensional (2D) finite element analyses of a single tunnel excavation are carried out assuming two different constitutive models for the soil: the simple linear elastic-perfectly plastic *Mohr-Coulomb* model (MC) and the more advanced *Hardening Soil model with small strain stiffness* (HSsmall), both available in the material model library of the numerical code used in the study (i.e. Plaxis) and carefully calibrated against *in situ* tests. The comparison of empirical and numerical settlement predictions with monitoring data highlights the capability of the HSsmall model to describe with accuracy the soil response during tunnelling. In fact, thanks to the dependency of the soil stiffness on the deformative level and to the early accumulation of plastic strains, it provides a computed profile in accordance with experimental observations in terms of maximum settlement and extension of the subsidence curve for volume loss typical for EPB-tunnelling in coarse-grained soils. This evidence is in contrast with the tendency of the more simple MC model to underpredict the maximum vertical displacement, overestimating the wideness of the subsidence trough.

The study is extended to the 3D numerical simulation of single and twin tunnel excavation under free-field conditions using a simplified step-by-step procedure which simulates the main aspects of the process (e.g. the action of face and grouting pressures, the conical geometry of the shield, the lining installation, etc.). The combination of this numerical technique to simulate the EPB-tunnelling with the adopted constitutive formulation leads to transversal and longitudinal surface subsidence troughs in agreement with measured settlements and empirical curves. It is found to be very effective also in capturing the unsymmetrical final settlement profile computed after the second excavation.

In this study, the response of simple framed structures subjected to different loading conditions is assessed by comparing the results of analyses performed on these models by two different codes, i.e. Plaxis 3D and the well-known program Sap 2000. The comparison confirms the realistic performance of the structural components implemented in Plaxis 3D, but it also highlights some limits of these elements, for example the inability of the *beams* to react to torsional actions.

The modification of the free-field transversal and longitudinal subsidence profiles due to the presence of ideal buildings with different properties of stiffness and weight is discussed in the first part of Chapter 5. The numerical outcomes highlight that, in general, the taller and heavier the structure, the larger the maximum settlements and the lower the differential ones. Larger vertical displacements are obtained, in particular, by neglecting the overall stiffness of the structure or the stiffening contribution provided by its external infill panels, although modelled in a simplified way (i.e. as equivalent cross-bracings).

Numerical analyses were carried out in the final part of the work to evaluate the effects induced by tunnelling on the real nine-storey framed structure interacting with the Milan metro-line 5. The building was introduced in the numerical scheme with different level of detail. The computed results clearly highlight, as expected, the role of the structure stiffness and weight on the settlement troughs, as compared to the free-field ones. Computation outcomes well reproduce the *in situ* observations in terms of building's displacements, being accurate in replicating the modification of the deformative patterns and the magnitude of settlements along its façades. This result proves the reliability of the proposed fully-coupled finite element approach to capture the essential mechanisms governing the problem. It is also demonstrated that the contribution of the infill panels on the overall displacement field appears to be

negligible for this specific structure, while it is shown to play a more significant role on the redistribution of the structural forces acting in the vertical columns of the building during the excavation process.

The numerical settlement profiles are found to nicely fit the monitoring data also when the building is simplified and reduced only to its buried portion, opportunely loaded to account for the weight of the above floors neglected in the model: in terms of displacement pattern, this model provides almost equivalent results to those obtained by the analysis with the complete structural scheme, highlighting the negligible stiffening role of the above structure in this reference case study.

In contrast, for this particular building and discrete foundation typology, the equivalent plate schematisation, often employed in the engineering practice, involves a large overestimation of the structure's stiffness, resulting in highly inaccurate settlement profiles as compared to that observed *in situ*. This schematisation does not allow to reproduce the real displacement field affecting this building in correspondence with its longitudinal sides, which rest on continuous strip footings, nor along the portions of the structure located between the discrete foundation elements. The equivalent plate model also prevents to capture the sagging and hogging type mechanisms highlighted along each side of the building and the stiffer structural response observed in correspondence with the single foundation beams.

The validation of this integrated approach in terms of subsidence field justifies the use of the proposed tool for a direct analysis of some features of the structural response. To illustrate this, the study proposes, as an example, the evaluation of the stress state within the cross-bracings during one of the most critical stage of the metro-line construction, corresponding to a prevailing mechanism associated to a hogging-type deformative mode in this multi-storey framed structure.

In conclusion, the procedure discussed and validated in this work, which refers to one particular interaction case, can be extended and generalised for future research. In addition to the effect of the structure weight and stiffness on the tunnelling-induced surface displacement field, already examined in this study, the influence of the building position and orientation with respect to the tunnel axis as well as the role of different foundation systems could be examined.

In the numerical analyses performed in this work the external infill panels of the building were schematised as weightless cross-bracings of equivalent stiffness properties. A more advanced modelling of these structural components, both in terms of geometry and constitutive hypothesis, can also represent a valuable improvement in the proposed numerical approach.

Acknowledgements

At the conclusion of this work, I wish to thank my supervisor Prof. Daniela Boldini and my co-supervisor Prof. Angelo Amorosi for their guidance, interest and enthusiasm for this research and for the great opportunity to work with them on the topic of this study.

Financial support provided by Astaldi S.p.A. in the person of Eng. Enrico Campa is gratefully acknowledged. Special thanks to Eng. Giuseppe Colombo of Milano Serravalle-Milano Tangenziali S.p.A. (formerly Astaldi S.p.A.) and to Eng. Davide Fraccaroli and Eng. Alessandro Caffaro of Astaldi S.p.A. for providing the monitoring data and for the technical support during the site activity.

A particular word of gratitude to my colleagues and friends, in particular to Annalisa Bandini and Carlo Cormio, for their kind welcome and for making my time at the University of Bologna so enjoyable.

Lovely thanks to my family and to Francesco for their patience and for absolutely supporting me during this experience.

References

Addenbrooke T.I. (1996). *Numerical analysis of tunnelling in stiff clay*. PhD. dissertation, University of London.

Addenbrooke T.I. and Potts D.M. (2001). Twin tunnel interaction - surface and subsurface effects. *International Journal of Geomechanics*, 1: 249-271.

Addenbrooke T.I., Potts D.M. and Puzrin A.M. (1997). *The influence of pre-failure soil stiffness on the numerical analysis of tunnel construction*. Géotechnique, 47(3): 693–712.

Al-Tabbaa A. (1987). *Permeability and stress strain response of speswhite kaolin*. Ph.D. dissertation, University of Cambridge.

Al-Tabbaa A. and Muir Wood D. (1989). *An experimentally based 'bubble' model for clay*. Proceedings of the Numerical Models in Geomechanics, NUMOG III, Niagara Falls, Canada, vol. 1, pp. 91–99.

Altamura G., Burghignoli A. and Miliziano S. (2007). *Modelling of surface settlements induced by tunnel excavation using the differential stress release technique*. Italian Geotechnical Journal, 41(3): 33–47.

Amorosi A., Boldini D., de Felice G., Malena M. and Sebastianelli M. (2014). *Tunnelling-induced deformation and damage on historical masonry structures*. Géotechnique, 64(2):118-130.

Ata A.A. (1996). *Ground settlements induced by slurry shield tunnelling in stratified soils*. Proc. North American Tunnelling '96, ed. L. Ozdemir, vol. 1, pp. 43–50.

Atkinson J.H. and Potts D.M. (1977). *Subsidence above shallow tunnels in soft ground*. ASCE, Journal of Geotechnical Engineering, vol. 103, GT4, 12872, pp. 307-325.

Attewell P.B. (1978). *Ground movements caused by tunnelling in soil*. In Geddes, J. D. (Ed.), Proc. Int. Conf. on Large Movements and Structures, Pentech Press, London, pp. 812–948.

Attewell P.B. and Yeates J. (1984). *Tunnelling in soil*. In P.B. Attewell and R.K. Taylor, editors, Ground movements and their effects on structures. Surrey University Press. pp. 132-215.

Attewell P.B., Yeates J. and Selby A.R. (1986). *Soil Movements Induced by Tunnelling and their Effects on Pipelines and Structures*. Blackie, Glasgow.

Attewell P.B. and Woodman J.P. (1982). *Predicting the dynamics of ground settlement and its derivatives caused by tunnelling in soil*. Ground Engineering 15(8): 13–22 (36).

Augarde C.E., Wisser C. and Burd H.J. (1999). *Numerical modelling of tunnel installation procedures*. Proc. 7th Int. Symp. on Numerical Methods in Geomechanics – NUMOG VII, Graz, pp. 329–334.

Barratt D.A. and Tyler R.G. (1976). *Measurements of ground movement and lining behaviour on the London Underground at Regent Park*. TRRL laboratory Report 684.

Bartlett T.I. and Bubbers B.L. (1979). *Surface movement caused by bored tunnelling*. Proceedings conference on subway construction; Budapest, pp. 513-89.

Baudet B.A. and Stallebrass S.E. (2004). *A constitutive model for structured clays*. Géotechnique, 54(4): 269–278.

Benz T. (2007). *Small-strain stiffness of soils and its numerical consequences*. Ph.D. dissertation, Universität Stuttgart.

Bilotta E. and Russo G. (2012). *Ground movements induced by tunnel boring in Naples*. Geotechnical Aspects of Underground Construction in Soft Ground – Viggiani (ed), Taylor & Francis Group, London, pp. 979-986.

Boldini D., Fargnoli V., Gragnano C.G. and Amorosi A. (2014). *Advanced numerical modelling of multi-storey buildings response to tunnelling*. 8th International Symposium on Geotechnical Aspects of Underground Construction in Soft Ground, Seoul. CRC PRESS TAYLOR & FRANCIS GROUP, vol. 1, pp. 239-244.

Boonpichetvong M. and Rots J.G. (2002). *Settlement damage of masonry buildings on soft-ground tunnelling*. In Finite Elements in Civil Engineering Applications – 3rd DIANA conference, Tokyo, pp. 285–294.

Boscardin M. and Cording E. (1989). *Building response to excavation-induced settlement*. ASCE Journal of Geotechnical Engineering, 115(1): 1–21.

Branque D., Subrin D. and Boutin C. (2002). *Etude sur modéle réduit du creusement des tunnels par la method du bouclier à pression de terre*. In: Proc. Int. Symposium on Geotechnical Aspects of Underground Construction in Soft Ground, Toulouse, pp. 324–329.

Breth H. and Chambosse G. (1974). *Settlement behaviour of buildings above subway tunnels in Frankfurt clay*. In Proc. Conf. Settlement of Structures, Cambridge, pp. 329–336.

Brinkgreve R.B.J., Kappert M.H. and Bonnier P.G. (2007). *Hysteretic damping in a small-strain stiffness model*. Numerical Models in Geomechanics-NUMOG X, pp. 737-742.

Burd H.J., Houlsby G.T., Augarde C.E. and Liu G. (2000). *Modelling tunnelling-induced settlement of masonry buildings*. Proc. Institution of Civil Engineers-Geotechnical Engineering, 143(1): 17–29.

Burghignoli A. (2011). *L'attraversamento sotterraneo del centro storico di Roma*. Italian Geotechnical Journal, 4: 13-50.

Burland J.B. (1995). *Assessment of risk of damage to buildings due to tunnelling and excavation.* Invited special lecture. In Proc. 1st Int. Conf. on Earthquake Geotech. Engineering-IS-Tokyo 95.

Burland J., Broms B.B. and de Mello V.F.B. (1977). *Behaviour of foundations and structures*. In Proc. 9th Int. Conf. Soil Mech. and Found. Eng., vol. 2, pp. 495–546.

Burland J.B., Simpson B. and St. John H.D. (1979). *Movements around excavations in London clay*. Proc. 7th Eur. Conf. Soil Mech., vol. 1, pp. 13-30.

Burland J.B. and Wroth C.P. (1974). *Settlement of buildings and associated damage*. In Proc. Conf. on Settlement of Structures, Cambridge, pp. 611–654.

Celestino T.B., Gomes R.A.M.P. and Bortolucci A.A. (2000). *Errors in ground distortions due to settlement trough adjustment*. Tunnel. Undergr. Space Technol., 15(1): 97–100.

Chambon J.F. and Corté J.F. (1994). *Shallow tunnels in cohesionless soil: stability of tunnel face*. Journal of Geotechnical Engineering, ASCE 120(7): 1150–1163.

Chapman D.N., Ahn S.K. and Hunt D.V.L. (2007). *Investigating ground movements caused by the construction of multiple tunnels in soft ground using laboratory model tests*. Canadian Geotechnical Journal, 44: 631-643.

Clough W. and Schmidt B. (1981). *Design and performance of excavations and tunnels in soft clay*. In E. Brand and R. Brenner, editors, Soft Clay Engineering, Elsevier, pp. 567–634.

Comodromos E.M., Papadopoulou M.C. and Konstantinidis G.K. (2014). *Numerical Assessment of Subsidence and Adjacent Building Movements Induced by TBM-EPB Tunneling*. J. Geotech. Geoenviron. Eng., 140(11): 04014061-1-12.

Cooper M.L., Chapman D.N., Roger C.D.F. and Chan A.H.C. (2002). *Movements of the Piccadilly Line tunnels due to Heathrow Express construction*. Géotechnique, 52(4): 243-257.

Cording E.J. (1991). *Control of ground movements around tunnels in soil*. General report, in 9th Pan-American Conference on Soil Mechanics and Foundation Engineering, Chile.

Cording E.J. and Hansmire W.H. (1975). *Displacements around soft ground tunnels*. In 5th Panamerican conference on soil mechanics and foundation engineering, Buenos Aires, pp. 571-632.

Cording E.J., Hansmire W.H., MacPherson H.H., Lenzini P.A. and Vonderohe, A.P. (1975). *Displacements around tunnels in soil*. Final Report by the University of Illinois on Contract No. DOT FR 30022 to the Office of the Secretary and Federal Railroad Administrator, Department of Transportation, Washington, D.C.

Dimmock P.S. and Mair R.J. (2008). *Effect of building stiffness on tunnelling induced ground movement*. Tunnelling and Underground Space Technology, 23(4): 438–450.

Dimmock P.S., Mair R.J. and Standing J.R. (2002). *Ground movements caused by tunnelling with an earth pressure balance machine: a greenfield case study at Southwark Park, London*. In: Proc. Int. Symposium on Geotechnical Aspects of Underground Construction in Soft Ground, Toulouse, pp. 356–361.

Fardis M.N. (1997). *Experimental and numerical investigations on the seismic response of RC infilled frames and recommendations for code provisions*. Report ECOEST-PREC8 No. 6. Prenormative research in support of Eurocode 8.

Fargnoli V., Boldini D. and Amorosi A. (2013). *TBM-tunnelling induced settlements in coarse-grained soils: The case of the new Milan underground line 5*. Tunnelling and Underground Space Technology, 38: 336-347.

Fargnoli V., Boldini D. and Amorosi A. (2015 *a*). *Twin tunnel excavation in coarse grained soils: observations and numerical back-predictions under free-field conditions and in presence of a surface structure.* Tunnelling and Underground Space Technology. Submitted.

Fargnoli V., Gragnano, C.G., Boldini D. and Amorosi A. (2015 *b*). *3D numerical modelling of soil-structure interaction during EPB tunnelling.* Géotechnique, 65(1): 23-37.

Farrell R.P. (2010). *Tunnelling in sands and the response of buildings*. PhD dissertation, University of Cambridge.

Farrell R.P. and Mair R.J. (2011). *Centrifuge modelling of the response of buildings to tunnelling.* Proceedings of 7th International Symposium on Geotechnical Aspects of

Underground Construction in Soft Ground, Rome. Viggiani (ed) 2012, Taylor & Francis Group, London, pp. 343-351.

Farrell R.P., Mair R.J., Sciotti A., Pigorini A. and Ricci M. (2011). *The response of buildings to tunnelling: A case study*. Proceedings of 7th International Symposium on Geotechnical Aspects of Underground Construction in Soft Ground, Rome. Viggiani (ed) 2012, Taylor & Francis Group, London, pp. 877-885.

Franzius J.N. (2003). *Behaviour of buildings due to tunnel induced subsidence*. PhD dissertation, Department of Civil and Environmental Engineering, Imperial College, University of London.

Franzius J.N. and Potts D.M. (2005). *Influence of mesh geometry on three-dimensional finite-element analysis of tunnel excavation*. Journal of Geotechnical Engineering, 5(3): 256-266.

Franzius J.N., Potts D.M. and Burland J.B. (2006). *The response of surface structures to tunnel construction*. Proc. Institution of Civil Engineers- Geotechnical Engineering, 159(1): 3-17.

Geddes J. D. and Kennedy D. (1985). *Structural implications of horizontal ground strains*. In Ground Movements and Structures, Proceedings of the 3rd International Conference. Pentech Press London England, pp. 610-629.

Giardina G., Dejong M. and Mair R. (2014). *Masonry response to tunnelling: A sensitivity study on the effect of cracking about building weight*. 9th International Masonry Conference, Guimarães, pp. 1-11.

Giardina G., Hendriks M.A.N. and Rots J.G. (2010). *Numerical analysis of tunnelling effects on masonry buildings: the influence of tunnel location on damage assessment*. Advd. Mater. Res. pp. 133–134, 289–294.

Giardina G., Marini A., Hendriks M.A.N., Rots J.N., Rizzardini F. and Giuriani E. (2012). *Experimental analysis of a masonry façade subject to tunnelling-induced settlement*. Engineering Structures, 45: 421–434.

Giardina G., van de Graaf A.V., Hendriks M.A.N., Rots J.G. and Marini A. (2013). *Numerical analysis of a masonry façade subject to tunnelling-induced settlements*. Engineering Structures, 54: 234–247.

Goh K.H. and Mair R.J. (2010). *Settlement response of framed buildings to movements from tunnelling and deep excavations*. Proc. of World Urban Transit Conference, Singapore.

Goh K.H. and Mair R.J. (2011). *The horizontal response of framed buildings on individual footings to excavation-induced movements*. Geotechnical Aspects of Underground Construction in Soft Ground – Viggiani (ed.), pp. 895-902.

Gonzalez N.A., Rouainia M., Arroyo M. and Gens A. (2012). *Analysis of tunnel excavation in London Clay incorporating soil structure*. Géotechnique, 62(12): 1095-1109.

Gragnano C. G., Fargnoli V., Boldini D., Amorosi A. (2014). *Comparison of structural elements response in PLAXIS 3D and SAP2000*. Plaxis Bulletin. Issue 35/Spring 2014, pp. 6-11.

Grammatikopoulou A., Zdravkovic L. and Potts D.M. (2006). *General formulation of two kinematic hardening constitutive models with a smooth elasto-plastic transition*. Int. J. Geomech., ASCE 6(5): 291–302.

Grant R.J. (1998). *Prediction of pre-failure ground movements due to tunnelling: physical and numerical modelling*. Workshop on Prediction and Performance in Geotechnical Engineering., Naples.

Grant R.J. and Taylor R.N. (2000). *Tunnelling-induced ground movements in clay*. Proc. Instn. Civ. Engrs. Geotech. Engng, 143: 43-55.

Guedes de Melo P. and Santos Pereira C. (2002). *Three-dimensional numerical modelling of the construction of an EPBS tunnel for Shanghai Metro – Line 2*. In: Proc. Int. Symposium on Geotechnical Aspects of Underground Construction in Soft Ground, Toulouse, pp. 318–323.

Gunn M.J. (1993). *The prediction of surface settlement profiles due to tunnelling*. Predictive Soil Mechanics-Proceedings Wroth Memorial Symposium, Houlsby GT, Schofield AN (eds). T Telford: London, pp. 304–316.

Hardin B.O. (1978). *The nature of stress-strain behaviour for soils-State of the art report*. Proceedings of specialty conference on earthquake engineering and soil dynamics, New York: American Society of Civil Engineering, pp. 3-90.

Hardin B.O. and Black W.L. (1968). *Vibration modulus of normally consolidated clay*. Journal of Soil Mechanics and Foundations Division, ASCE 95(SM6): 1531–1537.

Hardin B.O. and Drnevich V. (1972). *Shear modulus and damping in soils: design equations and curves*. Journal of Soil Mechanics and Foundations Division, ASCE 98(7): 667-692.

Harris D.I. and Franzius J.N. (2005). *Settlement assessment for running tunnels: a generic approach.* International Symposium on Geotechnical Aspects in Soft Ground. Amsterdam, Balkema, Rotterdam, vol. 1, pp. 13-18.

Harris D.I., Menkiti C.O., Pooley A.J. and Stephenson J.A. (1996). *Construction of low-level tunnels below Waterloo Station with compensation grouting for Jubilee Line Extension.* Aspects of underground construction in soft ground. Mair R.J. and Taylor R.N. Eds., Balkema, Rotterdam, pp. 751-756.

Hergarden H.J.A.M., van der Poel J.T. and van der Schrier J.S. (1996). *Ground movements due to tunnelling: Influence on pile foundations*. Proceedings of the international symposium on geotechnical aspects of underground construction in soft ground, London, pp. 519–524.

Higgins K.G., Mair R.J. and Potts D.M. (1996). *Numerical modelling of the influence of the Westminster Station excavation and tunnelling on the Big Ben clock tower.* Aspects of underground construction in soft ground. Mair R.J. and Taylor R.N. Eds., Balkema, Rotterdam, pp. 525-530.

Houlsby G.T. (1999). *A model for the variable stiffness of undrained clay*. In 2nd Int. Symp. on Pre-Failure Deformation Characteristics of Geomaterials, vol. 1, pp. 443–450.

Hulme T.W., Shirlaw S.N. and Hwang R.N. (1990). *Settlements during the underground construction of the Singapore MRT*. In: Proc. 10th Southeast Asian Geotechnical Conference, Taipei, Taiwan, pp. 521–526.

Hunt D.V.L. (2005). *Predicting the ground movements above twin tunnels constructed in London Clay*. Ph.D. dissertation, Birmingham University.

Imamura S., Hagiwara T., Mito K., Nomoto T. and Kusakabe O. (1998). *Settlement trough above a model shield observed in a centrifuge*. Proceedings of Centrifuge 98, pp. 713–719.

Jacobsz S.W. (2002). *The effects of tunnelling on piled foundations*. PhD dissertation, Engineering Department, Cambridge University.

Jacobsz S.W., Standing, J.R., Mair R.J., Hagiwara T. and Sugiyama T. (2004). *Centrifuge modelling of tunnelling near driven piles*. Soils Found., 44(1): 49–56.

Jardine R.J., Fourie A.B., Maswoswe J. and Burland J.B. (1985). *Field and laboratory measurement of soil stiffness*. Proceedings of the 11th International Conference on Soil Mechanics and Foundation Engineering, San Francisco, U.S.A., vol. 2, pp. 511–514.

Jardine R.J., Potts D.M., Fourie A.B. and Burland J.B. (1986). *Studies of the influence of non-linear stress–strain characteristics in soil–structure interaction*. Géotechnique, 36(3): 377-396.

Jenck O. and Dias D. (2004). *3D-finite difference analysis of the interaction between concrete building and shallow tunnelling*. Géotechnique, 54(8): 519-528.

Kasper T. and Meschke G. (2004). *A 3D finite element simulation model for TBM tunneling in soft ground*. Int. J. Numer. Anal. Methods Geomech., 28(14): 1441–1460.

Kasper T. and Meschke G. (2006 *a*). *A numerical study of the effect of soil and grout material properties and cover depth in shield tunneling*. Comput. Geotech., 33(4–5): 234–247.

Kasper T. and Meschke G. (2006 *b*). *On the influence of face pressure, grouting pressure and TBM design in soft ground tunneling*. Tunnelling and Underground Space Technology, 21(2): 160-171.

Kavvadas M. and Amorosi A. (2000). *A constitutive model for structured soils*. Géotechnique, 50(3): 263–273.

Keshuan M. and Lieyun D. (2008). *Finite element analysis of tunnel–soil–building interaction using displacement controlled model*. Wseas Transactions on Applied and Theoretical Mechanics, 3(1): 73–82.

Komiya K., Soga K., Hirokazu A., Hagiwara T. and Bolton M.D. (1999). *Finite element modelling of excavation and advancement processes of a shield tunnelling machine*. Soils and Foundations, 39(3): 37–52.

Kutter B. L., Chang J. D. and Davis B. C. (1994). *Collapse of cavities in sand and particle size effects*. Proc. Centrifuge 94, Singapore, pp. 809–815.

Lake L.M., Rankin W.J. and Hawley J. (1992). *Prediction and effects of ground movements caused by tunnelling in soft ground beneath urban areas*. CIRIA Special Report 30.

Lambrughi A., Medina L.R. and Castellanza R. (2012). *Development and validation of a 3D numerical model for TBM–EPB mechanized excavations*. Comput. Geotech., 40: 97–113.

Leblais Y. and Bochon A. (1991). *Villejust Tunnel: slurry shield effects on soils and lining behaviour and comments on monitoring equipment*. Tunnelling 91, London IMM, pp. 65-77.

Liu G., Houlsby G.T. and Augarde C.E. (2000). *Two-dimensional analysis of settlement damage to masonry buildings caused by tunnelling*. The Structural Engineer, 79(1): 19–25.

Liu J., Qi T. and Wu Z. (2012). *Analysis of ground movement due to metro station driven with enlarging shield tunnels under building and its parameter sensitivity analysis*. Tunnelling and Underground Space Technology, 28: 287–296.

Lo K.W., Lee S.L., Makino H., Chang L.K., Leung C.F. and Mihara T. (1987). *Tunnels in close proximity*. Proc. Singapore Mass Rapid Conference, Singapore, pp. 275-281.

Loganathan N. and Poulos H.G. (1998). *Analytical prediction for tunneling induced ground movements in clays*. Journal of Geotechnical and Geoenvironmental Engineering, 124(9): 846-856.

Losacco N. (2011). *Development and testing of a simplified building model for the study of soil-structure interaction due to tunnelling in soft ground*. PhD dissertation, Sapienza University of Rome.

Losacco N., Burghignoli A. and Callisto L. (2014). *Uncoupled evaluation of the structural damage induced by tunnelling*. Géotechnique, 64(8): 646-656.

Mainstone R.J. (1971). On the stiffnesses and strengths of infilles frames. *Proc. Inst. Civil. Engineers*,49(2): 59-70.

Mair R.J. (1979). *Centrifuge modelling of tunnel construction in soft clay*. Ph.D. dissertation, University of Cambridge.

Mair R.J. (1996). *Settlement effects of bored tunnels*. Session Report, Proc. Int. Symposium on Geotechnical Aspects of Underground Construction in Soft Ground, London (eds. R.J. Mair and R.N. Taylor), Balkema, pp. 43-53.

Mair R.J. (2003). *Research on tunnelling-induced ground movements and their effects on buildings-lessons from the Jubilee Line Extension*. Keynote Lecture. In Jardine, F. M. (Ed.), Proc. Int. Conf. on Response of Buildings to Excavation-induced Ground Movements, London, pp. 3–26.

Mair R.J. and Taylor R.N. (1997). *Theme lecture: bored tunnelling in urban environment*. Proc. of the 14th International Conference on Soil Mechanics and Foundation Engineering. Hamburg, vol. 4, pp. 2353-2385.

Mair R.J., Taylor R.N. and Bracegirdle A. (1993). *Subsurface settlement profiles above tunnels in clays*. Géotechnique, 43(2): 315–320.

Mair R.J., Taylor R.N. and Burland J.B. (1996). *Prediction of ground movements and assessment of risk of building damage due to bored tunnelling*. Proceeding of the International

Symposium on Geotechnical Aspects of Underground Construction in Soft Ground, London (eds Mair and Taylor), Balkema, pp. 713-718.

Maleki M., Sereshteh H., Mousivand M. and Bayat M. (2011). *An equivalent beam model for the analysis of tunnel-building interaction*. Tunnelling and Underground Space Technology, 26(4): 524–533.

Marshall A., Farrell R., Klar A. and Mair R. (2012). *Tunnels in sands: the effect of size, depth and volume loss on greenfield displacements*. Géotechnique, 62(5): 385-399.

Melis M., Medina L. and Rodriguez J.M. (2002). *Prediction and analysis of subsidence induced by shield tunnelling in the Madrid Metro extension*. Can. Geotech. J., 39(6):1273–1287.

Melis M.J. and Ortiz R. (2003). *Consideration of the stiffness of buildings in the estimation of subsidence damage by EPB tunneling in the Madrid Subway*. Proc. int. conf. on response of buildings to excavation-induced ground movements, CIRIA Special Publication, London, 199, pp. 387-394.

Migliazza M., Chiorboli M. and Giani G.P. (2009). *Comparison of analytical method, 3D finite element model with experimental subsidence measurements resulting from the extension of the Milan underground*. Comput. Geotech., 36(1–2): 113–124.

Moh Z.C. and Hwang R.N. (1993). *Underground construction of Taipei Transit Systems*. In: Proc. 11th Southeast Asian Geotechnical Conference, Singapore, pp. 15–24.

Moh Z.C., Hwang R.N. and Ju D.H. (1996). *Ground movements around tunnels in soft ground*. In Mair, R.J. & Taylor, R.N. (Eds.), Int. Symp. on Geotechnical Aspects of Underground Construction in Soft Ground, London, pp. 725–730.

Möller S. (2006). *Tunnel induced settlements and structural forces in lining*. PhD dissertation. Universität Stuttgart.

Möller S.C. and Vermeer P.A. (2008). *On numerical simulation of tunnel installation*. Tunnelling and Underground Space Technology, 23: 461-475.

Mroueh H. and Shahrour I. (2003). *A full 3-d finite element analysis of tunneling-adjacent structures interaction*. Computers and Geotechnics, 30(3): 245–253.

Mroz Z., Norris V.A. and Zienkiewicz O.C. (1978). *An anisotropic hardening model for soils and its application to cyclic loading*. Int. J. Numer. Anal. Meth. Geomech., 2: 203-221.

New B.M. and O'Reilly M.P. (1991). *Tunnelling induced ground movements; predicting their magnitude and effects*. Proceedings of the 4th International Conference on Ground Movements and Structures. Cardiff, invited paper, Pentech Press, pp. 671-697.

Nomoto T., Mori H. and Matsumoto M. (1995). *Overview on ground movements during shield tunnelling – a survey on Japanese shield tunnelling*. Proc. Int. Symposium on Geotechnical Aspects of Underground Construction in Soft Ground, Balkema, pp. 345–351.

Ohta Y. and Goto N. (1978). *Empirical shear wave velocity equations in terms of characteristic soil indexes*. Earthquake Engineering and Structural Dynamics, 6: 167-187.

O'Reilly M.P. and New B.M. (1982). *Settlements above tunnels in the United Kingdom-their magnitude and prediction*. Tunnelling '82, London, IMM, pp. 173-181.

Panagiotakos T.B. and Fardis M.N. (1996). Seismic response of infilled RC frames structures. Proceedings of the 11th world conference on earthquake engineering, Acapulco, Oxford, UK: Pergamon, paper no. 225.

Panet M. and Guenot A. (1982). *Analysis of convergence behind the face of a tunnel*. The Institution of Mining and Metallurgy, London. Tunnelling 82, pp. 197–204.

Peck R.B. (1969). *Deep excavations and tunnelling in soft ground*. Proceedings of the 7th international conference on soil mechanics and foundation engineering, Mexico City, pp. 225-290.

Peila D., Borio L. and Pelizza S. (2011). *The behaviour of a two-component back-filling grout used in a tunnel-boring machine*. Acta Geotechnica Slovenica, 1: 5–15.

Perez Saiz A., Garami J., Arcones A. and Soriano A. (1981). *Experience gained through tunnel instrumentation*. Proc. 10th International Conference on Soil Mechanics and Foundation Engineering, Stockholm, vol. 1, pp. 345-352.

Phienwej N., Sirivachiraporn A., Timpong S., Tavaranum S. and Suwansawat S. (2006). *Characteristics of Ground Movements from Shield Tunnelling of the First Bangkok Subway Line*. In: International Symposium on Underground Excavation and Tunnelling, Bangkok, Thailand, pp. 319–330.

Pickhaver J.A., Burd H.J. and Houlsby G.T. (2010). *An equivalent beam method to model masonry buildings in 3D finite element analysis*. Computers and Structures, 88: 1049–1063.

Plaxis (2012). Plaxis 2D and 3D user manuals. Delft, the Netherlands: Plaxis bv.

Polshin D. and Tokar R. (1957). *Maximum allowable non uniform settlement of structures*. In Proc. 4th Int. Conf. Soil Mechanics and Foundation Engineering, vol. 1, pp. 402–405.

Potts D.M. (1976). *Behaviour of lined and unlined tunnels in sand*. PhD dissertation, University of Cambridge.

Potts D.M. and Addenbrooke T.I. (1997). *A structure's influence on tunnelling-induced ground movements*. Proc. Institution of the Civil Engineers, Geotechnical Engineering, 125(2): 109–125.

Puzrin A.M., Burland J.B. and Standing J.R. (2012). *Simple approach to predicting ground displacements caused by tunnelling in undrained anisotropic elastic soil*. Géotechnique, 62(4): 341–352.

Rampello S. and Callisto L. (1999). *Numerical analysis of tunnel construction under an ancient massive structure*. In 2nd Int. Symp. on Pre-Failure Deformation Characteristics of Geomaterials, vol. 1, pp. 549–554.

Rampello S., Callisto L., Viggiani G. and Soccodato F.M. (2012). *Evaluating the effects of tunnelling on historical buildings: the example of a new subway in Rome*. Geomechanics and Tunnelling, 5(3): 275-299.

Rankin W.J. (1988). *Ground movements resulting from urban tunnelling: predictions and effects*. Geological Society, London, Engineering Geology Special Publications, 5(1): 79–92.

Rouainia M. and Muir Wood D. (2000). *A kinematic hardening constitutive model for natural clays with loss of structure*. Géotechnique, 50(2): 153–164.

Rowe R.K., Lo K.Y. and Kack G.J. (1983). *A method of estimating surface settlement above tunnel constructed in soft ground*. Canadian Geotechnical Journal, 20(1): 11–22.

Russo G., Viggiani C. and Viggiani G.M.B. (2012). *Geotechnical design and construction issues for lines 1 and 6 of the Naples underground*. Geomechanics and Tunnelling, 5(3): 300-311.

Santos J.A. and Correia A.G. (2001). *Reference threshold shear strain of soil. Its application to obtain a unique strain dependent shear modulus curve for soil*. 15th Int. Conf. on Soil Mechanics and Geotechnical Engineering, Istanbul, vol. 1, pp. 267-270.

Schanz T., Vermeer P.A. and Bonnier P.G. (1999). *The Hardening Soil Model: formulation and verification*. Plaxis symposium on beyond 2000 in computational geotechnics, Amsterdam, pp. 281–296.

Schmidt B. (1969). *Settlement and ground movement associated with tunneling in soils*. PhD dissertation, University of Illinois.

Shirlaw J.N., Doran S. and Benjamin B. (1988). *A case study of two tunnels driven in the Singapore "Boulder Bed" and in grouted coral sands*. Engineering Geology of Underground Movements, eds. F.G. Bell et al., Geological Society Engineering Geology Special Publication, vol. 5, pp. 93-103.

Shirlaw J.N., Ong J.C.W., Osborne N.H. and Tan C.G. (2002). *The relationship between face pressure and immediate settlement due to tunnelling for the North East Line, Singapore*. In: Proc. Int. Symposium on Geotechnical Aspects of Underground Construction in Soft Ground, Toulouse, pp. 306–311.

Sirivachiraporn A. and Phienwej N. (2012). *Ground movements in EPB shield tunnelling of Bangkok subway project and impacts on adjacent buildings*. Tunnelling and Underground Space Technology, 30: 10–24.

Skempton A.V. (1986). *Standard Penetration Test Procedures*. Géotechnique, 36**(**3): 425-557.

Skempton A.V. and MacDonald D.H. (1956). *Allowable settlement of buildings*. Proc. Institution of Civil Engineers, 5(6): 727–784.

Son M. and Cording E.J. (2005). *Estimation of building damage due to excavation-induced ground movements*. Journal of Geotechnical and Geoenvironmental Engineering, 131(2): 162-177.

Son M. and Cording E.J. (2011). *Responses of buildings with different structural types to excavation-induced ground settlements*. Journal of Geotechnical and Geoenvironmental Engineering, 137(4): 23-344.

Stallebrass S.A. (1990). *Modelling the effect of recent stress history on the deformation of overconsolidated soils*. Ph.D. dissertation, City University.

Stallebrass S.E. and Taylor R.N. (1997). *The development and evaluation of a constitutive model for the prediction of ground movements in overconsolidated clay*. Géotechnique, 47(2): 235–253.

Standing J.R., Nyren R.J., Longworth T.I. and Burland J.B. (1996). *The measurements of ground movements due to tunnelling at two control sites along the Jubilee Line Extension*. Proc.

Int. Symposium on geotechnical aspects of underground construction in soft ground, London, Mair R.J. and Taylor R.N. Eds., Balkema, pp. 751-756.

Sugiyama T., Hagiwara T., Nomoto T., Nomoto M., Ano Y., Mair R.J., Bolton M.D. and Soga K. (1999). *Observations of ground movements during tunnel construction by slurry shield method at the Docklands Light Railway Lewisham Extension – East London*. Soils and Foundations, 39(3): 99–112.

Suwansawat S. (2002). *Earth Pressure Balance Shield Tunnelling in Bangkok: Ground Response and Prediction of Surface Settlements using Artificial Neural Networks*. PhD dissertation, Massachussets Institute of Technology.

Suwansawat S. and Einstein H.H. (2007). *Describing settlement troughs over twin tunnels using a superposition technique*. J. Geotech. Geoenviron. Eng, 133: 445-468.

Swoboda G. (1979). *Finite element analysis of the New Austrian Tunnelling Method (NATM)*. In Proc. 3rd Int. Conf. Numerical Methods in Geomechanics, Aachen, vol. 2, pp. 581-586.

Tamagnini C., Miriano C., Sellari E. and Cipollone, N. (2005). *Two-dimensional FE analysis of ground movements induced by shield tunnelling: the role of tunnel ovalization*. Rivista Italiana di Geotecnica, 39(1): 11–33.

Tang D.K.W., Lee K.M. and Ng C.W.W. (2000). *Stress paths around a 3-d numerically simulated natm tunnel in stiff clay*. Proc. Int. Symp. on Geotechnical Aspects of Underground Construction in Soft Ground – IS-Tokyo 99, pp. 443–449.

Tatsuoka F. (2000). *Impacts on geotechnical engineering of several recent findings from laboratory stress–strain tests on geomaterials*. The 2000 Burmister Lecture, Department of Civil Engineering and Engineering Mechanics, Columbia University.

Taylor R.N. (1995). *Tunnelling in soft ground in the UK*. In K. Fujita and O. Kusakabe, editors, Proceedings of the 1994 International Symposium on Underground Construction in Soft Ground,. Balkema, New Delhi, pp.123-126.

Timoshenko S. (1955). *Strength of materials*. Part 1: Elementary theory and problems (3 ed.). D. Van Nostrand, New York.

Uriel A.O. and Sagaseta C. (1989). *Selection of design parameters for underground construction*. In: General Report, 12th International Conference on Soil Mechanics and Foundation Engineering, Rio de Janeiro, ed. Balkema, vol. 4, pp. 2521–2551.

Vermeer P.A. and Brinkgreve R. (1993). *Plaxis Version 5 Manual*. Rotterdam, Balkema edition.

Viggiani G. and Soccodato F.M. (2004). *Predicting tunnelling-induced displacements and associated damage to structures*. Italian Geotechnical Journal, (4): 11-25.

Viggiani G.M.B. and Standing J.R. (2001). *Building response to tunnelling: case studies from construction of the Jubilee Line Extension*. The Treasury. In J. B. Burland, J. R. Standing and F. Jardine, editors, CIRIA and Thomas Telford,. London, vol. 2, pp. 351-366.

Viggiani G.M.B. and Standing J.R. (2002). *The Treasury*. CIRIA and Thomas Telford, London, vol. 2, pp. 401–432.

Vinale F., Mancuso C. and Silvestri F. (1996). *Dinamica dei terreni*. Manuale di Ingegneria Civile, Ed. Scientifiche, A. Cremonese-Zanichelli.

Vorster T.E.B. (2005). *The effects of tunnelling on buried pipes*. PhD dissertation, Engineering Department, Cambridge University.

Vorster T.E.B., Kla, A., Soga K. and Mair R.J. (2005). *Estimating the effects of tunneling on existing pipelines*. J. Geotech. Geoenviron. Engng, 131(11): 1399–1410.

Vucetic M. and Dobry R. (1991). *Effect of the soil plasticity on cyclic response*. Journal Geotechnical Engineering, ASCE 117(1): 89-107.

Ward W.H. and Pender M.J. (1981). *Tunnelling in soft ground – General Report*. 10th International Conference on Soil Mechanics and Foundation Engineering. Stockholm, vol. 4, pp. 261-275.

Withers A. (2001). *Murdoch, Neptune and Clegg houses in Moodkee street, Rotherhithe*. In J. B. Burland, J. R. Standing and F. Jardine, editors, Building response to tunnelling case studies from construction of the Jubilee Line Extension, London, vol. 2, pp. 811–828.

Contents